WESTERN SYDNEY UNIVERSITY

The effects of two highly bioavailable curcumin preparations on the activation of glial cells and chronic neuroinflammation in GFAP-IL6 mice

Faheem Ullah (MSc in Neurobiology)

A thesis submitted in fulfilment of the requirements for the degree of Doctor of Philosophy School of Medicine, Western Sydney University, Australia 2019

Supervisor: **Dr Erika Gyengési**

Co-supervisors: **Prof Gerald Münch**

Dr Garry Niedermayer

Statement of Authentication

This is to certify that to the best of my knowledge that, the content of the thesis has not been submitted for the award of any degree or diploma. I hereby declare that the content of this thesis is the product of my own work, and to the best of my knowledge, this thesis contains no materials previously published by any person, except where references have been made.

Faheem Ullah

June 2019

Acknowledgment

In the Name of Allah, the Beneficent, the Merciful, the Almighty. May peace and salutation be upon the prophet Muhammad (PBUH).

Firstly, I would like to express my sincere gratitude to Dr Erika Gyengesi for being the greatest supervisor. I am grateful to you for the all the time, support and motivation throughout my PhD journey. I would like to thank my co-supervisor Prof Gerald Münch for his professional and scientific guidance throughout my journey. I would like to thank my co-supervisor Dr Garry Niedermayer for his help in breeding the mice and genotyping. I'm also thankful to Dr Andy Liang and Dr Alejandra Rangel for their help with tissue processing, precious advises and kindness. I would like to thank my fellow PhD student, Rustam Asgarov who monitored and fed the Longvida fed cohorts of mice weekly throughout the duration of the feeding experiment.

I also wish to thank the Graduate Research Office, here at Western Sydney University, for the award of postgraduate scholarship, the School of Medicine staff for their kind academic support and to the animal facility staff Miss Ashleigh Deschamps and Miss Nikola Mills for their work and support. I would also like to thank Indena S.P.A, Italy for the project grant.

I would like to thank the friendships and support from all the Pharmacology lab members, Dr Ritesh Raju, Dr Afia Akhtar, Sualiha Afzal, Dr Orsolya Kekesi, Madhuri Venigalla, Dr Karthik Dhananjyan, Ahilya Singh and my other old friends overseas.

I would like to thank my wife for her patience and mental support during these three years journey. Lastly, I wish to thank my parents and my all family members for their limitless moral support.

Table of Contents

List of Abbreviations

AD = Alzheimer's disease;

ROS = Reactive oxygen species;

TNF-α = Tumor necrosis factor-alpha;

IL6 = Interleukin-6;

LPS = Lipopolysaccharide;

COX-2 = Cyclooxygenase-2;

iNOS = Inducible nitric oxide synthase;

STATs = Signal transducers and activators of transcription;

Aβ = Amyloid-β;

TNFR1 = Tumor necrosis factor receptor 1;

TLRs = Toll-like receptors;

MAPK= mitogen-activated protein kinase;

JNK= c-Jun N-terminal kinase;

STZ= streptozotocin;

NF-κB = Nuclear factor kappa B;

AP-1= Activator protein 1;

APP23= Amyloid precursor protein 23

GFAP-IL6 = Glial fibrillary acidic protein- Interleukin-6;

NSAIDs = Nonsteroidal anti-inflammatory drugs;

CSAIDs =cytokine suppressive anti-inflammatory drugs;

FKN = Fractalkine;

IFNs = Interferons;

VCAM-1 = Vascular cell adhesion molecule-1;

ICAM-1 = Intracellular cell adhesion molecule-1;

gp130 = Glycoprotein 130;

MAPK = Mitogen-activated protein kinase;

PC = Phosphatidylcholine.

MCP= Meriva curcumin phytosome

SLCP= Solid lipid curcumin particle

LC= Longvida curcumin

List of the figures

List of the tables

Abstract

Neuroinflammation is a pathophysiological process present in a number of neurodegenerative disorders, including following acute insults such as stroke, traumatic brain injury including chronic traumatic encephalopathy as well as age-related CNS disorders such as Huntington's disease, Parkinson's disease and Alzheimer's disease (AD). Although there is still much debate over the initial trigger for these neurodegenerative disorders, neuroinflammation appears to be a major contributor, and therefore anti-inflammatory drugs including cytokine suppressive anti-inflammatory drugs (CSAIDs) might be promising therapeutic options to limit neuroinflammation, neurodegeneration and therefore improve the clinical outcome. One of the most promising CSAIDs is curcumin, which modulates the activity of several transcription factors (e.g., STAT, NF-κB, AP-1), most likely by interfering with upstream pro-inflammatory signaling pathways. Curcumin is a potent CSAID, but is not soluble in water and oily solvents like other polyphenols but soluble in methanol and ethanol, and degrades at low PH, it has low solubility and bioavailability *in vivo*. In order to increase its bioavailability, a variety of curcumin preparations have been designed, which lead to increased bioavailability, with the goal to achieve therapeutic concentrations in the brain.

The aim of this thesis was to investigate the effect of two different formulations of curcumin, Meriva curcumin phytosome (MCP) and Longvida curcumin (LC) in GFAP-IL6 mice, a model of chronic microglial activation. MCP preparations were fed for short term (one month) in three doses (140mg/kg bw, 70mg/kg bw and 35mg/kg bw whereas LC was fed long term (6 months) at a dose of 500ppm.

The following chapters will display the experiments undertaken to investigate the anti-inflammatory effects of these two curcumin formulations in the brain

The first experimental chapter focused on the effect of MCP on microglial and astroglial cells using stereology. The hippocampus of GFAP-IL6 mice fed with normal food had 438,550 ± 29,717 Iba-1$^+$ microglia, 147,803 ± 46,723 TSPO$^+$ microglia and 530,374 ± 30,447 GFAP$^+$ astrocytes, which was significantly higher than that of the WT mice [(175,192 ± 12,098), (474,7 ± 386,6), (169,908 ± 17,046)]. In the cerebellum, GPAP-IL6 mice had 1025,205 ± 104,467 Iba-1$^+$ microglia and 369,963 ± 152,991 TSPO$^+$ microglia, which was significantly higher than that

of WT mice [(154,058 ± 12,871), (12,402 ± 8,820)]. The main outcome was, all three doses of MCP significantly reduced the number of Iba-1^+ microglia in the cerebellum and the hippocampus and $GFAP^+$ astrocytes in the hippocampus with the high dose of MCP resulting in the most significant decrease.

The second experimental chapter investigated the effect of MCP on the morphology of microglial and astroglial cells. In the hippocampus, the Iba-1^+ microglial cells of GFAP-IL6 mice had significantly larger soma areas (66.36 ± 22.63μm^2), soma perimeters (33.93 ± 8.18μm) and more processes (5.62 ± 1.84) than those of WT mice [soma area (30.005 ± 13.93μm^2), soma perimeter (20.63 ± 5.50μm) and number of processes (3.66 ± 1.36)]. Whereas, in the cerebellum, microglial cells of GFAP-IL6 mice fed with normal food displayed significantly larger soma areas (66.64 ± 12.62) and soma perimeters (33.3 ± 2.84) as compared to those of WT mice [microglial soma area (30.03 ± 8.64) and soma perimeter (20.55 ± 0.28)]. The astrocytes in the GFAP-IL6 normal food fed mice had significantly larger convex area (1247.74 ± 371.77μm^2), convex perimeter (142.27 ± 26.27μm), dendritic length (224.35 ± 66.24μm), and number of nodes (7.33 ± 2.49), when compared to astrocytes of WT mice [convex area (601.93 ± 201.46 μm^2), convex perimeter (95.04 ± 27.79 μm), dendritic length (107.68 ± 29.17 μm) and number of nodes (4.68 ± 1.0)]. The key finding was that the 140mg/kg dose of MCP significantly reduced the de-ramification and aggregation of microglial cells in GFAP-IL6 mice. In addition, the high and medium dose of MCP significantly decreased the dendritic length of activated astrocytes in the hippocampus and reversed the astrocytes activation. The third and fourth experimental chapters focused on the impact of long term feeding of LC on microglial and astroglial cells stereology and morphology. The hippocampus of WT mice fed with normal food had 184,706 ± 19,037 Iba-1^+ microglia, 6,626 ± 3,952 $TSPO^+$ microglia and 211,968 ± 11,730 $GFAP^+$ astrocytes which was significantly increased in GFAP-IL6 mice normal food fed mice [383,588 ± 12,253 Iba-1^+ microglia, 236, 098 ± 28,005 $TSPO^+$ microglia and $GFAP^+$ astrocytes]. Whereas, in cerebellum, the wild type mice had 156,454 ± 33,721 Iba-1^+ microglia and 18,108 ± 2,933 $TSPO^+$ microglia, which was significantly increased in GFAP-IL6 mice [847,456 ± 46,120 Iba-1^+ microglia, 364,942 ± 28,577 $TSPO^+$ microglia]. The key findings were that LC significantly reduced Iba-1^+ microglia and $GFAP^+$ astrocytes the hippocampus while it slightly reduced the Iba-1^+ microglia in the cerebellum and $TSPO^+$ microglia in both cerebellum and hippocampus. Furthermore, in the hippocampus, Iba-1^+ microglial cells of normal fed GFAP-IL6

mice had significantly larger soma areas (57.25 ± 4.03μm^2), small convex areas (1035.60 ± 79.12μm^2) and convex perimeter (127.68 ± 4.39μm) than those of WT [soma areas (42.57 ± 3.82μm^2), convex areas (1535.63 ± 139.68μm^2) and convex perimeter (155.83 ± 6.11μm)]. Similarly, in cerebellum, Iba-1$^+$ microglial cells of GFAP-IL6 mice normal fed had significantly large soma area (77.68±7.89μm^2), soma perimeter (37.21±2.44μm) and small convex area (1087.96±150μm^2), convex perimeter (137.57±9.45μm) ($p < 0.026$) than those of the wild type non-fed mice [soma area (38.82 ± 2.80μm^2), soma perimeter (24.10 ± 0.82μm) and small convex area (1750.71 ± 148.98μm^2), convex perimeter (171.42 ± 7.98μm). Also, the astrocytes in the GFAP-IL6 normal-diet mice had a significantly larger dendritic length (275 ± 17.8μm), a number of processes (6.06 ± 0.51), convex area (1418 ± 128.3μm^2), convex perimeter (147.9 ± 6.01μm) and a number of nodes (7.62 ± 0.77) compared to the wild types. The LC significantly downregulated some of the morphological features of activated microglia and astrocytes and reversed the activation of both. Overall, our results suggest that the high dose MCP and LC formulation have the potential to overcome the chronic neuroinflammation and glial cells activation in GFAP-IL6 mice.

1. General Introduction

1.1. Neuroinflammation and neuroinflammatory cytokines

Inflammation is a protective reponse of the living tissues to injury, foreign bodies or trauma. Neuroinflammation is triggered by the activation of microglia and astrocytes that ultimately produce pro-inflammatory cytokines and neurotoxic factors, such as reactive oxidative species (ROS) leading to neuronal damage and the subsequent cognitive deficits (Agostinho, Cunha, and Oliveira 2010; Dantzer et al. 2008). Therefore, pro-inflammatory cytokines and oxidative stress could be associated with memory impairment and other cognitive deficits as manifested by neurodegenerative disorders like dementia and AD (Guerreiro et al. 2007).

Chronic neuroinflammation is now thought to be one the cause of AD, the most common neurodegenerative disease, characterized by senile plaques composed of amyloid-β (Aβ) peptide, neurofibrillary tangles, neuronal loss and neuroinflammation (Walsh and Selkoe 2004). Amyloid-β (Aβ) deposition in the brain and amyloid-β induced oxidative stress have been considered to play a vital role in AD pathogenesis (Swomley and Butterfield 2015; Walsh et al. 2002; Walsh and Selkoe 2004), but it has become more and more doubtful whether Aβ plaques and neurofibrillary tangles are actually causative factors for AD or biomarkers of a stressed and diseased brain. Recent studies have demonstrated that Aβ plaques accumulation in the brain poorly correlates with the progression and severity of dementia in AD (Davis and Laroche 2003). Moreover, studies on transgenic animals (APP mutated) showed widespread Aβ plaque deposition in the brain but only slight cognitive deficits in these mice (Braak and Braak 1998; Davis and Laroche 2003).

A number of studies of post-mortem human brain tissue have reported that the activation of the inflammatory processes such as activated microglia and astrocytes is also observed early stages of AD patients (Akiyama et al. 2000; Meda et al. 1995). Upon activation, microglia cells secrete various inflammatory mediators including cytokines such as tumor necrosis factor (TNF), interleukin (IL)-1β, IL-α, IL-6 and chemokines that promote the inflammatory state. Since inflammation is a defense mechanism, it activates the microglia and may enhance the amyloid β clearance (Meda, Baron, and Scarlato 2001; Morgan et al. 2014). However, various inflammatory mediators such as IL-1β, IL-6, and TNFα released upon activation of microglia may lead to brain damage (Meda, Baron, and Scarlato 2001; Tan and Seshadri 2010). Under

normal conditions, this process is monitored by immune cells which are recruited to the inflammatory site and remove the external stimulus/pathogen with subsequent resolution of the inflammatory response. In neurodegenerative diseases like AD, Aβ deposition and neurofibrillary tangles containing hyper-phosphorylated tau protein dysregulate this immune process. As a result, the recruited microglia and astrocytes are unable to clear the deposited Aβ within the inflammation site but to initiate excessive production of pro-inflammatory cytokines and chemokines (Heneka et al. 2015; Heneka, Kummer, and Latz 2014). Recent studies further supported the link between AD and the inflammatory state which is characterized by an increased level of cytokines (IL-1β, IL-6, TNF-α, TGF-β, and IL-18) in the peripheral blood stream (Swardfager et al. 2010). He P *et al* studied the effect of tumor necrosis factor receptor 1 (TNFR1) in APP23 transgenic mice and confirmed that the deletion of TNFR1 in APP23 transgenic mice leads to decrease in Aβ level in the brain and amelioration of cognitive deficits (He et al. 2007). Similarly, cytokines like IL-1α and IL-1β increase the APP level-up to 6-folds in primary human astrocytes and to 15-fold in human astrocytoma cells (Rogers et al. 1999).

Cytokines are small (~5–20 kDa) secreted proteins by diverse types of immune cells like monocytes and macrophages (microglia and astrocytes) at the sites of inflammation. The key functions of cytokines are the regulation of T-cell differentiation, cell proliferation, and responses against inflammation and T-cell differentiation from undifferentiated cells (Steinman 2007). Interleukins (ILs), TNFs, interferons (IFNs), colony stimulating factors (CSFs), and certain growth factors are in the same class of these regulatory proteins (Meager 2004). The activated macrophages produce pro-inflammatory cytokines that are involved in inflammatory responses (Zhang and An 2007). Similarly, activated astrocytes also produce pro-inflammatory cytokines and ROS intermediates in the central nervous system (Farina, Aloisi, and Meinl 2007; Hirsch and Hunot 2009). In stress conditions induced by microbial infection, a systemic body response is activated, which helps to fight against microbial invasion. This systemic response is characterized by pyrexia, leukocytosis, and changes in the balance of various proteins in the body. The most prominent pro-inflammatory cytokines produced to counteract the infections are TNF-α, IL-1β, and IL-6 (Gabay and Kushner 1999). IL-4, IL-10, IL-11, IL-13, and IL-1 receptor antagonists act as anti-inflammatory cytokines, whereas IL-6 and some of the growth factors are included in either anti-inflammatory or pro-inflammatory class of cytokines.

1.2. The role of microglia in neuroinflammation

Microglia demonstrate a certain population of the immune cells, found extensively in the CNS (Kettenmann, Kirchhoff, and Verkhratsky 2013). Apart from surveillance of the brain microenvironment, recent studies in microglial functions have found that microglia helps in the formation of synapses (Paolicelli et al. 2011), regulates neurogenesis (Sierra et al. 2010) and contains receptors which respond to different neuronal assaults and help to maintain the homeostasis (Pocock and Kettenmann 2007). Under normal physiological conditions, microglia were designated "resting" while the reactive morphology was termed "activated." In normal situations, microglial shows delicate branched processes oriented radially to a small elliptical soma. In diseased tissue, microglias appear quite different, with enlarged cell bodies, shortened and fewer processes and, a phagocytic appearance. Exposure of microglial cells *in vitro* to stimuli such as apoptotic cells, lipopolysaccharide, inflammatory cytokines or aggregated proteinsm, retract processes and, in response to appropriate stimuli, secreted factors typical of polarized macrophages (Ransohoff 2016). Ionized calcium binding adaptor molecule 1 (Iba1) is a microglial cell specific marker. It binds to fimbrin and helps to participate in membrane ruffling and phagocytosis in activated microglia (Ohsawa et al. 2004). Also, the mitochondrial translocator protein 18 kDa (TSPO) protein is observed to be expressed in the activated microglia (Betlazar et al. 2018). Numerous studies have shown that TSPO in the mitochondria of microglia is upregulated upon injury or progressive disease. However, it has long been reported that a low-level TSPO expression also occurs in the normal healthy (Liu et al. 2014). Neuroinflammation or aging may lead to changes in microglial number and morphology which often results in a decrease in microglial ability to respond to neuronal threats (Hefendehl et al. 2014). Therefore, different types of methods have been used to estimate their numbers. One of the studies used Smith and Guttman demonstrated a stereological method for estimating total length (*L)* and total length density (L_V) on random intersections with a two-dimensional sampling probe for linear objects in arbitrary tissue sections, found that microglia number in the hippocampus increased with age in female WT mice (Mouton et al. 2002). A recent study performed on chronic neuroinflammation mouse model (GFAP-IL6) and WT mice in our lab used stereological investigator (MBF) to investigate the microglial number. The study found that the microglial number significantly increased in the cerebellum region in four different age

groups (3,6,14 and 22 months) in GFAP-IL6 mice compared to WT mice using unbiased stereology (Gyengesi et al. 2019).

In situations of neuroinflammation or after injury, a stepwise activation and de-ramification of microglia have been observed (Davis, Foster, and Thomas 1994). The morphology of microglia is considered one of its major characteristics. According to several studies, the morphology of the microglia is not the same through the brain but they have different morphological shapes according to the areas in the brain. Moreover, one study has reported that the morphology of microglial cells was ramified in all cerebellar lobules of both young and adult mice but showed different sizes and ramification patterns in the different histological layers (Vela et al. 1995). Therefore, they have been classified into three subgroup compact, longitudinally branched and radially branched (Lawson et al. 1990). Several studies have reported that changes to the microenvironment of the brain, stress, injury to the brain and neuroinflammation can affect the structural remodeling of the ramified microglia (Tremblay, Lowery, and Majewska 2010). A recent study has suggested that microglia adopt different morphological structural characteristics after injury compared to the uninjured brain (Yamada and Jinno 2013). In normal circumstances, the resting microglia are characterized by small cell body and shorter and thick processes whereas, in the neuroinflammatory situation, ramified microglia are activated characterized by swollen cell body and shorter, thick processes, often exhibit rod-shape or amoeboid-like morphologies (Davis, Foster, and Thomas 1994).

1.3. The role of astrocytes in neuroinflammation

Astrocytes have an important role in brain homeostasis and it clear the metabolic waste from the brain (Iliff et al. 2012). It modulates the neuronal activity, potassium buffering and maintains the endothelial tight junctions (Parpura et al. 1994; Ballabh, Braun, and Nedergaard 2004; Iliff et al. 2012). Astrocytes provide structural and functional support neurons. They are activated (reactive) in response to different pathological assaults to CNS, such as injury, trauma, growth of a tumor, or neuroinflammation which is termed as “reactive gliosis” (**Fig 1**) (Pekny and Nilsson 2005). Previous few studies have quantified the number of astrocytes in adult murine CNS but these were based on assumptions to estimate the number per unit area. These studies have

reported an increase in astrocyte density in aged mice (Bronson, Lipman, and Harrison 1993; Mandybur, Ormsby, and Zemlan 1989; Sturrock 1980). One of the studies performed in the epilepsy model reported that aged rats present an increase in the expression of $GFAP^+$ astrocytes 26 days after neurodegeneration induced by intracerebroventricular kainite (KA) administration (Abdel-Rahman, Rao, and Shetty 2004).

The morphology of astrocytes is considered to be an important factor for their functions (Gulbransen and Sharkey 2012). Astrocytes are classified based on morphology such as soma size, the number, and thickness of processes, length of processes into type I, II and III. Type I astrocytes have small soma and short processes, type II astrocytes have a bipolar shape and long processes. Type III astrocytes are star shape with long processes (Gulbransen and Sharkey 2012; Şovrea and Boşca 2013). Astrocytes are activated in response to many neuropathological situations which is characterized by high expression of GFAP protein, and an increase in number and length of $GFAP^+$ processes. These findings have been interpreted as cellular hypertrophy (Kimelberg and Norenberg 1989).

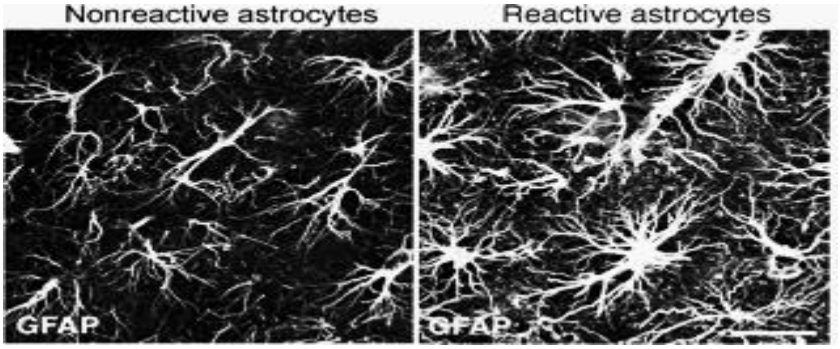

Figure 1. Entorhinal cortex lesion triggers reactive gliosis in the hippocampus. Unilateral entorhinal cortex lesion triggers astrocyte activation in the outer and middle molecular layer of the ipsilateral dentate gyrus of the hippocampus (Wilhelmsson et al. 2006)

A study conducted in Friend Virus B NIH Jackson (Fvb/n) mice, in which the mice were exposed to contextual fear condition, and checked for morphological changes in astrocytes. One hour after fear conditioning, astrocytes exhibited cellular hypertrophy with an increased number and length of processes which differed from the typical resting or reactive state (Choi et al. 2016). One of the studies performed on the human brain to compare morphometric analyses of

protoplasmic and fibrous astrocytes in Golgi-stained postmortem anterior cingulate cortex (ACC) samples from depressed suicides and non-psychiatric controls. The study found some significant differences between depressed and control groups such as a number of astrocytes processes, nodes, and spines that could reflect a state of chronic inflammation affecting the white matter in depression and suicide (Torres-Platas et al. 2011).

1.4. Acute and chronic neuroinflammatory models in rodents

Neuroinflammation is considered as an important component in the development of neurodegenerative diseases due to its presence in all neurodegenerative diseases along with reactive glial cells (Glass et al. 2010). To further investigate the role of neuroinflammation in neurodegenerative diseases, a number of rodent models have been used for the induction of chronic neuroinflammation. It includes toxin-induced models such as lipopolysaccharide (LPS)-induced neuroinflammatory model, neurotoxin-induced models including colchicine-induced neuroinflammation, okadaic acid-induced neuroinflammation, and Streptozotocin-induced neuroinflammation. Apart from these, genetically manipulated models or transgenic models such as anti-nerve growth factor (NGF) transgenic models, IL-1β and IL-6 overexpression models have been used (Nazem et al. 2015).

1.4.1 Toxin-induced models

A number of studies demonstrated that LPS activates microglia both *in vitro* and *in vivo*, which subsequently triggers the release of NOS and a series of pro-inflammatory cytokines such as interleukin (IL)-1β, IL-6, tumor necrosis factor (TNF)-α, and interferons (IFNs) (Palsson-McDermott and O'Neill 2004; Block, Zecca, and Hong 2007a). Studies have found that after systemic administration, LPS induced inflammation via the up-regulation of different pro-inflammatory cytokines and this lead to the activation of the inflammatory process which includes phosphorylation of P38 mitogen-activated protein kinase (MAPK) and c-Jun N-terminal kinase (JNK). Another study reported that LPS has a direct impact on IL-6 release from glial

cells and its signalling pathway. Incubation of glial cells with LPS for 2 h increased JAK2 and STAT1 phosphorylation, which ultimately results in the release of IL-6 and subsequent neuroinflammation (Minogue, Barrett, and Lynch 2012). LPS injection induced a potent activation of inflammatory signaling pathways in astrocytes and microglia in the brain through Toll-like receptor 4 (TLR4) and nuclear factor kappa B (NF-κB) signaling pathways (Noble et al. 2007). The activation of these pathways, in turn, results in the release of pro-inflammatory cytokines such as tumor necrosis factor alpha (TNF-α) and interleukin-1beta (IL-1β) (Kielian 2006). The production of these cytokines and ROS ultimately leads to neuronal loss in the hippocampus and the subsequent cognitive impairment (Henry et al. 2008). Recently, the GFAP-IL6 mouse model (transgenic model) is being used to induce neuroinflammation (Campbell et al. 1993b; Campbell, Hofer, and Pagenstecher 2010). In this model, the IL6 gene was inserted into the promoter region of the glial fibrillary acidic protein (GFAP) gene and as a result, IL6 was constantly expressed along with GFAP.

Similarly, another reliable model used in rodents is neurotoxin-induced neuroinflammation. Among them, the streptozotocin-induced neuroinflammatory model is considered as the most effective one. Glucosamine-nitrourea compound streptozotocin (STZ) damages beta cells of the pancreas, which makes it an animal model of diabetes mellitus (Like and Rossini 1976). Surprisingly, the STZ-induced diabetes model display impaired neuronal plasticity and learning deficits in rodents (Stranahan et al. 2008). A study performed in rats demonstrated that a single Intracerebroventricula (ICV) injection of 1 or 3 mg/ml STZ in rats has been proved to induce neuroinflammation, neurodegeneration, and atrophy of the septum in rats (Kraska et al. 2012). Moreover, STZ also contributes to ROS production, DNA damage, and apoptosis (Takasu et al. 1991; Murata et al. 1999).

D-galactose is a substance naturally exists in the body in a small amount. D-galactose model is also considered as a senescent model for age-related neurodegenerative diseases and neuroinflammation. One of the studies conducted on rats has used a chronic D-galactose model. D-galactose administered to the rats at dose of 50–500 mg/kg for 4–8 weeks showed a significant increase in inflammatory mediators e.g. COX-2, NOS2, IL-1β, and TNFα in D-galactose treated rats compared to those of the controls (Ullah et al. 2015)(Zhang and An 2007), hence attributed neuroinflammation, oxidative stress, and neurodegeneration (Zhang and An 2007).

1.4.2. Transgenic mouse models of neuroinflammation

A number of genetically modified animal models have been used to study acute and chronic neuroinflammatory responses as well as for AD research. These include the p25 transgenic model, the anti-nerve growth factor (NGF) transgenic model (AD11 model), the TGF-β-deficient model, the IL-1β overexpression model, and the GFAP-IL6 mouse model. Regarding the GFAP-IL6 mouse model, Campbell *et al* generated transgenic mice in which IL6 was overexpressed under the control of glial fibrillary acidic gene (GFAP) promoter and demonstrated the direct pathogenic impact of IL6 on inflammation and neurodegeneration of the CNS (Campbell et al. 1993b). In the GFAP-IL6 transgenic mice, an increase in the levels of IL-6 is observed in most brain areas including the cerebellum, striatum, hippocampus, hypothalamus, neocortex, and pons, which results in accelerated age-related structural changes observed in 3–6 months old mice, but not in the WT mice (Vallieres et al. 2002).

Most of the neurodegenerative diseases like AD are associated with inflammation characterized by activated microglia and astrocytes, increased cytokines and ROS production (Munch et al. 1998). Amyloid precursor protein (APP) transgenic mice that show dementia pathology do not show all features of AD. For example, these mice generally develop a much weaker neuroinflammatory phenotype and do not share the same features of pro-inflammation compared with human AD patients (Johnston, Boutin, and Allan 2011). Whereas, GFAP-IL6 mice represent clear and severe neurological abnormalities characterized by seizures, tremors, and ataxia. These transgenic mice also show a clear neuropathological sign that includes neuroinflammation, gliosis, angiogenesis, and neurodegeneration, more proximal to that of human neurodegenerative diseases like MCP and HIV-associated dementia (Campbell 1998) (**Fig 2**).

IL6 was discovered as an inflammatory cytokine involved in B cell differentiation (Kishimoto 2010). Later on, a landmark study revealed that IL6 is supposed to be involved in the pathogenesis of various pathologic states including infection, autoimmunity, neurodegeneration, neuroinflammation, and trauma (Spooren et al. 2011). Based on the fact that IL6 is involved in the physiologic and pathophysiologic processes of the central nervous system, GFAP-IL6 transgenic mice were generated to explore the neuropathological impact of IL6 overexpression. In this model, the mouse shows localized neuroinflammatory reaction and this might be

associated with a variety of neurological deficits manifested by various neurological disorders (Campbell, Hofer, and Pagenstecher 2010). Therefore, the GFAP-IL-6 animal model is a suitable animal model for studying neuroinflammation related neurodegenerative disorders (Campbell 1998).

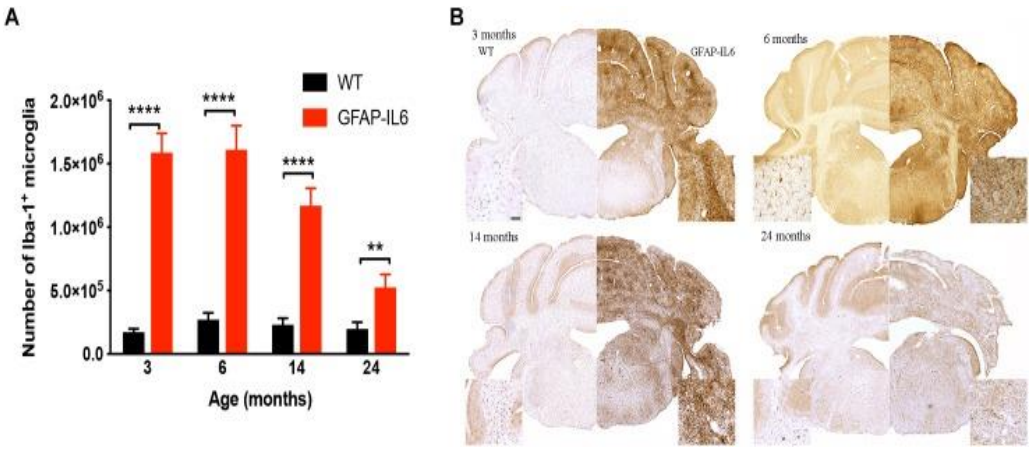

Figure 2. **Activation of microglia (Iba-1) increased in the cerebellum of GFAP-IL-6 mice with the passage of age** (Gyengesi et al. 2019).

1.4.3. Interleukin-6 (IL-6)

IL-6 is a four-helical protein consisting of 184 amino acids. In the early 1980s, IL-6 was discovered as an inflammatory factor involved in B cell differentiation (Spooren et al. 2011). For more than two decades, IL-6 has been known to have a prominent role in stimulating the final maturation of B cells to antibody-producing cells (Hirano et al. 1986). Researchers claimed that IL-6 is involved in the pathogenesis of various pathologic states including infection, autoimmunity, trauma, acute phase response, liver regeneration, metabolic processes, gliogenesis and neurodegeneration (Spooren et al. 2011). Similarly, IL-6 expression is impaired in different diseases like atherosclerosis, asthma, rheumatoid arthritis, diabetes mellitus, cancers, and in different neurological and neuroinflammatory disorders (Hirano et al. 1990). In brain inflammation, there is activation of brain immune cells like microglia and astrocytes. In response to neuroinflammation, cytokines, chemokines, prostaglandins and reactive oxygen species (ROS)

are produced, which eventually leads to a number of neurodegenerative diseases such as AD and epilepsy (Wyss-Coray 2006).

The source of IL-6 production is very diverse but astrocytes are considered to be the main CNS producers of IL-6. Neurotransmitters (e.g. norepinephrine), neuropeptides (e.g. vasoactive intestinal peptide, substance P), inflammatory cytokines (e.g. TNF-α, IL-1β), microbial pathogens (e.g. LPS), and IL-6 itself are the stimuli that trigger the production of IL-6 (Van Wagoner and Benveniste 1999; Gruol and Nelson 1997; Munoz-Fernandez and Fresno 1998). A number of studies have reported that IL-6 in the CNS is produced by the neuron as well. Therefore, astrocytes are not the only source of IL-6 (Streit et al. 2000).

The function of IL-6 is variable and multipolar. Researchers claimed that IL-6 exerts both beneficial and destructive effects on the brain. (Loddick, Turnbull, and Rothwell 1998) reported the beneficial role of IL-6 in neuronal survival, protection, and differentiation, similar to what has been shown before that IL-6 increased survival and differentiation of primary neurons (Hama et al. 1991; Satoh et al. 1988). It has been reported that the injection of IL-6 into the ischemic region significantly reduced brain damage. On the other hand, several neurologists have correlated IL-6 with neurological disorders (Loddick, Turnbull, and Rothwell 1998). To support the neurotoxic effect of IL-6, Campbell *et al*, generated transgenic mice in which the IL-6 was overexpressed under the control of the promotor of glial fibrillary acidic protein (GFAP) gene (Campbell et al. 1993b). The GFAP-IL-6 transgenic mice have a high level of IL-6 protein expression characterized by a number of neurological diseases such as neurodegeneration, ataxia, seizure, tremor, and neuroinflammation. Furthermore, performed the immunolabeling of the brain sections with Anti-alpha 1 Antichymotrypsin (anti-ACT), showed an increase expression in the hippocampus and cerebellar white matter of GFAP-IL-6 mice compared to the control mice. As ACT production shoots up in AD and other neurological disorders, this study confirmed the claim that overexpression of IL-6 is a prominent cause of neurological diseases (Campbell et al. 1993b).

Cytokines have their own effect on the blood-brain barrier (BBB). IL-6 plays a prominent role in the maintenance of the blood-brain barrier integrity. In normal conditions, IL-6 acts as an anti-inflammatory cytokine, helping to maintain blood-brain barrier integrity. In neuroinflammatory conditions, IL-6 block TNF-α-induced vascular cell adhesion molecule-1 (VCAM-1)

upregulation and inhibits TNF-α-induced intracellular adhesion molecule-1 (ICAM-1) expression in primary astrocytes, and ultimately, prevents the detrimental effect of TNF-α (Shrikant et al. 1995). Another study claimed that the increased level of IL-6 in the brain led to a proliferation of astrocytes and endothelial cells, which ultimately resulted in BBB breakdown (Campbell et al. 1994). Brett *et al* described that BBB never developed in IL-6 transgenic mice while in normal mice the BBB develops between 7 and 14 days. They studied two types of transgenic animals and found that the BBB was partially permeable until one month after birth in the low IL6 expression mice and complete absence of BBB was observed in the high IL6 expression animals and they only survived for 6 months (Brett et al. 1995). It was also reported that axonal degeneration, macrophage accumulation, astrocytic foot process vacuolation, and gliosis widely spread in low and high expression IL-6 mice at the age of 6 and 12 months, respectively, compared to the control mice. These results clearly suggest the role of astrocytes and the effect of IL-6 overproduction on BBB breakdown and other neurophysiological functions (Brett et al. 1995).

1.4.4. IL-6 signaling pathway and its pathogenic action in the brain

IL-6 acts via interleukin receptors (membrane-bound IL-6Rα or soluble (s) IL-6Rα). The existence of interleukin receptors was discovered for the first time in urine (Novick et al. 1989) and later in the plasma (Honda et al. 1992). IL-6 belongs to a cytokine family in which almost all the cytokines have a common signal transducer, namely gp130 (glycoprotein 130/ CD130). Due to the presence of two types of IL-6 receptors, IL-6 mediates two types of cellular mechanisms: classic and trans-signaling pathways. In the classic signaling pathway, IL-6 binds to a specific transmembrane receptor termed IL-6Rα and forms a complex with gp130 protein, which induces homodimerization of gp130 (Campbell et al. 2014). The soluble form of the IL-6Rα (sIL-6R) is generated by cleavage of the ectodomain of the transmembrane IL-6Rα (Lust et al. 1992). In both types of pathways, dimerization leads to activation of the associated Janus kinases (JAK-1 and JAK-2), which phosphorylates specific conserved tyrosine residues in the cytoplasmic domains of gp130. The phosphorylation of tyrosine residues leads to activation and translocation

of STATs to the nucleus where they modulate gene transcription. Therefore, this is also termed the JAK/STAT signaling pathway (**Fig. 3**) (Heinrich et al. 2003).

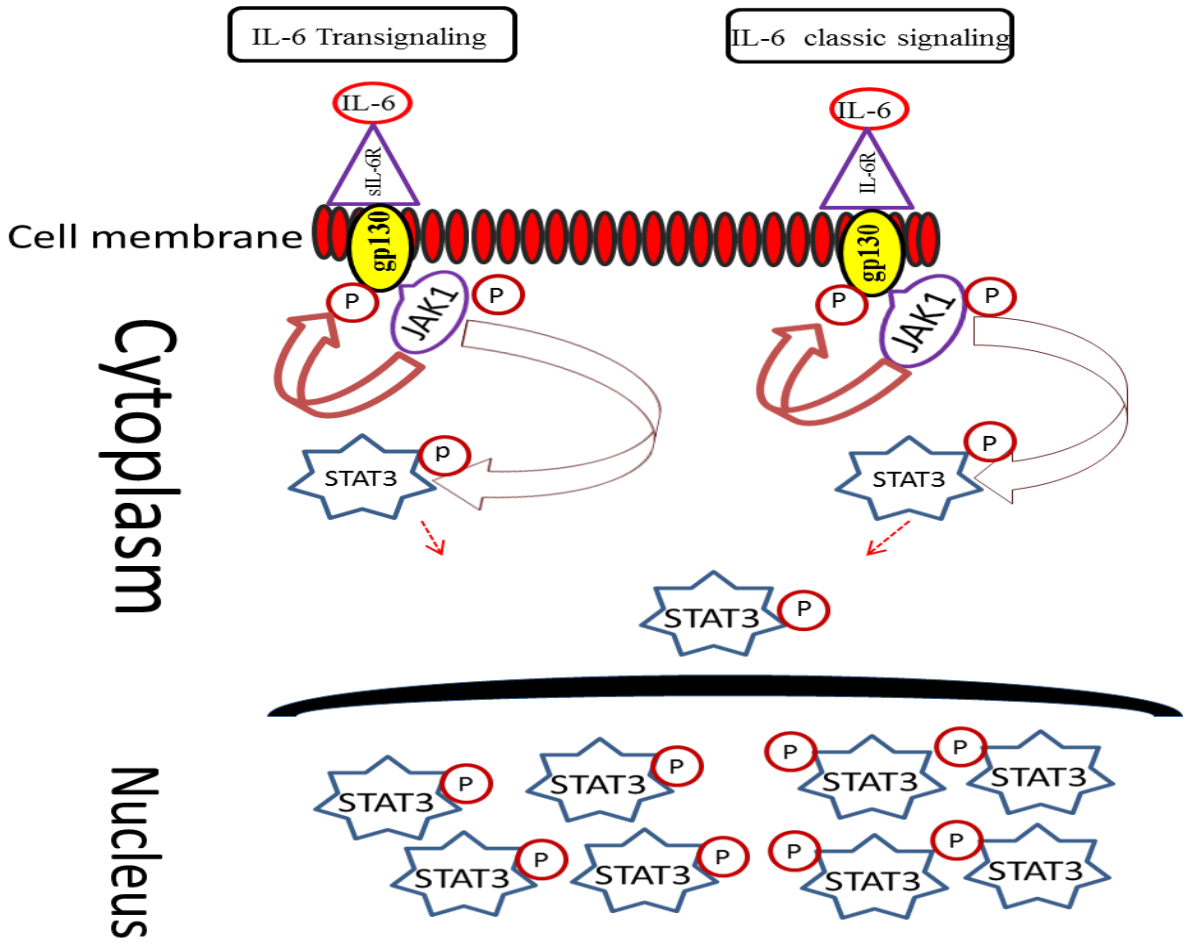

Figure 3. IL-6 Signalling mechanisms: IL-6 binds to either non-transducing IL-6R or sIL-6R, which causes homodimerization of the transducer protein gp130. This leads to activate the association of JAKs and phosphorylation designated tyrosine residues in the cytoplasmic domains of gp130. After phosphorylation, STATs form homodimers, translocate to the nucleus and finally switch on the gene transcription. [Adopted from (Spooren et al. 2011) (Ullah et al. 2017)].

Studies have classified trans-signaling as pro-inflammatory and classic signaling as an anti-inflammatory pathway on the bases of their action (Campbell et al. 2014). A study performed on

the trans-signaling mechanism of IL-6 and claimed that the pro-inflammatory activity of IL-6/sIL-6R is blocked by a naturally occurring, soluble form of gp130 (sgp130). By generating single GFAP-IL6 transgenic mice and bigenic GFAP-IL-6/sgp130 transgenic mice, they found that blockade of trans-signaling by sgp130 protein significantly attenuates Serpina3n gene expression, angiogenesis, and blood-brain barrier leakage. In GFAP-IL6/ sgp130 mice degenerative changes in the cerebellum, blood vessels, and hippocampal neurogenesis were significantly decreased compared to those of GFAP-IL6 mice. As their previous study reported that neurodegeneration developed in the cerebellum of the GFAP-IL6 mice (Campbell et al. 1993) and the signaling pathway of IL-6 was mediated through the activation of STAT-3 phosphorylation. In bigenic mice, sgp130 was able to block IL-6 trans-signaling and hence, pY-STAT3 activation was reduced 2.5 folds in the GFAP-IL6/sgp130 bigenic mice compared to GFAP-IL6 mice (Campbell et al. 2014).

1.4.5. IL-6 signalling and microglial activation.

Interleukin-6 (IL-6) was originally identified as a B-cell differentiation factor (BSF-2) that induced the maturation of B cells into antibody-producing cells (Hirano et al. 1985). It is a unique cytokine that can act as both pro- and anti-inflammatory depending on the anatomical site and conditions under which it gets activated (Bobbo et al. 2019). There is very limited information about the direct role of IL-6 in the regulation of microglia in the literature. Stress situations or any kind of foreign insult lead to the activation of microglia which release cytokines, including IL-6, in addition to other chemokines and growth factors, in order to mitigate or prevent damage to the brain due to the insult. The relationship between microglia and IL-6 in the brain remains very unclear. The activation of IL6 in the brain occur due to different kinds of stimulus such as LPS, diet, trauma or neuroinflammation which leads to actiation of many signalling pathways (Mendes et al. 2018). LPS from the diet are recognized by TLR4 in microglial cells, increasing the production and release of several inflammatory cytokines including IL-6 (Milanski et al. 2009) whereas, neonatal overfeeding beginning early in life increases the TLR4 expression in the hypothalamus and the number of Iba-1 (microglia) positive cells, followed by increased expression of IL-6 (Ziko et al. 2014). Emerging shreds of evidence suggest that microglial IL-6 production is more strongly associated with the activation of P2Y

receptors (Shigemoto-Mogami et al. 2001). Several studies have reported that curcumin is able to inhibit the IL-6 signalling by inhibiting the phosphorylation and nuclear localization of STAT3, a well-known downstream mediator of IL-6 signalling (Devi et al. 2015)

1.5. Cytokine suppressive anti-inflammatory drugs (CSAIDs) as a potential therapeutic agent, molecular signalling and curcumin concentrations in the brain.

The pharmacotherapy of inflammatory conditions is based mainly on the use of non-steroidal anti-inflammatory drugs (NSAIDs). However, NSAIDs have limited anti-inflammatory action, as they are specific inhibitors of cyclooxygenases (COXs). Epidemiological studies suggest that current or former NSAID is significantly associated with reduced risk of AD compared with those who did not use NSAIDs. However, the ADAPT study results revealed that treatment for 1 – 3 years with naproxen or celecoxib did not protect against cognitive decline in older adults with a family history of AD (Breitner et al. 2011).

NSAIDs do not influence the production of pro-inflammatory cytokines such as IL1, IL6, TNF-α or nitric oxide produced by iNOS (Gunawardena et al. 2015). Therefore, drugs with a broader range of anti-inflammatory effects than NSAIDs may be more effective for the prevention and treatment of AD. One promising drug class in this respect might be cytokine suppressive anti-inflammatory drugs (CSAIDs) which target the pro-inflammatory AP1 and NF-κB signaling pathways and inhibit the expression of many pro-inflammatory cytokines in the low μM range (Zhang, Li, et al. 2013).

One of the most interesting CSAIDs is the main ingredient of the spice turmeric (*Curcuma longa*), curcumin. Curcumin has a broad cytokine-suppressive anti-inflammatory action, down-regulating the expression of cyclooxygenase-2 (COX-2), inducible nitric oxide synthase (iNOS), TNF-α, IL-1, -2, -6, -8, and -12. It inhibits IL-6 mediated signaling via inhibition of IL-6 induced STAT3 phosphorylation and consequent STAT3 nuclear translocation (Bharti, Donato, and Aggarwal 2003), and interferes with the first signaling steps downstream of the IL-6 receptor (“the inflammatory trigger”) in microglial activation (Ray and Lahiri 2009).

Numerous studies have reported that curcumin suppresses IL-6-induced STAT3 phosphorylation and IFN-alpha-induced STAT1 phosphorylation and promotes survival. A study performed in human multiple myeloma (MM) cells has reported that curcumin inhibited IL-6-induced STAT3 phosphorylation and consequent STAT3 nuclear translocation (Bharti, Donato, and Aggarwal 2003). Another study investigated the effect of curcumin on IL-6 induced expression in HuF cells, primary human fibroblast cells, and UIII cells, a rodent non-transformed decidual cell line. The study reported that curcumin inhibited the expression of gp130, a critical molecule in IL-6 signalling and inhibited phosphorylation and nuclear localization of STAT3, a well-known downstream mediator of IL-6 signalling (Devi et al. 2015). Curcumin targets numerous signalling pathways associated with neuroinflammation and related disorders. One of the studies reported that curcumin significantly reduced spatial memory deficit and promoted the function of cholinergic neurons in mice by the inhibition of NF-kappaB signalling pathways and enhanced transcription by PPAR-gamma (Liu et al. 2016). One study performed in the LPS mouse model has reported that curcumin inhibited the Toll-like receptor 4 (TLR4)-mediated downstream signalling and effectively lowered the production of inflammatory mediators (Youn et al. 2006). Curcumin has several potential receptors through which it gets into the cell. A study characterized the accumulation of curcumin in membrane structures of mammalian cancer cells (Ishikawa cells), derived from a human endometrial carcinoma, and HT-29 cells, derived from human colon adenocarcinoma. The results indicated that curcumin rapidly penetrates the plasma membrane of mammalian cells and binds to the membranes of the endoplasmic reticulum (Dempe, Pfeiffer, and Metzler 2007). Despite its various pharmacological and therapeutic activities, the instability of curcumin at physiological pH and its susceptibility to intestinal and hepatic metabolism have limited its therapeutic use. Although curcumin is well absorbed in glucuronidated and sulfated forms by the intestine and liver, which increases hydrophobicity, and therefore limits blood-brain barrier permeability and lowers bioavailability to the brain (Wang et al. 1997; Anand et al. 2007). However, free curcumin is membrane permeable because it is lipophilic and fulfills the Rule of 5 characteristics of blood-brain barrier permeable molecules. To decrease the glucuronidation of curcumin, the use of piperine has been recommended (Jager et al. 2014). To increase its stability and subsequent bioavailability, a number of different encapsulation approaches have been employed including the use of liposomal curcumin, including Longvida (LC) curcumin.

Several literature studies have reported that curcumin gets into the brain and can achieve a steady state concentration. One study conducted in the LPS mouse model has identified the concentration of curcumin in the mice brain and plasma. Curcumin was orally fed to mice 50 mg/kg dose, once daily for 2 consecutive days and then i.p. injected with 5 mg/kg LPS or vehicle. Two hours after LPS injection the mice were culled and the brain concentration of curcumin was 41.1 ± 6.7 ng/g and plasma contained very low concentrations of curcumin (8.2 ± 1.8 ng/g), with the sulphate and glucuronide metabolites being more abundant (67.0 ± 10.2 ng/ml and 453.2 ± 110.2 ng/ml, respectively) (Sorrenti et al. 2018). Another study performed in rats has localised the nanocurcumin formulation in the rat brain. Three different types of liposomal formulation were injected intravenously and one hour later, up to 0.5% of the injected material localized in the brain stem, the striatum, and the hippocampus with different accumulation and clearance rates using HPLC sensitive assay (Chiu et al. 2011). Pharmacokinetics of unmodified curcumin is unfavorable, and its bioavailability is low. However, highly bioavailable curcumin formulations (encapsulated in liposomes or micelles) such as LC (VS Corp) can achieve μM concentrations in the rodent brain (Begum et al. 2008a; Ma et al. 2013b). A study conducted in APPSw mice, have used a low (160 ppm) and a high dose of dietary curcumin (5000 ppm), which reported that the low and high doses of curcumin significantly lowered oxidized proteins and interleukin-1, the astrocytic marker GFAP was reduced, plaque formation was significantly decreased by 43-50% (Lim et al. 2001).

1.5.1. Origin and efficacy of curcumin

Turmeric spices have been a source of drug and traditional medicines since ancient times. They have been used for at least 2,500 years, mostly in Asian countries. They have derived from the dry rhizomes of plant *Curcuma longa* which belongs to the Zingiberaceae family or ginger family (Mathew and Pushpanath 2005). Turmeric is widely produced in India as well as in Pakistan, Bangladesh, China, Indonesia and South America (Norman 1991). The most active component of turmeric is curcumin, which constitutes up to 2–5% of the spice. Besides curcumin, turmeric may contain essential oils, carbohydrates, polyphenols, proteins, fat, minerals and moisture (Chattopadhyay et al. 2004). Turmeric is an effective traditional medicine and has

been used as a remedy to treat various disorders including rheumatism, body aches, skin diseases, wounds, intestinal worms, diarrhea, hepatic disorders, biliousness, urinary discharges, dyspepsia, inflammation, constipation, leukoderma, amenorrhea, and colic inflammation (Aggarwal, Surh, and Shishodia 2007). In addition to its traditional medicinal use, it has been used by the food industry as a flouring and coloring agent in soft drinks and beverages as well as Ayurveda medicine in oxidative stress, pyrexia and as an anti-inflammatory agent (Aggarwal, Surh, and Shishodia 2007).

Curcumin, a polyphenolic compound, has a yellow pigment and aromatic smell (Jayaprakasha, Jagan Mohan Rao, and Sakariah 2005). Recently, considerable attention has been drawn towards curcumin because of its numerous pharmacological applications including antioxidant, anti-inflammatory, antiviral, antibacterial activities as well as the therapeutic potential for cancer, AD and other neurological disorders (Goel, Kunnumakkara, and Aggarwal 2008; Goel and Aggarwal 2010). It has been reported that curcumin scavenges free radicals such as reactive oxygen species (ROS) and inhibits ROS-generating enzymes like xanthine dehydrogenase/oxidase and lipoxygenase/cyclooxygenase (Menon and Sudheer 2007). It was reported that curcumin has anti-carcinogenic, antibacterial, and anti-inflammatory activities (Anand et al. 2008). It inhibits TNF-α induced or IL-1-induced activation of NF-κB and decreases pro-inflammatory cytokines in cells (Singh and Aggarwal 1995).

1.5.2. Structure and chemistry of curcumin and curcuminoids

Curcumin is a bis-α, β-unsaturated β-diketone with a molecular weight of 368.38g/mol. Its chemical name is: (E, E)-1, 7-bis (4-hydroxy-3-methoxyphenyl)-1, 6-heptadiene-3, 5 dione) with a melting point of 179–183 °C. In 1815, Vogel and Pelletier purified curcumin from turmeric for the first time while its structure as diferuloylmethane was not established until 1910 (Milobedzka J 1910). Its chemical structure was confirmed in 1973 by Roughley and Whiting (Roughley and Whiting 1973). Turmeric contains a group of compounds called curcuminoids which make up 2% to 9% of turmeric. The group of curcuminoids includes three compounds named curcumin/diferuloylmethane, desmethoxycurcumin, and bisdemethoxycurcumin with a

proportion of approximately 77%, 18%, and 5% respectively (**Fig. 4**) (Basnet, Tho, and Skalko-Basnet 2010).

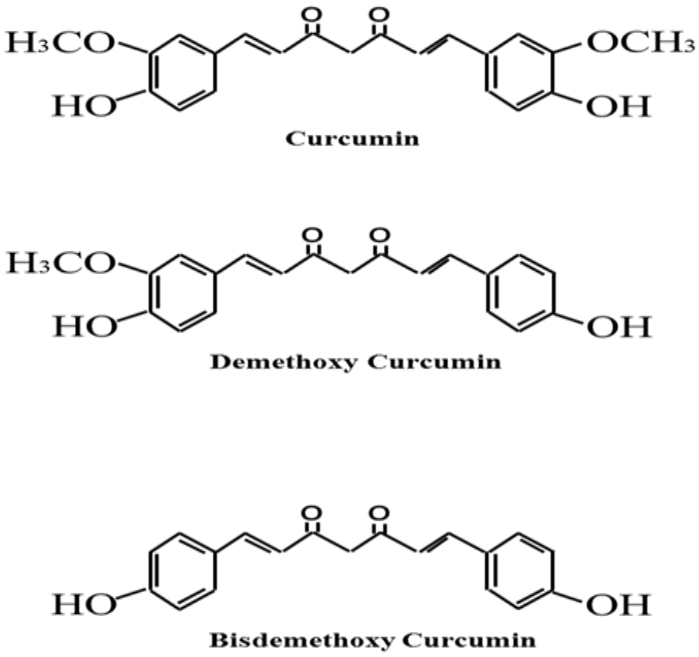

Figure 4. **Chemical Structure of three different curcuminoids adapted from** (Wilken et al. 2011)

As far as the structure of curcumin is concerned, it belongs to the diaryl hepatanoid class of compounds. It has a seven carbon chain with two aromatic rings attached at both ends. The two phenolic rings are linked via an aliphatic unsaturated heptene linker in the para-position that also contains β diketonic functionality on carbon-3 and -5 (Priyadarsini 2013). Curcumin probably exists in equilibrium between keto and enol tautomer. A number of studies have demonstrated that enolic- and ketonic-forms of curcumin interconvert in solution in a reversible manner (Payton, Sandusky, and Alworth 2007). Tautomerization of curcumin occurs under the influence of temperature, the polarity of the solvent, the substitution of the aromatic rings, and pH (Cornago et al. 2008). At pH 3-7, the curcumin molecules remain in bis-keto form and act as a potent proton donor but at pH > 8 the enolate form of the heptadienone chains predominates and it behaves as an electron donor (Wang et al. 1997). The enolate form of curcumin is found to have the radical scavenging ability which entitles curcumin to its antioxidant property (Sharma, Gescher, and Steward 2005).

1.5.3. Role of curcumin as an anti-inflammatory agent

Experiments have demonstrated that curcumin treatment reverses the activation of microglial cells in the brain by inhibiting the production of NO in the brain and decreases the secretion of pro-inflammatory cytokines such as IL1β, IL6, and TNF-α (Jung et al. 2006; Jin et al. 2007). It is well known that lipopolysaccharide (LPS) is able to induce iNOS in microglial cells of CNS. Studies showed that curcumin counteracts the LPS- induced cyclooxygenase-2 (COX2) by targeting different signaling pathways like NF-κB inhibition pathway, activator protein 1 (AP1), signal transducers and activators of transcription (STATs) (Kang et al. 2004; Kim et al. 2003).

Curcumin can attenuate IL6 induced neuroinflammation both *in vitro* and *in vivo*. Curcumin attenuates LPS induced neuroinflammation and cytokine production in BV2 microglia cell line (Cheng et al. 2001). In this study, BV2 microglia cells were incubated with curcumin (0, 5, 10, and 20 μM/L) in the presence or absence of LPS (0.5 μg/ mL). The level of cytokines (IL-1β, IL-6, and TNF-α) in the culture media was measured using ELISA. Interestingly, pre-treatment with curcumin resulted in a dose-dependent decrease in cytokine production (Cheng et al. 2001). Another study performed in Dalton's lymphoma (DL) mouse model also revealed the protective effect of curcumin against IL6 induced inflammation. They reported that the level of IL-6 in DL and DL+DMSO mice was up-regulated to double that of normal mice, treatment with curcumin significantly reduced the level of IL-6 to 65%, 53% and 71% of that of DL+DMSO mice with doses of 50, 100 and 150 mg/kg bw, respectively (Das and Vinayak 2014). The protective effect of curcumin against inflammatory cytokines has been reported by many researchers. A recent study reported that curcumin pre-treatment reverses or stops the secretion of TNF-α and IL6 by MPP+ treated astrocytes (Yu et al. 2016). Another study reported the effect of curcumin on LPS-stimulated microglia (BV2) cell line and the regulation of pro-inflammatory cytokines (IL-1β, IL-6, and TNF-α). Curcumin had no effect on the production of IL-1β, IL-6, and TNF-α in normal BV2 microglia, but decreased the cytokine production level in a dose-dependent manner in LPS-treated microglia (Jin et al. 2007).

In a study, curcumin was studied in a traumatic brain injury (TBI) model. Many activated TLR4-positive microglia/macrophages were observed post-trauma and various inflammatory mediators like interleukins and cytokines were found in the injured brain of TBI groups compared to the

control. Curcumin, administered at 100 mg/kg, significantly reduced the expression of cytokines and the number of activated microglia compared to the untreated group (Zhu et al. 2014). Similar results were observed in other animal models of neurological disorders like depression. Olfactory bulbectomy (OBX) is used to create a depression model by inducing changes in behavioral and biochemical actions in experimental subjects (Song and Leonard 2005). Levels of TNF-α and caspase 3 were raised in olfactory bulbectomized (OBX) rats compared to controls. Treatment with curcumin (100, 200 mg/kg) and piperine (20 mg/kg) significantly reduced the level of TNF-α and caspase 3 and this effect was much more effective than using curcumin or piperine alone (Rinwa, Kumar, and Garg 2013).

For neuroinflammation therapeutics, curcumin is a compound of choice compared to the α-tocopherol (vitamin E), a poor scavenger for NO-related oxidative and to nonsteroidal anti-inflammatory drugs (NSAIDs) that have adverse effects including gastric ulcer, liver, and kidney toxicity (Chan et al. 1998; Hanai et al. 2006). A couple of studies demonstrated that curcumin administration reverses neuroinflammation and attenuates cognitive impairment in AD models (Yang et al. 2005; Garcia-Alloza et al. 2007). Moreover, curcumin fed orally has been reported to be effective in animal models for conditions like oxidative stress, cancer, diabetes, atherosclerosis, arthritis, stroke, peripheral neuropathy, inflammatory bowel disease (Aggarwal, Surh, and Shishodia 2007).

Studies have shown that astrocytes and microglia play a pro-inflammatory role through toll-like receptor (TLRs) and the subsequent production of various inflammatory mediators including cytokines, chemokines, and reactive oxygen species (Farina, Aloisi, and Meinl 2007; Hirsch and Hunot 2009). Toll-like receptors (TLRs), a group of receptors (TLR2, TLR3, TLR4, and TLR9) present in immune cells like astrocytes and microglia (Bowman et al. 2003), are activated by exogenous stimuli or pathogens, leading to the activation of the intracellular signal pathways (Akira, Takeda, and Kaisho 2001; Zhang, Tang, et al. 2013). A recent study on curcumin reported that it decreases the level of pro-inflammatory cytokines and ROS in the brain, confirming the pro-inflammatory role of curcumin (Aggarwal, Gupta, and Sung 2013).

One of the other studies reported that fructose in the diet induces fractalkine (FKN) and modulates the inflammatory status of microglia via CX3CR1 in animal models of obesity through Toll-like receptor 4 (TLR4)/nuclear transcription factor κB (NF-κB) signaling pathway.

Curcumin treatment reverses the neuronal damage, microglial activation, neuroinflammation and downregulated FKN/CX3CR1 up-regulation in the neural network by decreasing the level of IL-1β, TNF-α, IL-6, and Iba1- a microglial marker in both hippocampus and hypothalamus of fructose-fed mice (Cardona et al. 2006).

1.5.4. Available curcumin formulations

Despite its multi neuroprotective properties, curcumin's use is limited due to its low brain bioavailability which attributes to its poor absorption, rapid metabolism, rapid systemic elimination, and limited blood-brain barrier (BBB) permeability (Tsai et al. 2011). The most challenging factor is its low water solubility (0.4μg/ml at normal pH). The solubility of curcumin is very sensitive to physiological pH (Tonnesen 1989, 2002). Preclinical studies on rodents and clinical studies on humans have reported low bioavailability of curcumin shown by the lower level of serum curcumin (50ng/ml) after feeding with 10-12 g/ml of orally administered curcumin (Vergoni et al. 2009). Many approaches have been applied to enhance the bioavailability of curcumin such as using the structural analogs of curcumin, the use of adjuvants like piperine and phospholipids. To cope with these limiting factors and to improve its bioavailability in the brain, biodegradable nanoparticle-mediated delivery of curcumin may be the best approach to increase its intracellular transport and prevent degradation (Tsai et al. 2011). A couple of recent studies suggest that delivery of an encapsulated compound of low aqueous solubility, poor absorption, rapid metabolism, and low BBB permeability is more effective than delivering parent compound, which yields a higher BBB permeability (Vergoni et al. 2009; Hoppe et al. 2013).

Several studies have compared raw curcumin and various curcumin formulations and reported the bioavailability of the curcumin formulations. A human study was conducted to quantify the plasma levels of free curcumin after dosing of a solid lipid curcumin particle (SLCP) formulation versus unformulated curcumin in healthy volunteers and osteosarcoma patients. Doses of 2, 3, and 4 g of SLCP were evaluated. Using a high-performance liquid chromatography method, the mean peak concentration of curcumin achieved from dosing 650 mg of SLCP was 22.43 ng/mL, whereas plasma curcumin from dosing an equal quantity of unformulated 95% curcuminoids extract was not detected (Gota et al. 2010). The molecular modification of MCP was designed

for human consumption and was proved to be more effective in humans in other studies, such as lecithin formulation (Meriva) and standardized curcuminoid mixture was investigated in a randomized, double-blind, crossover human study. The study investigated that the total curcuminoid absorption was about 29-fold higher for Meriva than for its corresponding unformulated curcuminoid mixture. This better plasma curcuminoid profile might underlie the clinical efficacy of Meriva at doses significantly lower than unformulated curcuminoid mixtures (Cuomo et al. 2011).

Table. 1 Available curcumin formulations

	Curcumin formulation	Company Name and Address	Type of Formulation/Dosage form	Composition	Dosage	Reference	Study Human/Animals	Cmax	Comments
1	Meriva®	Indena S.p.A. Italy	Phytosome	Curcumin (20%), hydroxypropyl methylcellulose and Calcium Citrate Laurate, Hypromellose (derived from cellulose) capsule, Leucine, Silicon Dioxide, Microcrystalline Cellulose & phytosome	MCP high & MCP low{200-300mg}	Cuomo et al.,2010	Human	538.0±130.7ng/ml 272.6± 68.52ng/ml	A randomized, double-blind, crossover study was carried out in nine volunteers by five (low-dose) or nine (high-dose) capsules of MCP
2	Longvida®	Verdure Sciences, USA.	Liposome	Curcumin (20%), Plant derived cellulose, soy lecithin, stearic acid (from vegetable), dextrin, ascorbyl palmitate (vitamin c),	80 mg/day for 4 weeks	DiSilvestro et al.,2012	Human	N.R	The study was conducted in healthy middle aged people (40–60 years old). Subjects were given either curcumin (N = 19) or placebo (N = 19)

				silicon dioxide and microcrystalline cellulose					
3	Curcumin C3 complex®	Sabinsa Corporation, Australia	Curcuminoids with BioPerine®	Curcuminoids (including: Bisdemethoxycurcumin – 2.2% to 6.5% Demethoxycurcumin – 15% to 19% Curcumin – 75% to 81%) BioPerine®† Black Pepper Standardized Extract (Piper nigrum)	Dose = 10 g (n = 6) Dose = 12 g (n = 6)	Shaiju K et al.,2008	Human	3.2±0.56 µg/ml 2.1±0.73 µg/ml	Twelve healthy human subjects 18 y of age or older, with normal organ function were recruited.Subjects included five males and seven females
4	Sabinsa C^3 complex®				Dose = 10 g Dose = 12 g	Vareed et al.,2014		2.3±0.56 µg/ml 1.7±0.73 µg/ml	This study was conducted in healthy human volunteers for 0.25-72 hours after a single oral dose.
5	Theracurmin®	Curcumin Rich™, USA	Capsules containing colloidal particles	Curcumin (10%) from turmeric *(Curcuma longa)* (rhizome)	150 mg and after an interval of two weeks 210 mg	Kanai et al.,2012	Human	150 mg = 189 ± 48 & 210 mg =275 ± 67	Six healthy human volunteers were recruited and received THERACURMIN at a single oral dose of 150 mg and after an interval of two weeks, the same subjects then received THERACURMIN at a single dose of 210 mg
6	Biocurcumax™BCM95®	DolCas Biotech ,USA	Capsules	Combination of curcuminoids (86%) plus essential oils (7-9%)	4×500 mg capsules	Antony et al., 2008	Human	456.88 ng/g	11 individuals, the study was performed in India, no information on diet except to avoid foods containing turmeric two days prior to the study date

7	NovaSOL® Curcumin	AQUANOVA AG (Darmstadt, Germany	Curcumin micelles (Capsules)	Curcumin, Polysorbate, Ascorbic Acid, Medium Chain Triglycerides	500mg	Schiborr et al., 2014	Human	3228±1408.2 nmol/l	Total 23 healthy subjects (13 women, 10 men) took, a single oral dose of 500 mg curcuminoids, micronized powder, or liquid micelles randomly. Blood and urine samples were collected for 24 h
8	Pure curcumin powder	Provided by the National Cancer Institute's Division of Cancer Prevention	Capsules	Curcumin powder	2 g (8 capsules) once daily 4 g(16 capsules) once daily	Carroll et al., 2011	Human	Pre-intervention 7.3±8.1 ng/ml Post-intervention 3.8±1.3	A phase IIa cancer prevention trial of oral curcumin given daily for 30 days in two stages on 40 participants.
9	Curcumin phytosome (CP),	Indena USA Inc., Seattle, WA, USA		Curcumin plus phosphatidylcholine (PC)	376 mg	Jäger et al., 2014	Human	2.8 ± 0.3ng/ml	Fifteen subjects (11 males, 1 female) were recruited for this study. One subject never started the study and the other two drop-outs. Each volunteer passed through screening and completed 4 trials in 7 days.
	Curcumin turmeric rhizome (CTR)	DolCas Biotech, LLC, Landing, NJ, USA	Gel capsules	Curcumin formulation with volatile oils	376 mg			0.5 ± 0.0ng/ml	

	Curcumin with hydrophilic carrier, (CHC)	Health Technologies, Inc., Morristown, NJ, USA		Curcumin with a combination of hydrophilic carrier, cellulosic derivatives and natural antioxidants	376 mg			$27.3 \pm 6.4^{\#}$ ng/ml	
	Standardized curcumin mixture (CS)	Sabinsa Corporation, East Windsor, NJ, USA		Standard curcumin	1,800 mg			2.3 ± 0.3ng/ml	

1.5.4.1. Curcumin Phytosome, Meriva by Indena

Phytosome technology emerged in the late 80s (Bombardelli et al. 1989). The term phytosome refers to the molecular-level association of the polyphenol chemically bound with a phospholipid preparation, consisting mainly of phosphatidylcholine (PC). Researchers have found from systematic bioavailability comparison that oral administration of phytosome enhances and strengthens the blood level of polyphenol constituents by at least 2-6 times (Indena SA). Most of the polyphenol molecules have a large chemical structure and cannot be absorbed by simple processes of diffusion due to their poor solubility in the water or lipids (Manach et al. 2004). On the other hand, PC is an amphipathic molecule with a unique structure having a positively charged head group and two neutrally charged tail groups that proffer it miscible in both water and lipid (Kidd and Head 2005). MCP® is a patented curcumin formulation from Indena S.p.A. Milan, Italy. It is formulated in a 1:2 weight ratio of curcumin and soy lecithin with an overall 20% of curcumin content in the final product. Some preliminary data on MCP curcumin have been collected so far and clinical trials have been conducted on MCP curcumin against osteoarthritis, diabetic mellitus, and microangiopathy.

MCP is the embedded dosage from Indena, designed to improve the bioavailability of compounds like polyphenolics and triterpenoid acids, that are normally characterized by poor water solubility and low solubility in organic solvents as well (Kidd 2009). Meriva® is a Curcumin phytosome, a patented complex with phosphatidylcholine (Semalty et al. 2010). There are two factors which mainly influence the bioavailability of natural products: hydrophilicity and lipophilicity. Most of the polyphenolics like curcumin have good water solubility but are poorly absorbed because of their poor miscibility with oils and their large particle size (Manach et al. 2004). In order to counteract the low bioavailability of these phytoconstituents, polyphenolics are modified into a lipid-compatible molecular complex known as Phytosome®. The phytosome® is made up of Phospholipids (small lipid molecules) mainly phosphatidylcholine, and a lipophilic substance which is more bioavailable than phytoextract due to its high capacity to cross the lipid-rich biomembranes and reach the circulation (Bombardelli et al. 1989; Citernesi and Sciacchitano 1995; Mauri et al. 2001). It is amphiphilic in nature having the property of improving solubility and bioavailability of both high lipids insoluble and poorly water-soluble phytoconstituents. Moreover, it improves systemic bioavailability of the attached substances

when administered orally (Barzaghi et al. 1990; Morazzoni et al. 1992; Maiti K 2005). There are a number of available Pytosome® complexes in the market owned by Indena S.p.A. Milan, Italy such as Crataegus Phytosome® (Antioxidant), Escin ß-sitosterol Phytosome (Anti-oedema), Silymarin Phytosome® (Antihepatotoxic) and MCP ™ (Anti-inflammatory) (Semalty et al. 2010).

By complexing a polyphenol like curcumin with PC to make phytosome, the embedded curcumin adopts some of the PC's versatile solubility properties. Moreover, PC molecules enhance the dispersion and bioavailability of the poorly water-soluble curcumin molecules. In order to evaluate the hypothesis that curcumin phytosome with soy phosphatidylcholine MCP might improve the systemic availability of curcumin. Various studies have been performed to compare the effect of MCP with curcumin to figure out its efficacy and bioavailability. One of the comparative pharmacokinetic studies performed on male Wistar rats has confirmed the high bioavailability of biocompatible curcumin. They feed to male Wistar rats orally raw curcumin and MCP at the dosage of 340 mg/kg and 1.8 g/kg respectively. After 15, 30, 60 and 120 minutes of administration, the presence of curcumin and other metabolites in the plasma, liver and intestinal mucosa was analyzed. It turned out that 99% of curcumin was present in plasma as glucuronides, with the remaining 1% being curcumin sulphate and free curcumin whereas curcumin formulation with phospholipids (MCP) increased the plasma concentration of curcumin up to 20-fold (Marczylo et al. 2007).

It has been shown that the phytosome® complexes have a better anti-inflammatory effect than uncompleted herbal extracts (Bombardelli et al. 1989; Bombardelli, Cristoni, and Morazzoni 1994). Several clinical trials are going in support of MCP curcumin. The absorption and ultimate bioavailability were examined in human subjects for both curcuminoid and MCP at the same time. The absorption of the unformulated curcuminoid mixture was 29-fold less as compared to MCP (Cuomo et al. 2011). Another study investigated the activity of curcumin in neurogenesis in AD brain. It was found that curcumin-encapsulated PLGA nanoparticles (Cur-PLGA-NPs potently induce NSC proliferation and neuronal differentiation *in vitro* and in the hippocampus and subventricular zone of adult rats as compared to uncoated bulk curcumin (Tiwari et al. 2014).

Taken together all these studies, it is concluded that the curcumin efficacy and potency can be enhanced by delivering it in a controlled and embedded manner to a target site and phytosome is expected to be the better candidate for delivery for curcumin particles.

Figure 5. Meriva curcumin. The MCP in raw form **(http://www.indena.com/)**

1.5.4.2. Solid lipid curcumin particle (SLCP), Longvida by Verdure Sciences

The SLCP preparation (Longvida, SLCP), consist of dispersible solid lipid curcumin particles, and a curcumin extract (containing 95% curcuminoids) patented by Verdure Sciences (Noblesville, IN, USA). Briefly, dry turmeric root extract powder was mixed with phosphatidylcholine, vegetable stearic acid, ascorbic acid (vitamin C) Palmitate, and other inert ingredients manufactured under cGMP standards for precise chemical and physical characteristics. This patented Solid Lipid Curcumin Particle (SLCP) Technology enables the uptake of free curcumin to the blood and target tissues.

Curcumin has a broad cytokine-suppressive anti-inflammatory action, down-regulating the expression of cyclooxygenase-2 (COX-2), inducible nitric oxide synthase (iNOS), TNF-α, IL-1, -2, -6, -8, and -12. It inhibits IL-6 mediated signalling via inhibition of IL-6 induced STAT3

phosphorylation and consequent STAT3 nuclear translocation (Bharti, Donato, and Aggarwal 2003), and interferes with the first signalling steps downstream of the IL-6 receptor ("the inflammatory trigger") in microglial activation (Ray and Lahiri 2009). Pharmacokinetics of unmodified curcumin is unfavourable, and its bioavailability is low. However, highly bioavailable curcumin formulations (encapsulated in liposomes or micelles) such as Longvida curcumin (VS Corp) can achieve μM concentrations in the rodent brain (Begum et al. 2008a; Ma et al. 2013b). As mentioned earlier, due to the poor bioavailability and extensive phase-II metabolism of curcumin, the oral dosage form of curcumin formulations has very limited bioavailability and absorption, which limits its potential as a preventive and/or therapeutic agent (Anand et al. 2007). Several clinical studies have reported low systemic bioavailability of normal curcumin even after 12 g/day oral administration (Olivera et al. 2012).

Studies have been conducted on LC with positive outcomes. A study conducted in aged human tau transgenic mice have reported that the LC selectively suppressed soluble Tau dimers and attenuated the synaptic and behavioral deficits in transgenic mice (Ma et al. 2013a). Moreover, acute and chronic animal studies and the No Observed-Adverse-Effect Level (NOAEL) were determined to be 720 mg/kg bw/day (Dadhaniya et al. 2011).

Clinical studies conducted on LC have reported the increased bioavailability and absorption compared to free curcumin (Gota et al. 2010). A study demonstrated that a low dose of LC (80 mg/day) have shed health-promoting effects on aged-human (DiSilvestro et al. 2012). Highly bioavailable curcumin preparations, the LC has achieved higher concentrations in the brain and significantly improved working memory and mood after a 4 week treatment in a randomized, double-blind, placebo-controlled human trial (Begum et al. 2008b; Wu et al. 2014). From the previous studies, it could be assumed that the curcumin efficacy and potency can be enhanced by delivering it in a controlled and embedded manner to a target site and SLCP is expected to be the better candidate for delivery for curcumin particles.

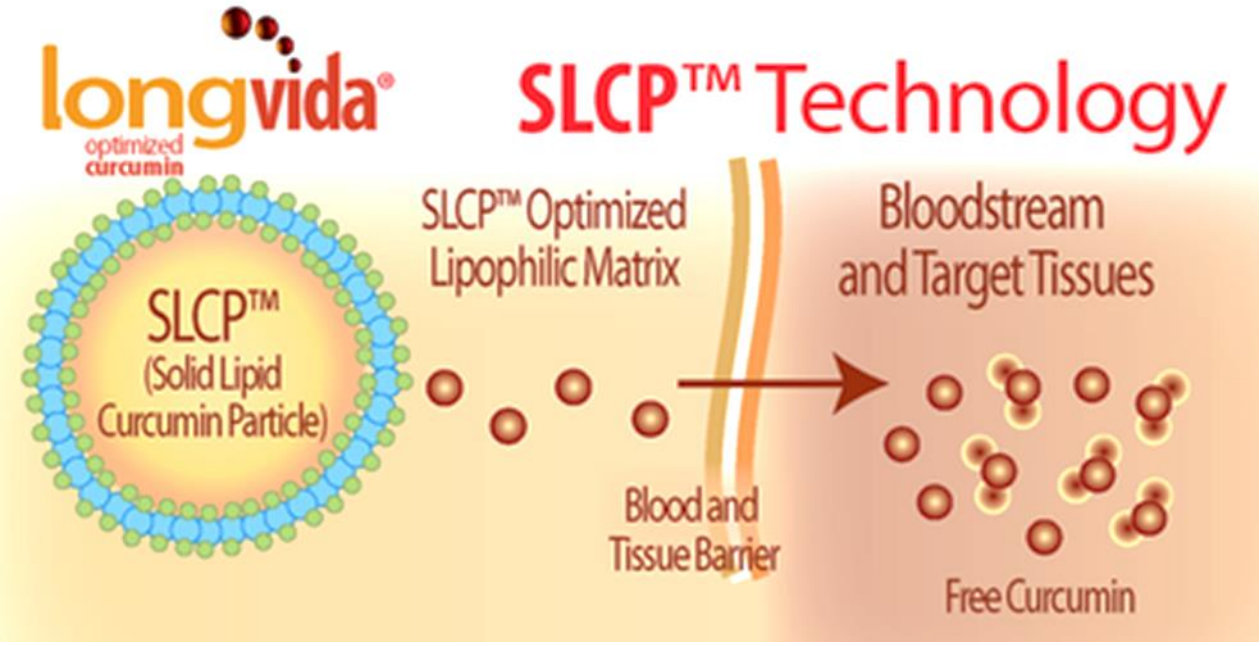

Figure 6. Longvida curcumin (https://vs-corp.com/l)

2. Hypothesis and Research aims

2.1 Hypothesis

In the GFAP-IL6 mouse model, chronic neuroinflammation starts early from the age of 3 months, having a higher number of activated microglia and astrocytes (Campbell et al. 1993b; Suresha and Srinivasan 2013). Feeding these mice at an age of 2 months with LC and 3 months with MCP will downregulate the number and activation state of activated microglia and astrocytes.

2.2 Specific Aims

Aim 1: To investigate if MCP can downregulate the activated higher number of microglia (Iba1, TSPO) and astroglial (GFAP) cell numbers in the hippocampus and the cerebellum Inflammation in the GFAP-IL6 mouse model.

Aim 2: To investigate if MCP can reverse the microglia and astroglial cells morphology from the activated state to the resting state in the hippocampus and the cerebellum in the GFAP-IL6 mouse model.

Aim 3: To investigate if LC can downregulate the activated higher number of microglia (Iba1, TSPO) and astroglial (GFAP) cell numbers in the hippocampus and the cerebellum.in the GFAP-IL6 mouse model.

Aim 4: To investigate if LC can reverse the microglia and astroglial cells morphology from the activated state to the resting state in the hippocampus and the cerebellum in the GFAP-IL6 mouse model.

3. Materials and methods

3.1. Materials

3.1.1. Preparation of curcumin containing food pellets

3.1.1.1 Meriva

MCP was prepared using phytosome technology. The curcumin was supplied by Indena SpA, Italy and the MCP curcumin food pellets were prepared locally. Briefly, the food pellets consisted of 1:2 weight ratio of curcumin and soy lecithin with overall 20% of curcumin content in the final product and two parts of microcrystalline cellulose are then added to improve followability and bioavailability.

3.1.2.1 Longvida

Similarly, LC was prepared using solid lipid curcumin particle technology. Briefly, curcumin powder was supplied by Vendure science, USA and LC food pellets were prepared locally. Briefly, the curcumin powder was mixed with phosphatidylcholine, vegetable stearic acid, ascorbic acid (vitamin C) Palmitate, and other inert ingredients with 20% curcumin (Nahar, Slitt, and Seeram 2015).

Table.2. MCP and LC doses

	Amount in grams of MCP/LC per Kg of finished feed	**Dose(s) in mg/kg bw**	**Dose(s) in ppm**
1. MCP	4.37g	35mg/kg/bw	320ppm
2. MCP	2.18g	70mg/kg/bw	636ppm
3. MCP	1.09g	140mg/kg bw	1272ppm
4. LC	2.5g	51-60mg/kg bw	500ppm
5. NC	0.87g	140mg/kg bw	1272ppm

3.2. Animals

3.2.1 Housing and ethics

WT (C57BL/6) and GFAP-IL6 heterozygous mice of mixed genders weighing 20-30g were housed in the animal facility of the School of Medicine, Western Sydney University under a temperature-controlled environment, with a normal 12h/12 h light/dark cycle at 23 ˚C, 60 ± 10% humidity, and provided with food and water *ad libitum*. The experimental procedures were approved by the Western Sydney University Animal Care and Ethics Committee (A11393) and carried out in accordance with the rules established by the National Health and Medical Research Council of Australia. Heterozygous GFAP-IL6 mice and their non-transgenic littermates (WT C57BL/6) were used at the age of 3 months.

3.2.2. Grouping of animals and feeding with MCP food pellets

Animals were randomly assigned to 6 groups: WT C57BL/6 mice fed with control food pellets and GFAP-IL6 mice fed with control food pellets as well. The rest of the four groups of GFAP-IL6 mice were fed with food pellets containing 140mg/kg bw/d, 70mg/kg bw/d, or 35mg/kg bw/d of MCP, 140mg/kg bw/d of normal curcumin **(Table 3)**. At the age of 3 months, the mice were fed for one month. The weight of the mice was monitored throughout the feeding period In addition, the cage food trays were monitored weekly and noticed that each mouse was eating 3-4 g/day of the food pellets. At the age of 4 months, they were perfused for histology.

3.2.3 Grouping of animals and feeding with LC food pellets

In this long term feeding study, animals were randomly assigned to 4 groups: Wild type C57BL/6, GFAP-IL6 mice fed with control food pellets and GFAP-IL6, GFAP-IL6 mice fed with LC diet **(Table 2)**. The Longvida® curcumin food pellets were supplied by Verdure Sciences Corp.; Noblesville, IN. The pellets consisted of natural antioxidant curcumin with enhanced followability and bioavailability. At the age of 2 months, the mice were put on feeding at one defined dose for the duration of 6 months. Animals were monitored, body weight and the amount of food consumed was recorded. It was observed that the mice were constantly gaining

weight during the entire feeding tenure. At the age of 8 months, the behavioral test was performed followed by perfusion for histology.

Table. 3 Cohort information and the number of mice used

Cohorts	Type of food	Number of mice used		
		Iba-1	GFAP	TSPO
WT	Normal food	6	4	6
GFAP-IL6	Normal food	7	4	5
GFAP-IL6	MCP 35 mg	7	5	6
GFAP-IL6	MCP 70 mg	6	6	5
GFAP-IL6	MCP 140 mg	7	7	7
GFAP-IL6	Normal Curcumin 140 mg	8	8	7
WT	Normal food	4	6	3
GFAP-IL6	Normal food	6	6	6
WT	LC (500ppm)	5	6	3
GFAP-IL6	LC (500ppm)	6	6	6

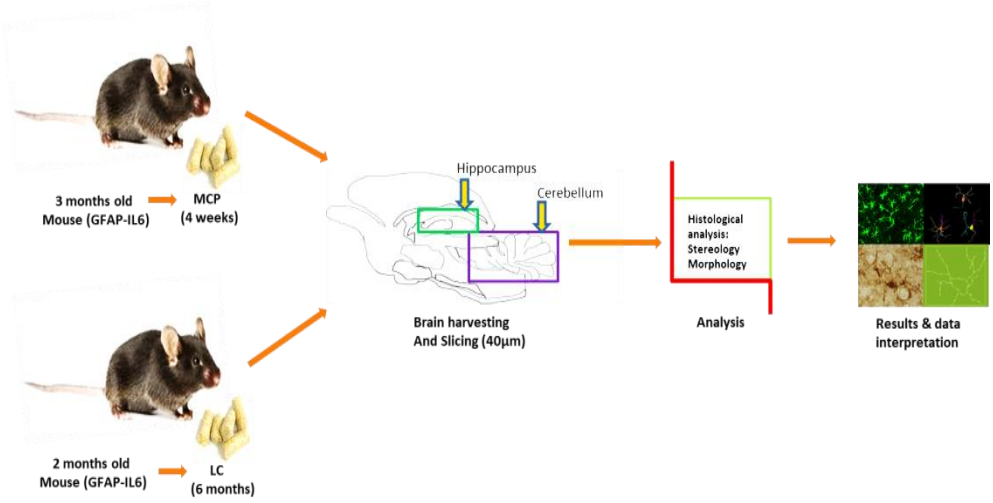

Figure 7. Graphical representation of age and feeding differences between the MCP and the LC feeding paradigms.

3.2.4. Histology and tissue sample preparation

For histological analysis, the tissue samples were prepared from all experimental cohorts. Mice were anesthetized with Pentobarbitone (30-50 mg/kg bw IP (20-40 min. of anesthesia) and transcardially perfused with 30 ml of 0.9 % normal saline using a peristaltic pump, followed by 60 ml of 4 % cold paraformaldehyde (Merck) (in 0.1 M phosphate buffer). Brains were harvested and post-fixed in 4 % paraformaldehyde for 24 hrs at 4 °C, and then transferred to 30% sucrose (in 0.1 M PB solution) for cryoprotection. After the brains sank to the bottom of the container, they were embedded and frozen with 6% gelatine. Forty μm thick coronal sections were cut in eight series using a Leica CM 1950 cryostat.

3.2.5. Immunohistochemistry

For bright field microscopy, immunohistochemistry assays were performed on every 8th section from the brains to identify microglial activation using microglia markers (Iba-1 and TSPO). All washing and incubation procedures were performed using 0.1M PBS unless stated otherwise. The sections were washed 3 times and treated with 1 % H_2O_2 before being incubated for 2 hrs in the blocking solution (2% goat serum) to block non-specific antigen binding sites. Then they were incubated in the primary rabbit-anti-Iba1 antibody (1:500, Wako, # 019-19741) and rabbit anti TSPO (1:500, Merck, #ABC139) solutions for two days at 4 ˚C and subsequently in the secondary antibody (1:200, biotinylated goat anti-rabbit IgG; Life Technologies, #656140) for 2 hrs. The sections were washed 3 times and ABC solution (1:250, Vector Laboratories, # PK-6100) was applied for 2 hrs. Sections were then incubated in the developer solution containing 0.4 mg/ml DAB and 0.0006% hydrogen peroxide until an optimal color developed. In the end, the sections were washed, mounted, dehydrated, coverslipped and images were captured with a Zeiss microscope (MBF Bioscience).

3.3. Microscopy and anatomical data analysis

3.3.1 Fluorescence microscopy

Immunofluorescent staining against GFAP was performed on every 8th section from the brains to identify astroglial activation using GFAP as an astroglial marker. The sections were washed with 0.1M PBS in order to remove the gelatine and incubated in the primary rabbit-anti-GFAP antibody (1:500, Dako, #20023331) solution for one day at 4 ˚C followed by fluorescence secondary antibody (1:200, goat anti-rabbit IgG, Alexa 488; Thermo Fisher Scientific, # 1853312) for 2 hrs. The sections were washed, mounted and coverslipped with a fluorescent mounting medium (Vector Laboratories, #H1400).

3.3.2. Stereological counting

In order to do the stereological quantification, the estimated number of glial cells in both the cerebellum and the hippocampus was counted on Iba1, TSPO and GFAP stained sections using

the Zeiss AxioImager M2 microscope equipped with MBF Biosciences StereoInvestigator (Bastide et al. 2014; Morgan et al. 2014). Briefly, the objective for the contour of the cerebellum and hippocampus was first drawn under the 2.5x objective. The size of the counting frame was 130 x 130 μm for WT for cerebellum while, 120 x 120 μm for the hippocampus, 60 x 60 μm for GFAP-IL6 non-fed mice as well as for MCP fed mice. The counting grid was 1500 x 1000 μm for the cerebellum and 800 x 800 μm for the hippocampus for the entire cohorts. The guard zone was 1 μm at the top and the bottom of the sections. Microglia and astrocytes were plotted on the screen using a marker as the focus moved from the top to the bottom of the sections using a 63x oil objective. This led to the Gunderson coefficient error of less than 0.1 in all cases (m=1). The average estimated population of the cells has been obtained from each mouse brain Due to technical limitations, it was not possible to discriminate between individual astrocytes in the cerebellum. Therefore, for this time point, only the representative pictures are shown. However, the number of $GFAP^+$ cells in the hippocampus was measured under the above-mentioned parameters.

3.3.3. Three-dimensional reconstruction of astrocytes and microglia

Samples were prepared as described above and the images were taken using Confocal ZEISS laser Scanning Microscope (LSM-5) with an argon laser and processed using the Zen 2009 software package. Z-stacks were captured using a 20 x objective, NA1.0 for reflective imaging, at a step size of 0.1um (unless specified otherwise). Reflective imaging was achieved using the 488 nm wavelength. For the three-dimensional reconstruction of both astrocytes and microglia, Neurolucida 360 (MBF Bioscience) software was used. To better identify the objects and provide greater accuracy, all the images were taken using a 20x high power objective with the laser scanning confocal microscope. A total of 16-20 cells in the hippocampus and the cerebellum of the brain were traced in each experimental cohort. The cells and their processes were analyzed in three dimensions within single sections by using a computer-based tracing system (Neurolucida 360; MBF Bioscience, Williston, VT). Only somas were analyzed in two dimensions (area at its largest cross-sectional diameter) because of limitations associated with tracing and measuring and the cell body area as well as the number, length, diameter, and branching points (nodes) of its processes were measured in three dimensions. We further observed thorny protrusions along

the length of processes. In order to further assess the spatial distribution of astrocytic processes, a 3D version of the Sholl analysis (Sholl 1956) was used.

3.3.4. Analysis of reconstructed cells

Morphometric data of each astrocyte and microglia were extracted by the software and thus, each reconstructed cell was subject to multiple parameters. The soma area, soma perimeter, convex 2D area, convex perimeter, the total length of all processes, the total volume of all processes, total density and number of nodes (Branch points) and dendrites of all the processes were measured. In order to determine changes in the size of the cell in relation to distance from the cell soma, Sholl analysis was performed for each microglial and astroglial cell (Bento-Torres et al. 2017). Z-stack images of live microglia and astrocytes were condensed into a maximum intensity and applied the Sholl analysis in Neurolucida 360 software. Concentric circles (radii) originating from the soma were spaced 5 μm apart in this case. This analysis determined the number of intersections, process length (μm), the surface area of the cells (μm^2), process volume (μm^3), process diameter (μm) and a number of nodes of the cells for each radius.

3.3.5 Data analysis

The estimated number of microglia and astrocytes in both the cerebellum and the hippocampus were compared between groups using one-way ANOVA in GraphPad Prism 6. Results were presented as mean ± SEM. Significance was indicated when p was less than 0.05. Distinct morphological features of microglia and astrocytes in the brain were compared between groups using One-way ANOVA with Turkey's post-test (*$p < 0.05$, **$p < 0.001$, ***$p < 0.0001$, mean ± SEM). Correlations of the Convex Hull Area with distinct morphological features of microglia and astrocytes were analyzed using linear regression (R^2) and correlation (*$p < 0.05$) tests in GraphPad Prism 7. ANCOVA test was used to compare slope differences in each specific morphological feature (*$p < 0.05$) between different experimental cohorts.

4. RESULTS

4.1. Effect of Meriva® curcumin phytosome on microglia and astrocytes numbers in the GFAP-IL6 mouse model

4.1.1. Introduction

Neuroinflammation is a defense response of the central nervous system to injury, infection or toxic metabolites. Acute neuroinflammation is a self-protective reaction aimed at eliminating deleterious stimuli and restoring tissue integrity. However, if neuroinflammation becomes chronic it can be harmful. Chronic neuroinflammation is both a feature and a potential cause of many neurodegenerative diseases like AD and dementia (Arends et al. 2000). Interleukin 6 (IL-6) is a multifactorial, regulatory cytokine that may play a pathogenic role in dysregulating inflammatory responses (Akira et al. 1990). Microglia and astrocytes play a key role in the CNS's innate immunity. The major role of microglia is to clear damaged neurons and foreign pathogens, while astrocytes help to remove debris and toxins from the cerebrospinal fluid. When activated, microglia produces a variety of pro-inflammatory cytokines and neurotoxic factors, such as reactive oxidative species (ROS), leading to neuronal damage, neuroinflammation and subsequent cognitive deficits (Rosenblat et al. 2014; Heneka, Golenbock, and Latz 2015). Microglial cells are the key neuroinflammatory cells as they are activated in response to brain inflammation and release ROS as well as cytokines that cause neurotoxicity (Block, Zecca, and Hong 2007b; Beggs and Salter 2007). TSPO is a translocator protein expressed in the nervous system, specifically on the outer mitochondrial membrane (Chen and Guilarte 2008). It is predominantly expressed in the microglia, astrocytes, neurons and macrophages in the blood vessels (Kuhlmann and Guilarte 2000; Wilms et al. 2003). TSPO represents a novel macrophage marker, as neurological insults and chronic neuroinflammation induce TSPO expression in the nervous system (Casellas, Galiegue, and Basile 2002; Kuhlmann and Guilarte 2000). Astrocytes are vital cells of the CNS, playing an important role in coupling neuronal organization to blood flow and maintaining, regulating, and altering neuronal synaptic junctions (Zhang and Haydon 2005). Astrocytes are highly reactive cells respond to adverse neural insults, such as neuroinflammation, trauma, and neurodegeneration (Sofroniew 2009). Previous studies conducted on GFAP-IL6 mice have shown a larger number of $GFAP^+$ astrocytes in both the cerebellum and cortical areas compared to WT mice (Chiang et al. 1994).

GFAP-IL6 mice have been used in this study as a chronic glial cell activation mouse model. In the GFAP-IL6 mouse model, the murine IL-6 gene is expressed by astrocytes under the

transcriptional control of the glial fibrillary acidic protein (GFAP) promoter, results in brain-specific overexpression of IL6 and chronic neuroinflammation. This has been demonstrated via a significant increase in Iba-1$^+$, TSPO$^+$ microglia, GFAP$^+$ astroglia, and neurodegeneration mostly in the cerebellum (Campbell et al. 1993a). This model presents with prolonged neuroinflammation (activation of microglia and microgliosis) (Gyengesi et al. 2018) and a range of structural and functional neurological impairments, which typify various neurodegenerative diseases (Campbell et al. 1993a). Previous studies have reported that GFAP-IL6 transgenic mice display a high level of IL6 expression in the cerebellum compared to other brain regions (Campbell et al. 1993a; Quintana et al. 2009). A recent study conducted by our lab in the same animal model has confirmed that the number of Iba-1$^+$ cells in GFAP-IL6 mice is significantly larger compared to that of the WT mice (Gyengesi et al. 2018). This is the first study to evaluate the effect of a high bioavailability curcumin formulation MCP curcumin in the GFAP-IL6 mouse model. MCP could be a potential suppressive agent against chronic neuroinflammation through the modulation of astroglial and microglial activity. To determine how MCP affects the number of activated (Iba-1$^+$, TSPO$^+$) microglia and activated (GFAP$^+$) astroglia in the brain, stereological counting, were applied to assess the number activated microglia and astrocytes in the hippocampus and the cerebellum in an unbiased manner.

4.1.2. Results

4.1.2.1 Curcumin formulations decreased the number of Iba-1$^+$ microglia in the hippocampus of GFAP-IL6 mice

First, the phenotype difference between WT and GFAP-IL6 mice and the effect of MCP and normal curcumin on the elevated number of Iba-1$^+$ microglial cells in the GFAP-IL6 mice was determined. Immunohistochemistry and stereological counting of Iba-1$^+$ microglia were performed in the hippocampus in GFAP-IL6 mice fed with normal food, increasing doses of MCP and normal curcumin.

The hippocampus of GFAP-IL6 mice fed with normal food had 438,550 ± 29,717 Iba-1$^+$ microglia, which was significantly higher than that of the WT mice (175,192 ± 12,098) (Fig 8A-

B, G). In the MCP fed GFAP-IL6 mice, a reduction in the number of Iba-1$^+$ microglia was observed. The low doses 35mg/kg bw/d and 70mg/kg bw/d of MCP reduced the number by 17.5% (361,644 ± 54,484) and 22% (338,483 ± 81,353) (Fig 8C-D,G), whereas, 140mg/kg bw/d of MCP significantly reduced the number of microglia by 26.2% (323,451 ± 21,520) compared to the GFAP-IL6 normal food fed cohort (Fig 8 E,G). In contrast, the 140 mg/kg bw/d normal curcumin decreased the number of microglia by 18.3% (357,955 ± 26,079) compared to GFAP-IL6 normal food fed cohort (Fig 8F, G).

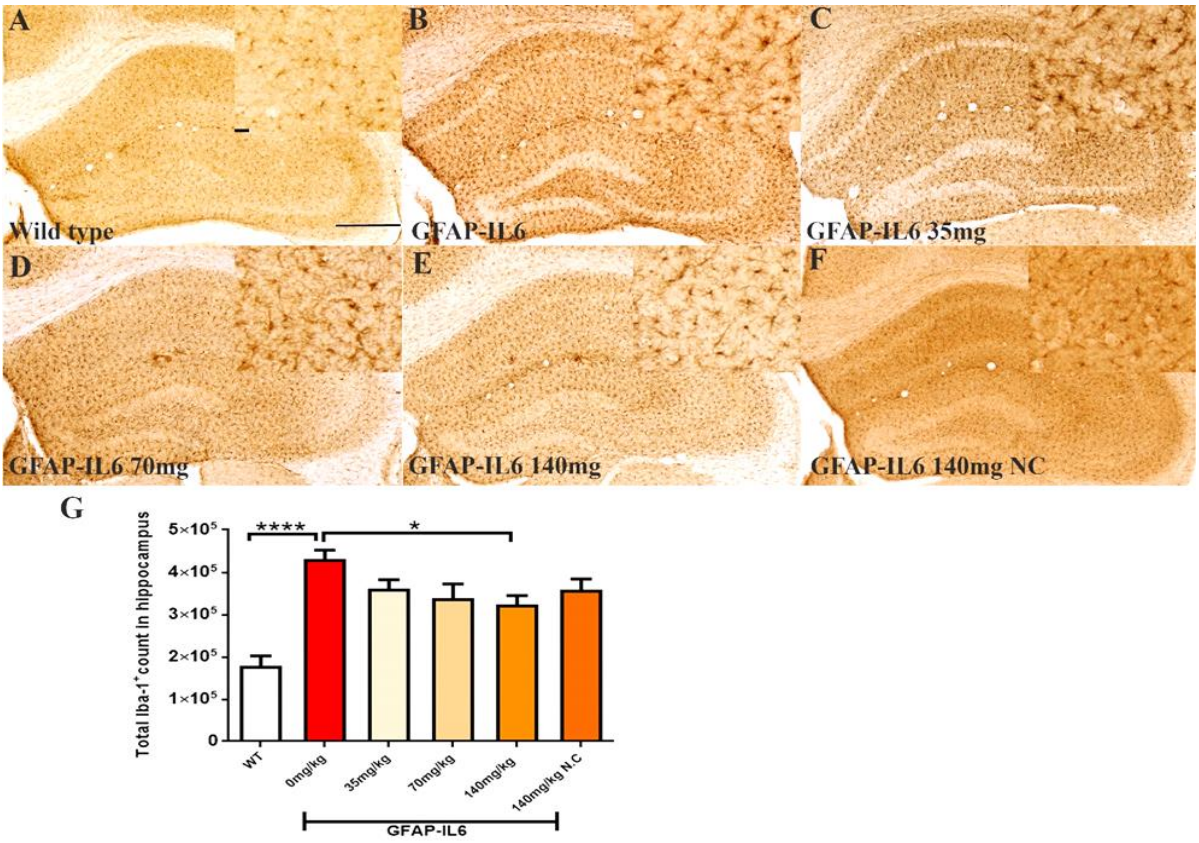

Figure 8. Curcumin formulations decreased the number of Iba-1$^+$ microglia in the hippocampus of GFAP-IL6 mice. (A-F) Representative photomicrographs of immunohistochemical staining for the microglia (Iba-1$^+$ cells) of the hippocampus. (Magnification 10x objective field, scale bar = 500µm and 100µm in inserts). Images are representative of at least six animals per group (n=6). (G) Graphical representation of total Iba-1$^+$ count in the hippocampus. The graph represents the mean ± SEM and significant differences were determined using a one-way analysis of variance (ANOVA). Significance = ****$p < 0.0001$, *$p < 0.05$.

4.1.2.2 Curcumin formulations decreased the number of Iba-1$^+$ microglia in the cerebellum of GFAP-IL6 mice

In the cerebellum, GPAP-IL6 mice had 1025205 ± 104467 Iba-1$^+$ microglia which was significantly higher than that of WT mice (154,058 ± 12,871) (Fig 9A-B, G). A significant reduction in the total number of microglial cells was observed in high dose of MCP and normal curcumin groups compared to the normal food fed GFAP-IL6 group. GFAP-IL6 mice fed with 140mg/kg MCP and 140mg/kg normal curcumin significantly downregulated the Iba-1$^+$ microglia by 40% (605,085 ± 63,857) and 38% (629,122 ± 54,363), respectively (Fig 9 E – F, G). Whereas, in case of 35mg/kg and 70mg/kg doses of MCP, the Iba-1$^+$ microglial reduced by 32% (693,938 ± 117,878), 42% (592,373 ± 48,489) , respectively (Fig 9 C – D, G).

No significant difference in the number of Iba-1$^+$ microglia was observed between 140mg/kg bw/d MCP and 140mg/kg bw/d normal curcumin in either brain region.

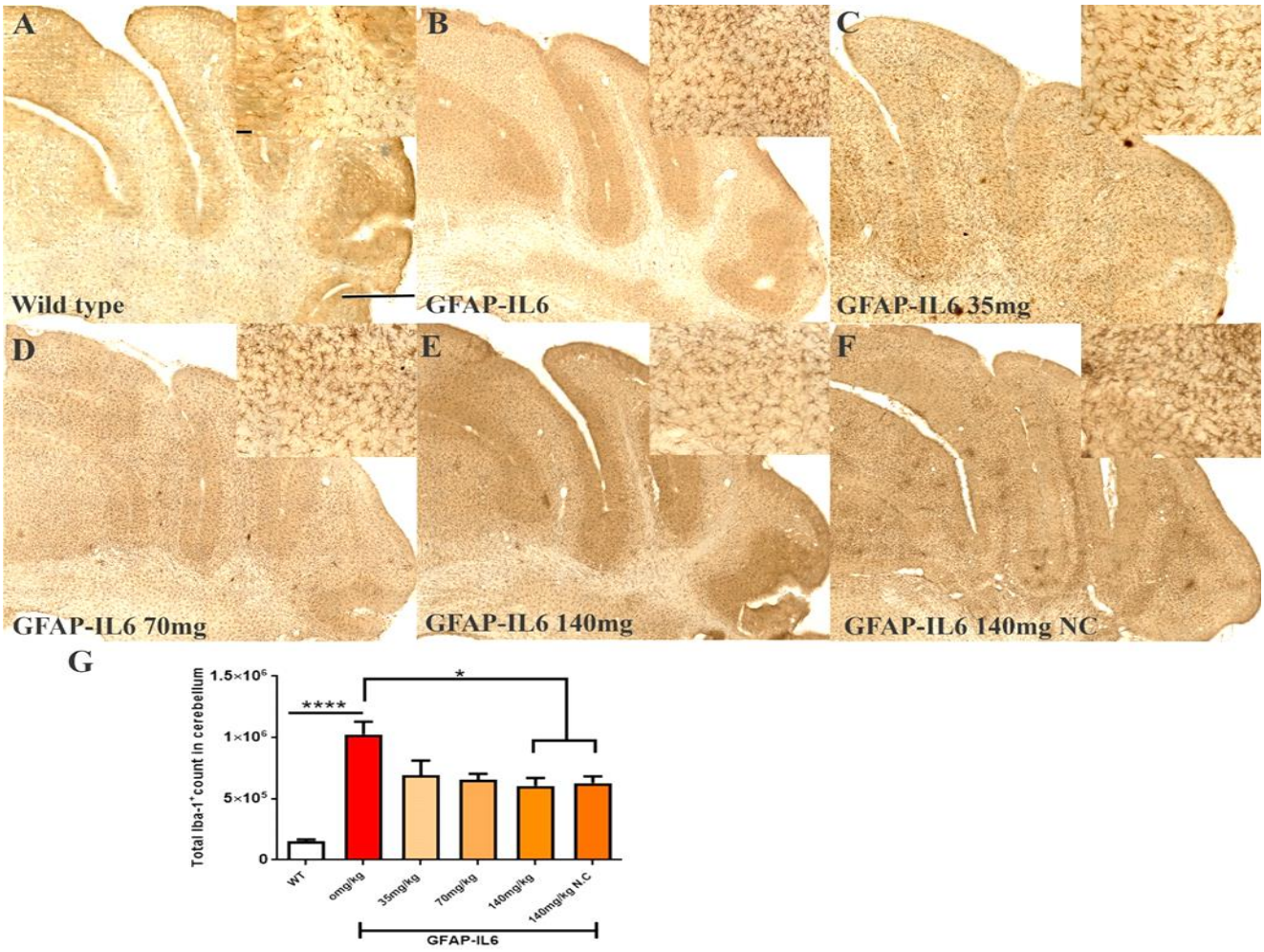

Figure 9. Curcumin formulations decreased the number of Iba-1$^+$ microglia in the cerebellum of GFAP-IL6 mice. (A-F) Representative photomicrographs of immunohistochemical staining for the microglia (Iba-1$^+$ cells) of the cerebellum. (Magnification 10x objective field, scale bar = 500µm and 100µm in inserts). Images are representative of at least six animals per group (n=6). (G) Graphical representation of total Iba-1$^+$ count in the cerebellum. The graph represents the mean ± SEM and significant differences were determined using a one-way analysis of variance (ANOVA). Significance = ****$p < 0.0001$.

4.1.2.3 Curcumin formulations decreased the number of TSPO$^+$ microglial cells in the hippocampus of GFAP-IL6 mice

The mitochondrial translocator protein (TSPO) is expressed in both macrophages and a portion of microglia in the brain and has been shown to be upregulated in reactive microglia in

inflammation (Mirzaei et al. 2016; Cosenza-Nashat et al. 2009). In addition to Iba-1, immunostaining was performed for TSPO as a microglial marker. Stereological quantification was performed in order to test whether there is a difference in $TSPO^+$ microglia/macrophages between WT and GFAP-IL6 mice, whether MCP changes the number of $TSPO^+$ cells in the brains of GFAP-IL6 mice, and to investigate the difference between MCP and normal curcumin diet fed mice.

In the hippocampus, GFAP-IL6 mice had 147,803 ± 46,723 $TSPO^+$ microglia compared to WT mice (4,747 ± 3,866)(Fig 10A-B,G). Low doses of MCP such as 35mg/kg and 70mg/kg reduced the number of $TSPO^+$ microglia by 16% (123,769 ± 6266) and 19% (119,213 ± 11,229) respectively. The 140mg/kg dose of MCP significantly decreased the number by 33% (98,941 ± 21,413) while, the 140mg/kg normal curcumin decreased the number by 26% (108,323 ± 8124) compared to GFAP-IL6 non-fed mice (Fig 10E-F, G). No significant difference was observed between 140mg/kg bw/d MCP and 140mg/kg bw/d normal curcumin.

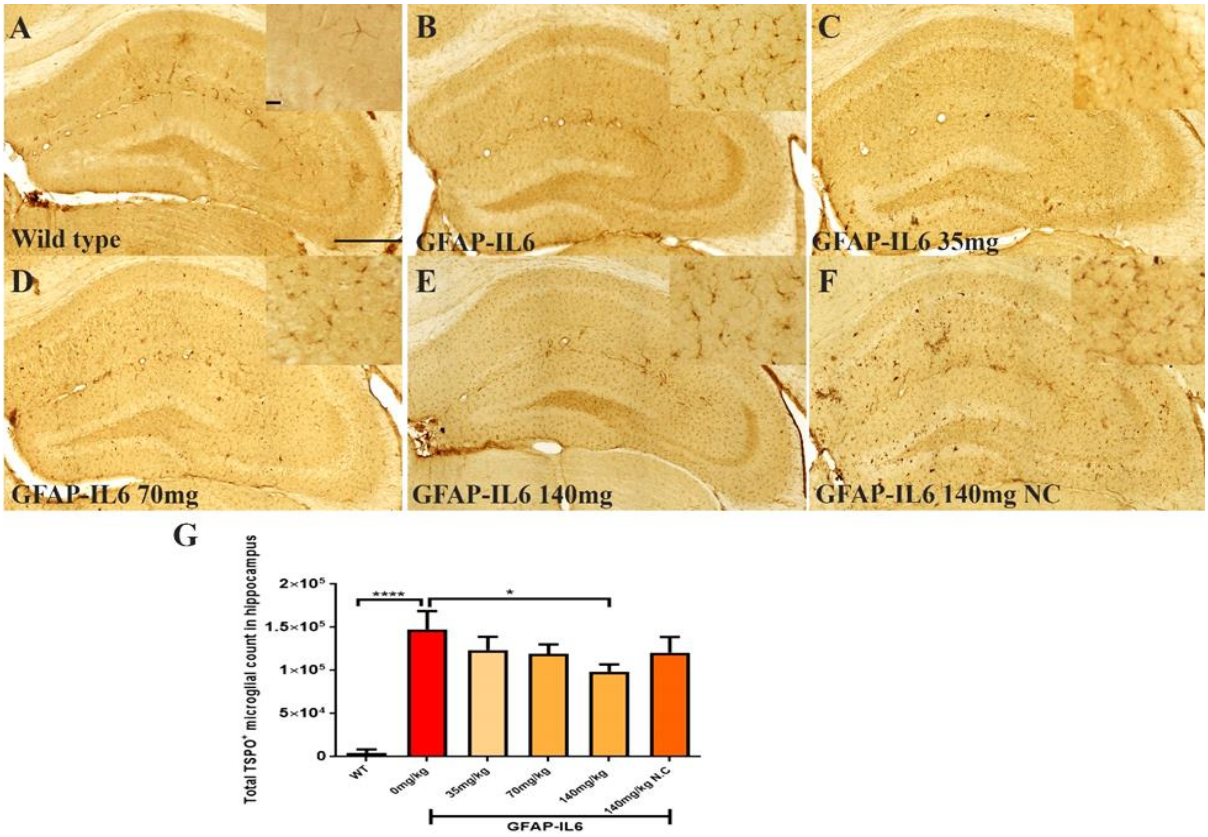

Figure 10. Curcumin formulations decreased the number of TSPO$^+$ microglial cells in the hippocampus of GFAP-IL6 mice. (A-F) Representative photomicrographs of immunohistochemistry staining for the microglia (TSPO$^+$ cells) of the hippocampus. (Magnification 10x objective field, scale bar = 500µm and 100µm in inserts). Images are representative of at least six animals per group (n=6). (G) Graphical representation of total TSPO$^+$ microglial count in the hippocampus. The Graph represents the mean ± SEM and significant differences were determined using a one-way analysis of variance (ANOVA). Significance = $*p < 0.01$, $****P < 0.0001$.

4.1.2.4 Curcumin formulations decreased the number of TSPO$^+$ microglial cells in the cerebellum of GFAP-IL6 mice

In the cerebellum, GFAP-IL6 mice had 369,963 ± 152,991 TSPO$^+$ microglia, which was significantly higher than that of WT mice (12,402 ± 8820) (Fig 11A-B,G). Lower doses of MCP such as 35mg/kg and 70mg/kg reduced the number of TSPO$^+$ microglia by 26% (276,303 ± 40,166) and 24% (278,235 ± 35,052) respectively (Fig 11C-D). The 140mg/kg MCP reduced TSPO$^+$ microglial number by 42% (215,912 ± 80,444) whereas, 140mg/kg normal curcumin reduced the number only by 34% (242,110 ± 12,527) compared to GFAP-IL6 normal food fed mice (Fig 11E,F-G).

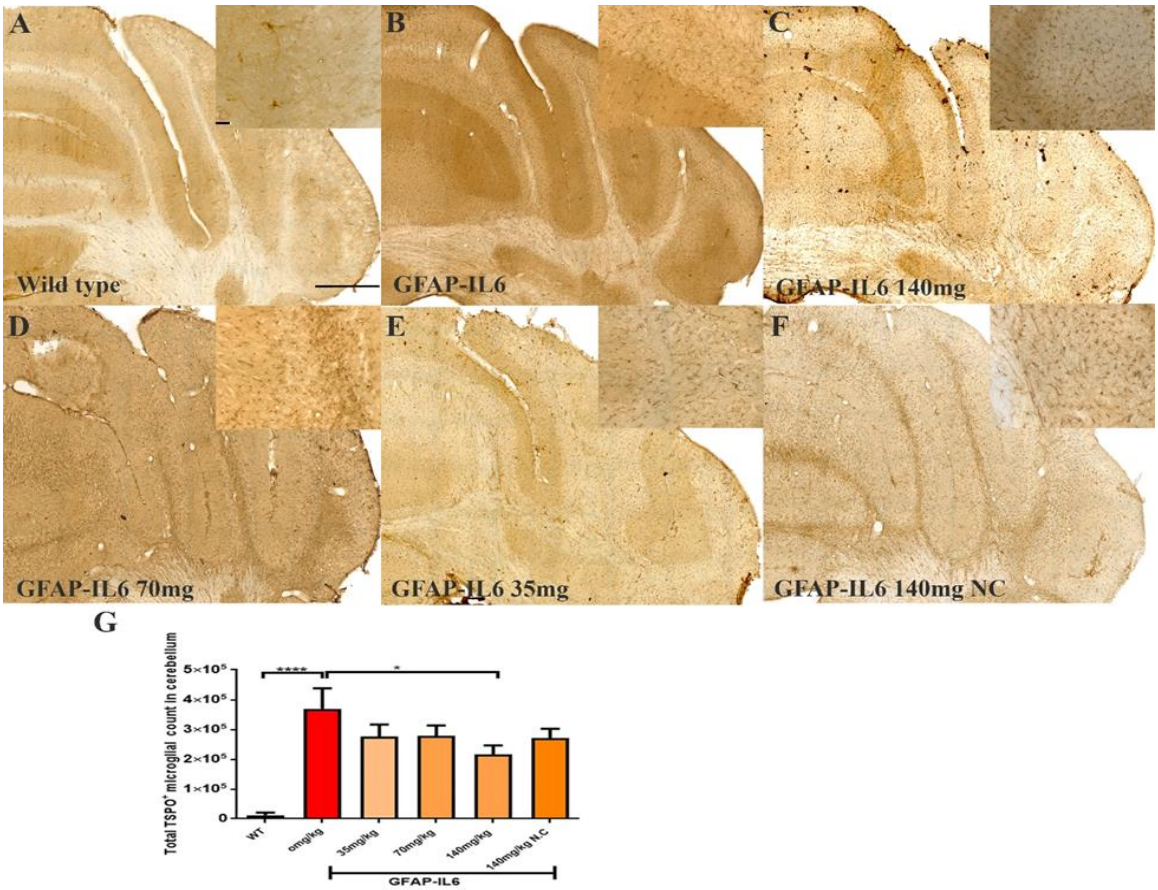

Figure 11. Curcumin formulations decreased the number of TSPO$^+$ microglial cells in the cerebellum of GFAP-IL6 mice. (A-F) Representative photomicrographs of immunohistochemistry staining for the microglia (TSPO$^+$ cells) of the cerebellum. (Magnification 10x objective field, scale bar = 500µm and 100µm in inserts). Images are representative of at least six animals per group (n=6). (G) Graphical representation of total TSPO$^+$ microglial count in the cerebellum. The Graph represents the mean ± SEM and significant differences were determined using a one-way analysis of variance (ANOVA). Significance = *p <0.01, ****P < 0.0001.

4.1.2.5 Curcumin formulations decreased GFAP$^+$ astrocytes in the hippocampus of GFAP-IL-6 mice

To quantify the number of astrocytes, GFAP immunostaining and stereological quantification were performed to investigate the genotype difference between WT and GFAP-IL6 mice. Furthermore, the effect of MCP and normal curcumin on the elevated number of GFAP$^+$ astrocytes in the GFAP-IL6 mice was investigated in the hippocampus and cerebellum.

In the hippocampus, GFAP-IL6 mice had a significantly larger number of $GFAP^+$ astrocytes (530,374 ± 30,447) compared to WT mice (169,908 ± 17,046) (Fig 12A-B,G). In MCP fed GPAP-IL6 mice, a significant reduction in the number of $GFAP^+$ astrocytes were observed in a dose-dependent manner compared to the GFAP-IL6 normal fed group. MCP at a dose of 35mg/kg and 70mg/kg reduced the number by 30% (369,401 ± 64,227) and 37% (333,646 ± 85,311) respectively (Fig 12C-D, G). The 140mg/kg downregulated the total GFAP+ astrocytes by 42% (304,668 ± 62,649) whereas, the normal curcumin decreased the number by 25% (395,739 ± 23,531) (Fig 12E-F, G) Based on this stereological data, a dose-response curve was plotted showing that the IC_{50} value for MCP is 46.70mg/kg bw in the hippocampus of GFAP-IL6 mice (Fig 12H).

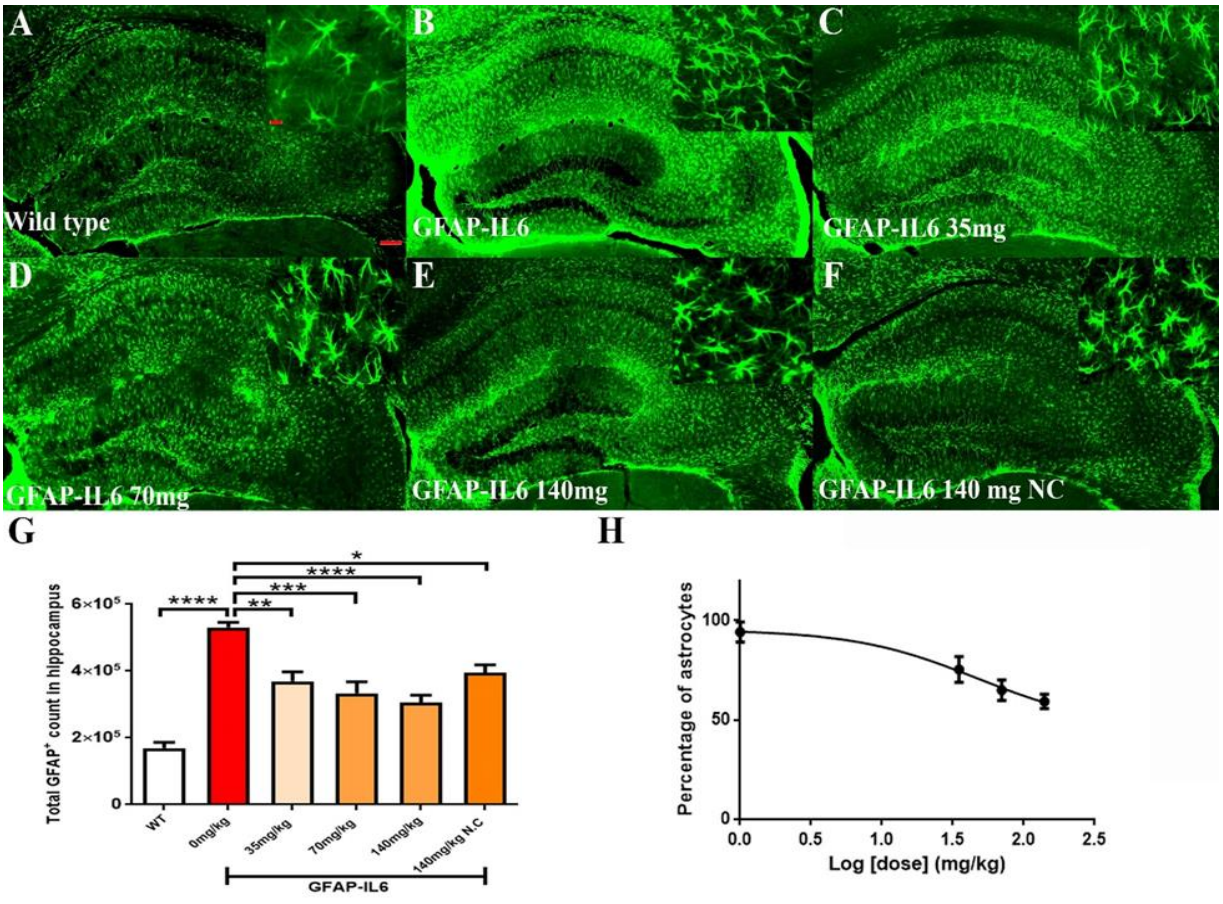

Figure 12. Curcumin formulations decreased $GFAP^+$ astrocytes in the hippocampus of GFAP-IL-6 mice. (A-F) Representative photomicrographs of immunofluorescence staining for the astrocytes ($GFAP^+$ cells) in the hippocampus. (Magnification 5x, scale bar=100µm in 5x and 50µm in inserts). Images are representative of at least

six animals per group (n=6). (BG) Graphical representation of total GFAP count in the hippocampus. The Graph represents the mean± SEM and significant differences were determined using a one-way analysis of variance (ANOVA). Significance = *p <0.05, **p <0.001, ***P <0.0001, ****p < 0.0001. (H) A dose-response curve showing the percentage decrease in a number of astrocytes against log dose concentration (mg/kg) of MCP in the hippocampus

4.1.2.6 Curcumin formulations decreased GFAP$^+$ astrocytes in the cerebellum of GFAP-IL-6 mice

In the cerebellum, the astrocytes and their processes were very abundant and densely packed, making stereological counting difficult, hence the numbers of GFAP$^+$ cells were not analyzed. However, high-level expression of GFAP protein was observed in GFAP-IL6 mice compared to WT mice, located mostly but not exclusively in the gray matter of the cerebellum, with a strong presence of elongated microglia in the white matter and molecular layer. The difference in the distribution of astrocytes between the WT and GFAP-IL6 animals was substantial. No conclusions could be drawn in the absence of quantitative stereology. (Fig 13).

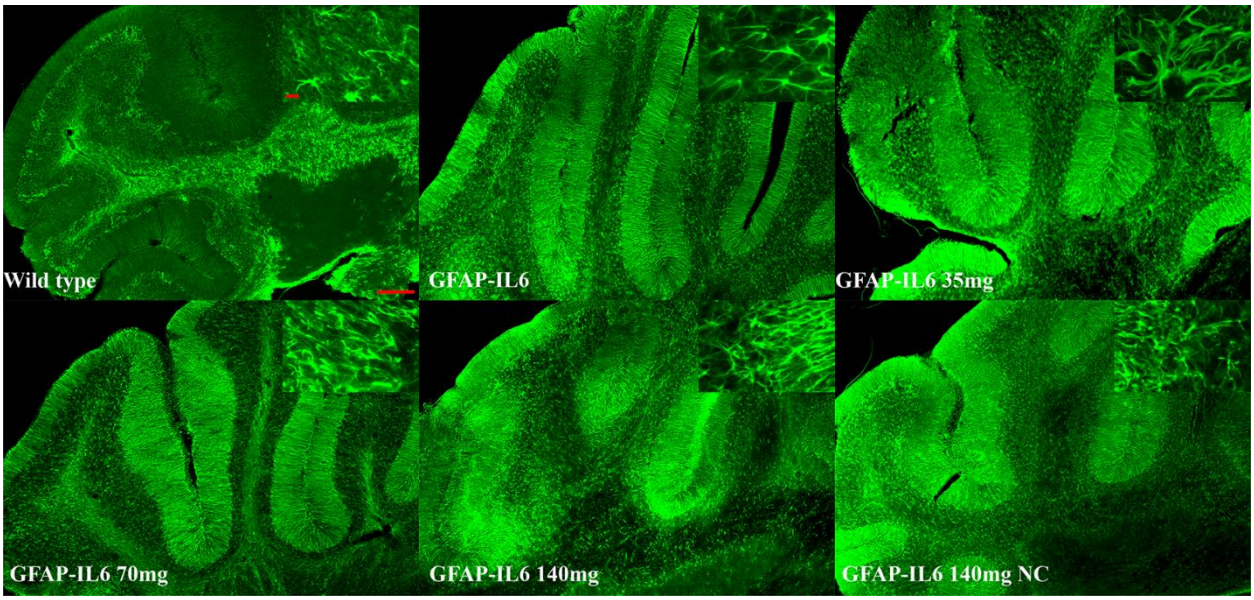

Figure 13.Effect of curcumin formulations on the GFAP$^+$ astrocytes in the cerebellum of GFAP-IL-6 mice. Representative photomicrographs of immunofluorescence staining for the astrocytes (GFAP$^+$ cells) in the cerebellum. (Magnification 5x, scale bar=100µm in 5x and 50µm in inserts). Images are representative of at least six animals per group (n=6).

Table 4. Stereological counting summary of the Iba-1, TSPO positive microglia in the hippocampus and the cerebellum and GFAP positive astrocytes in the hippocampus. All values are presented as mean ± SEM

Cohorts	Diet	Iba-1 hippocampus (Mean+/- SEM)	Iba-1 cerebellum (Mean+/- SEM)	TSPO hippocampus (Mean+/- SEM)	TSPO cerebellum (Mean+/- SEM)	GFAP hippocampus (Mean+/- SEM)
WT	Normal food	175192±12098	154058± 12871	4747±1579	12402±3601	169908±8523
GFAP-IL6	Normal food	438550±29717	1025205±104467	147803±20895	369963±68420	530374±15224
GFAP-IL6	MCP 35mg	361644±20593	693938±117878	123769±6266	276303±40166	369401±28724
GFAP-IL6	MCP 70mg	338483±33212	592373±48489	119213±11229	278235±35052	333646±34828
GFAP-IL6	MCP 140mg	323451±21520	605085±63857	98941±8094	215912±30405	304668±23679
GFAP-IL6	NC 140mg	357955±26079	629122±54363	108323±8124	242110±12527	395739±23531

4.1.2.7 Correlation analysis among the Iba-1$^+$ microglia, TSPO$^+$ microglia, and GFAP$^+$ astrocytes

Since the activation of the glial cell were assessed through Iba-1, TSPO and GFAP markers, therefore, in order to see whether Iba-1$^+$ microglia correlate with the TSPO$^+$ microglia and GFAP$^+$ in WTs, GFAP-IL6 normal fed and GFAP-IL6 fed, the Iba-1$^+$ microglial count was plotted against TSPO$^+$ cell count. A strong correlation was observed between the two markers in both the cerebellum (R = 0.76, and the hippocampus (R=0.54) (Fig 15A-B). There was also a strong correlation between the Iba-1$^+$ microglial number and GFAP$^+$ astrocytes number (R=0.50) in the hippocampus (Fig 14C). Additionally, the numbers of TSPO$^+$ microglia and GFAP$^+$ astrocytes were also correlated in the hippocampus (R = 0.54) (Fig 14D).

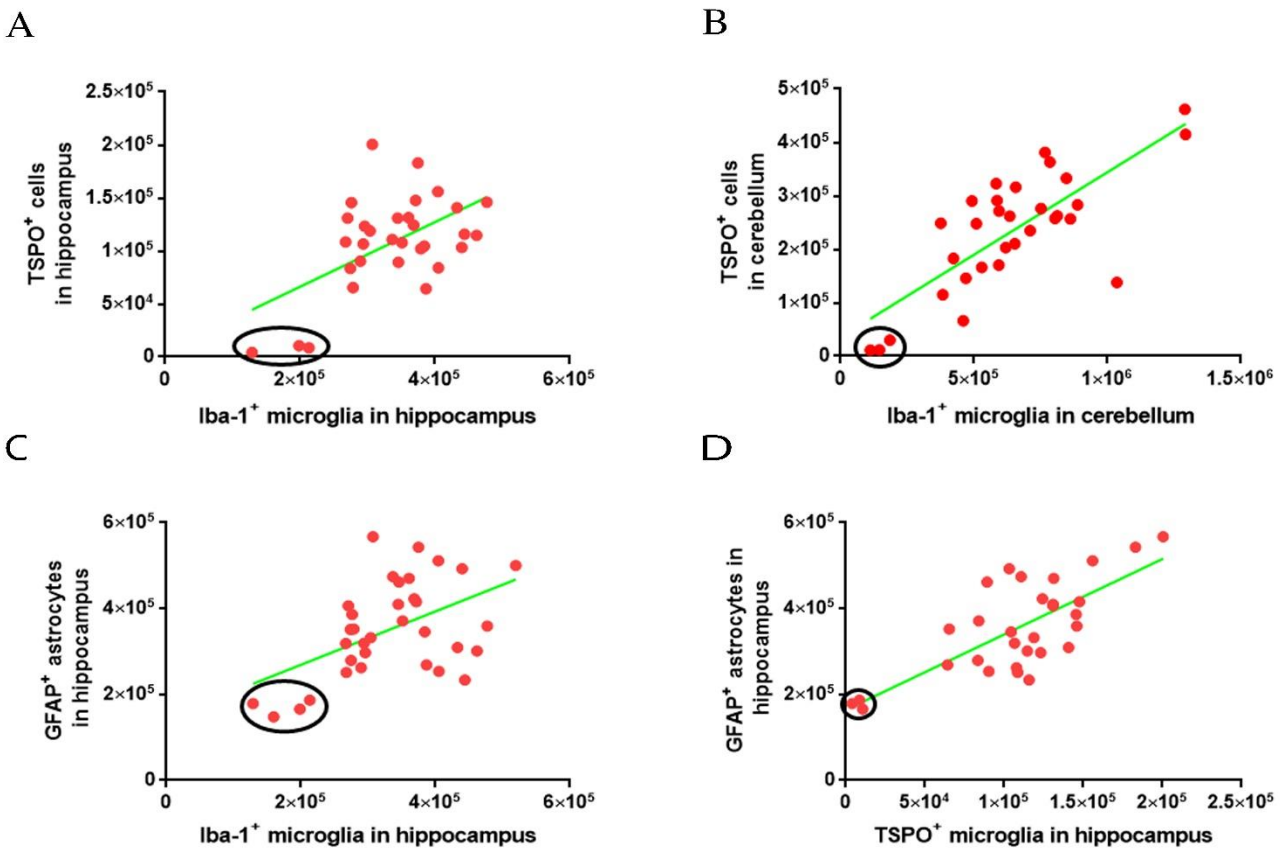

Figure 14. Correlation analysis among the Iba-1$^+$ microglia, TSPO$^+$ microglia, and GFAP$^+$ astrocytes. (A) Graphical representation of the correlation between Iba-1$^+$ microglia and TSPO$^+$ cells in the cerebellum. The data were analyzed using linear regression and correlation. ****p <0.0001, R^2=0.58 (n=31) (B) Graphical representation of the correlation between Iba-1$^+$ microglia and TSPO$^+$ cells in hippocampus. The data were analyzed using linear regression and correlation. **p <0.001, R^2=0.29 (n=31) (C) Graphical representation of the correlation between Iba-1$^+$ microglia and GFAP$^+$ astrocytes in hippocampus. The data were analyzed using linear regression and correlation. **p <0.002, R^2=0.25 (n=34) (D) Graphical representation of the correlation between TSPO$^+$ microglia and GFAP$^+$ astrocytes in hippocampus. The encircled dotes are WT mice. The data were analyzed using linear regression and correlation. ****p <0.0001, R^2=0.54 (n=30)

4.1.3. Summary

Our results indicate that the high dose of highly bioavailable curcumin is able to attenuate the chronic neuroinflammation. After feeding the mice with MCP for four weeks, it was observed that all three doses of MCP significantly reduced the number of Iba-1^+ microglia in the cerebellum and the hippocampus, with the high dose of MCP resulting in the most significant decrease.

This study found that the total estimated number of $TSPO^+$ cells was significantly larger in the GFAP-IL6 group than that of the WT group in the cerebellum and the hippocampus. The 140mg/kg of MCP significantly downregulated chronic neuroinflammation in GFAP-IL6 mice in both the hippocampus and the cerebellum compared to the non-fed group. TSPO is a translocator protein that is mainly expressed in microglia, astrocytes and at low levels in neurons in diseased brains (Cosenza-Nashat et al. 2009). In a study conducted in mice has measured the fluorescence intensity and the number of $TSPO^+$ per $0.1mm^2$, has reported that TSPO expression is elevated in the brain after exposure to an injury or inflammation (Bonsack, Alleyne, and Sukumari-Ramesh 2016). This is consistent with our findings which showed that the number of Iba-1^+ and TSPO+ microglia in GFAP-IL6 mice was significantly larger compared to WT mice.

Additionally, all three doses of MCP significantly decreased the number of reactive astrocytes in the hippocampus compared to the GPAP-IL6 control mice. These results indicate that the high dose MCP is effective in attenuating neuroinflammation.

4.2. Effect of Meriva® curcumin phytosome on the morphological characteristics of astroglial cells in the GFAP-IL6 mouse model

4.2.1 Introduction

As discussed earlier, microglia and astrocytes play a key role in CNS's innate immunity. Microglial cells are the key neuroinflammatory cells as they are activated in response to brain inflammation and release ROS as well as cytokines that cause neurotoxicity (Block, Zecca, and Hong 2007b; Beggs and Salter 2007).

The morphological features are one of the important characteristics of microglial cells. Under normal circumstances, the resting microglia continuously scans the nervous system which is termed as ramified morphology (Nimmerjahn, Kirchhoff, and Helmchen 2005). During inflammatory conditions, the microglial cells have been observed to go into an "activated state" characterized by swollen cell body and thick processes and can adopt an amoeboid-like morphology termed as "de-ramified microglia" (Davis, Foster, and Thomas 1994). Similarly, the astrocytes morphology is also considered as a hallmark for neurodegenerative diseases. Astrocytes have bushy or spongiform shapes and fine and delicate processes emerging from the soma (Bushong et al. 2002). In neuroinflammation, when astrocytes are activated, they are characterized by high-level expression of GFAP and an increase in size and the number of processes compared to the non-reactive astrocytes (Silver and Miller 2004; McGraw, Hiebert, and Steeves 2001).

The study represents the effect of a high bioavailability curcumin formulation MCP curcumin on the morphology of astroglial cells in the GFAP-IL6 mouse model. To determine how MCP affects the morphology of activated (Iba-1^{+}) microglia and activated ($GFAP^{+}$) astroglia in the brain, 3D reconstruction techniques were applied to assess the morphology of reactive and nonreactive microglia and astrocytes in the hippocampus and the cerebellum in an unbiased manner.

4.2.2 Results

4.2.2.1 Effect of curcumin formulations on the morphological characteristics of microglial cells in the hippocampus

In order to demonstrate how chronic inflammation affects the morphology of the microglia, we analyzed the anatomical features of the Iba-1^+ microglia in the WT and GFAP-IL6 animals in the hippocampus. Then, to investigate the effects of MCP on microglia morphology, GFAP-IL6 mice fed with MCP at different doses and normal curcumin at a dose of 140mg/kg bw/d were included in the analysis.

In the hippocampus, a difference between the genotypes was observed, as Iba-1^+ microglial cells of GFAP-IL6 mice had significantly larger soma areas (66.36 ± 22.63μm^2), soma perimeters (33.93 ± 8.18μm) and more processes (5.62 ± 1.84) than those of WT mice [soma area (30.005 ± 13.93μm^2), soma perimeter (20.63 ± 5.50μm) and number of processes (3.66 ± 1.36)]. GFAP-IL6 mice fed with 140mg/kg dose of MCP had significantly decreased soma area (42.55 ± 9.45), soma perimeter (25.47 ± 3.44) and increased the number of nodes compared to GFAP-Il6 mice on normal food (10.75 ± 3.49) (Fig. 15 A-H, Table 5). The rest of the lower MCP doses and the 140mg NC did not result in significant changes in any of the measured parameters.

A

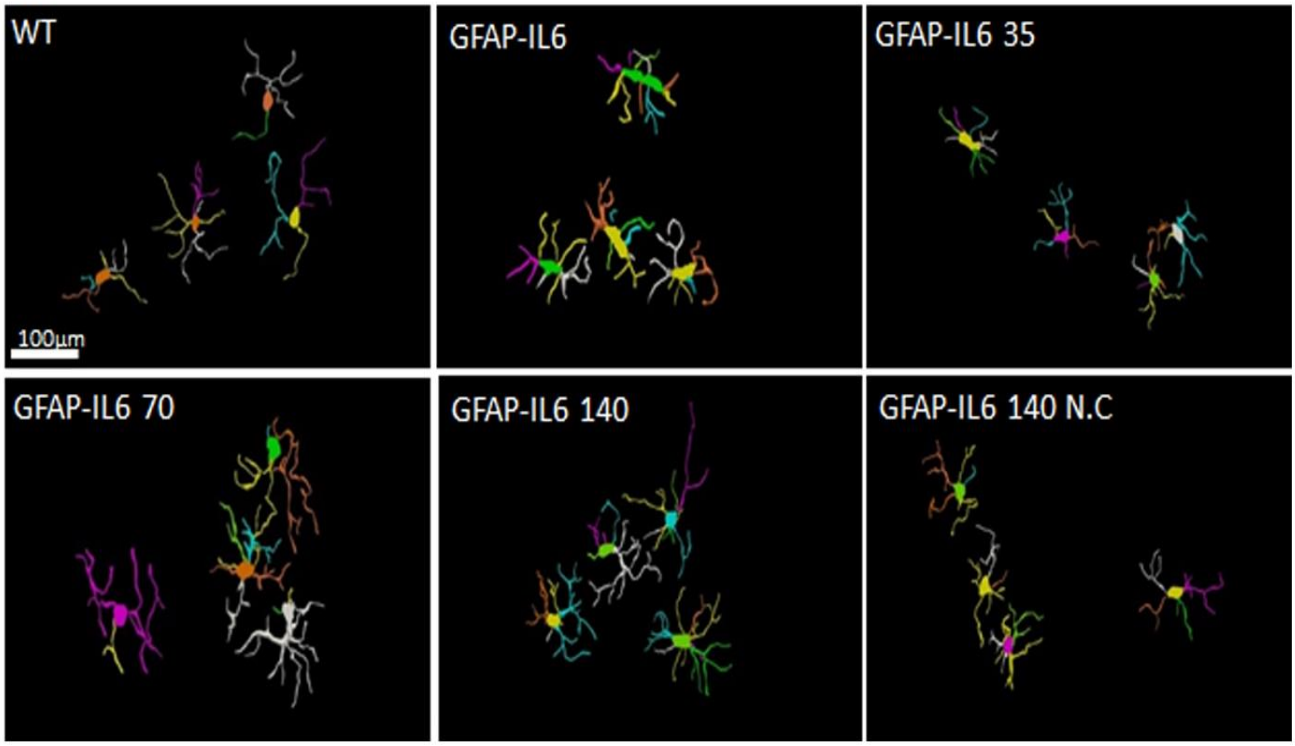
WT
GFAP-IL6
GFAP-IL6 35
100µm
GFAP-IL6 70
GFAP-IL6 140
GFAP-IL6 140 N.C

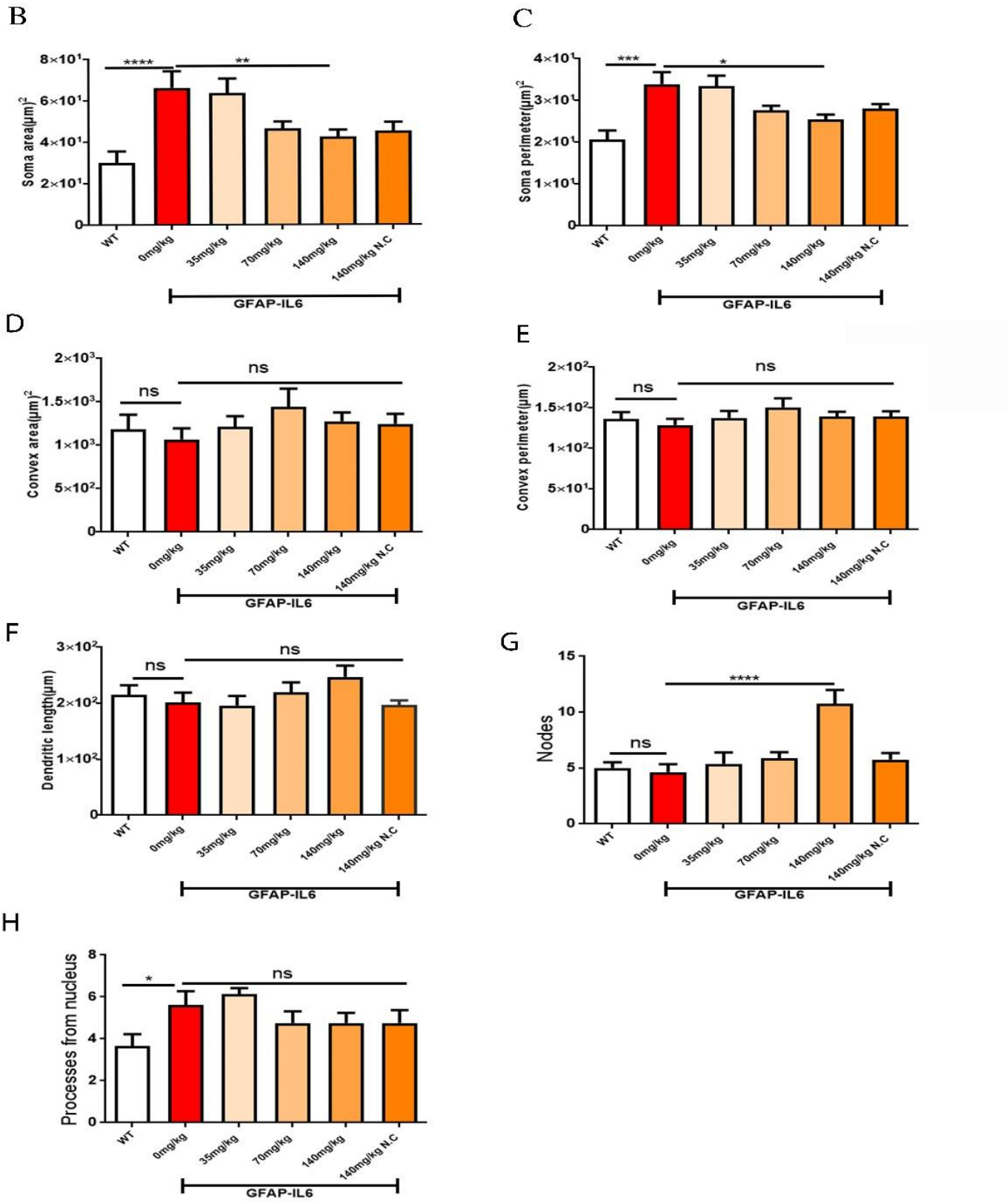
B
Soma area(μm)²
8×10¹
6×10¹
4×10¹
2×10¹
0
****
**
WT
0mg/kg
35mg/kg
70mg/kg
140mg/kg
140mg/kg N.C
GFAP-IL6
C
Soma perimeter(μm)²
4×10¹
3×10¹
2×10¹
1×10¹
0
***
*
WT
0mg/kg
35mg/kg
70mg/kg
140mg/kg
140mg/kg N.C
GFAP-IL6
D
Convex area(μm)²
2×10³
1.5×10³
1×10³
5×10²
0
ns
ns
WT
0mg/kg
35mg/kg
70mg/kg
140mg/kg
140mg/kg N.C
GFAP-IL6
E
Convex perimeter(μm)
2×10²
1.5×10²
1×10²
5×10¹
0
ns
ns
WT
0mg/kg
35mg/kg
70mg/kg
140mg/kg
140mg/kg N.C
GFAP-IL6
F
Dendritic length(μm)
3×10²
2×10²
1×10²
0
ns
ns
WT
0mg/kg
35mg/kg
70mg/kg
140mg/kg
140mg/kg N.C
GFAP-IL6
G
Nodes
15
10
5
0
****
ns
WT
0mg/kg
35mg/kg
70mg/kg
140mg/kg
140mg/kg N.C
GFAP-IL6
H
Processes from nucleus
8
6
4
2
0
*
ns
WT
0mg/kg
35mg/kg
70mg/kg
140mg/kg
140mg/kg N.C
GFAP-IL6

Figure 15. Effect of curcumin formulations on the morphological characteristics of Iba-1^{+} microglial cells in the hippocampus. (A) Morphological assessment of reactive and nonreactive microglia in the hippocampus. (B-H) Microglias in the inflamed mice have significantly larger soma area, soma perimeter and processes compared to the WT mice. High dose MCP significantly reduced soma area and soma perimeter compared to GFAP-IL6 mice. However, the same high dose MCP significantly increased the number of nodes compared to the GFAP-Il6 mice. It has no effect on the convex area, convex perimeter, dendritic length and number of processes.

Sholl analysis, a quantitative analysis to investigate the morphological characteristics, of microglial cells from the hippocampus revealed some further variations in morphology between WT and GFAP-IL6 normal food fed, GFAP-IL6 MCP fed and normal curcumin-fed mice characteristics. In the hippocampus, the microglias of GFAP-IL6 mice have a significantly larger surface area, process volume, and process diameter than that of WT mice. In MCP fed mice, the 70mg/kg and 35mg/kg significantly reduced the process volume and diameter whereas, 140mg/kg significantly decreased the process volume and surface area, while it significantly increased the number of nodes compared to the microglia of normal fed GFAP-IL6 mice (Fig. 16 A-F).

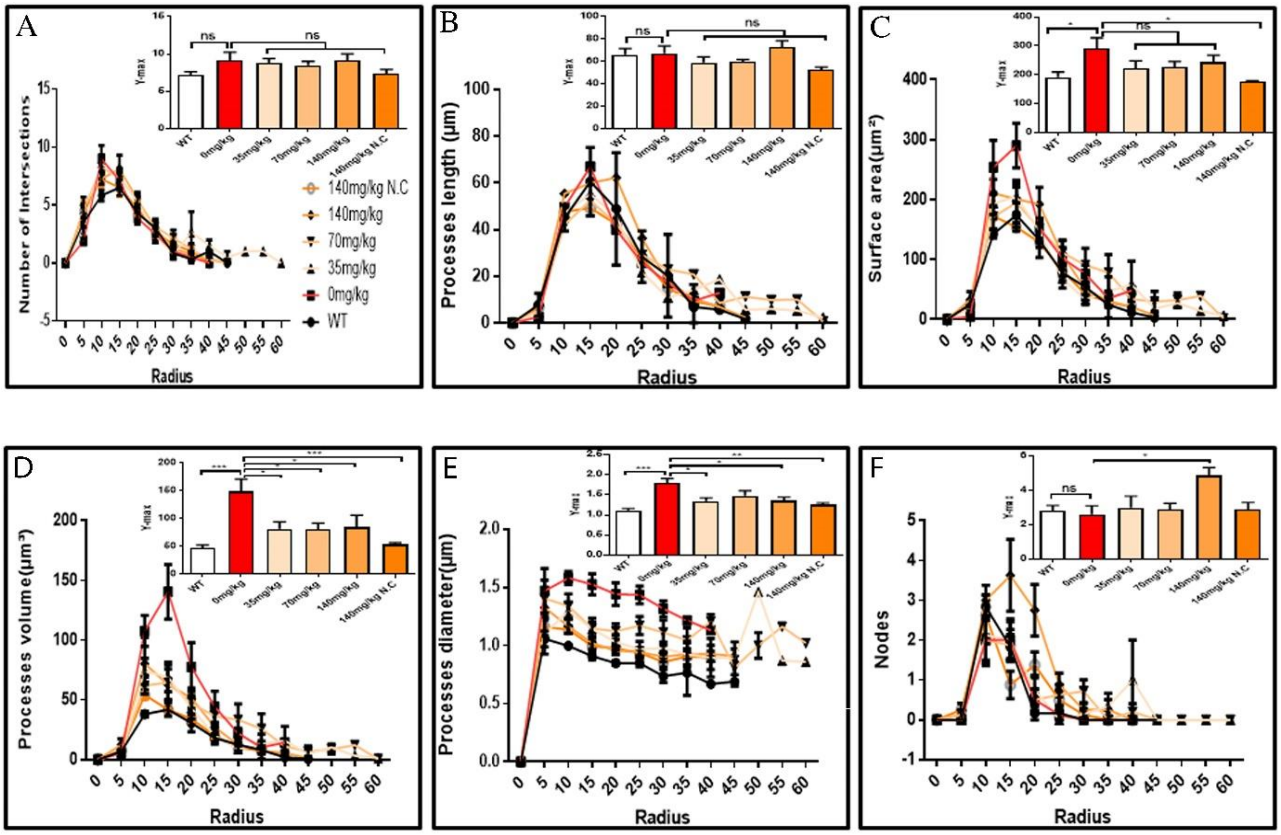

Figure 16. Effect of curcumin formulations on the morphological characteristics of Iba-1^{+}microglial cells in the hippocampus. A Sholl analysis revealed a significant change in the surface area, processes volume and processes diameter of microglia between wild type and GFAP-IL6 inflamed microglia both in the hippocampus. (A-F) MCP retracted processes volume and processes diameter compared to the GFAP-IL6 mice whereas; the normal curcumin significantly affected the surface area and a number of nodes.

In the hippocampus, correlation analysis of microglial cell size with each morphological characteristic revealed significant correlations with soma area in WT and 70mg/kg, with convex perimeter in all cohorts, and with dendritic length in curcumin-treated cohorts, which revealed that microglial cells of WT and 70 mg/kg fed groups tended to increase the size of the soma area. It also shows that the convex perimeter of the microglia of each cohort increased with the increasing size of the cells, whereas, the dendritic length of the microglia of the fed cohorts were increased with the overall cell size. Despite these changes, soma area, soma perimeter, nodes and number of dendrites of microglia of all treated cohorts remained consistent regardless of the cell size (Fig 17, Table 6).

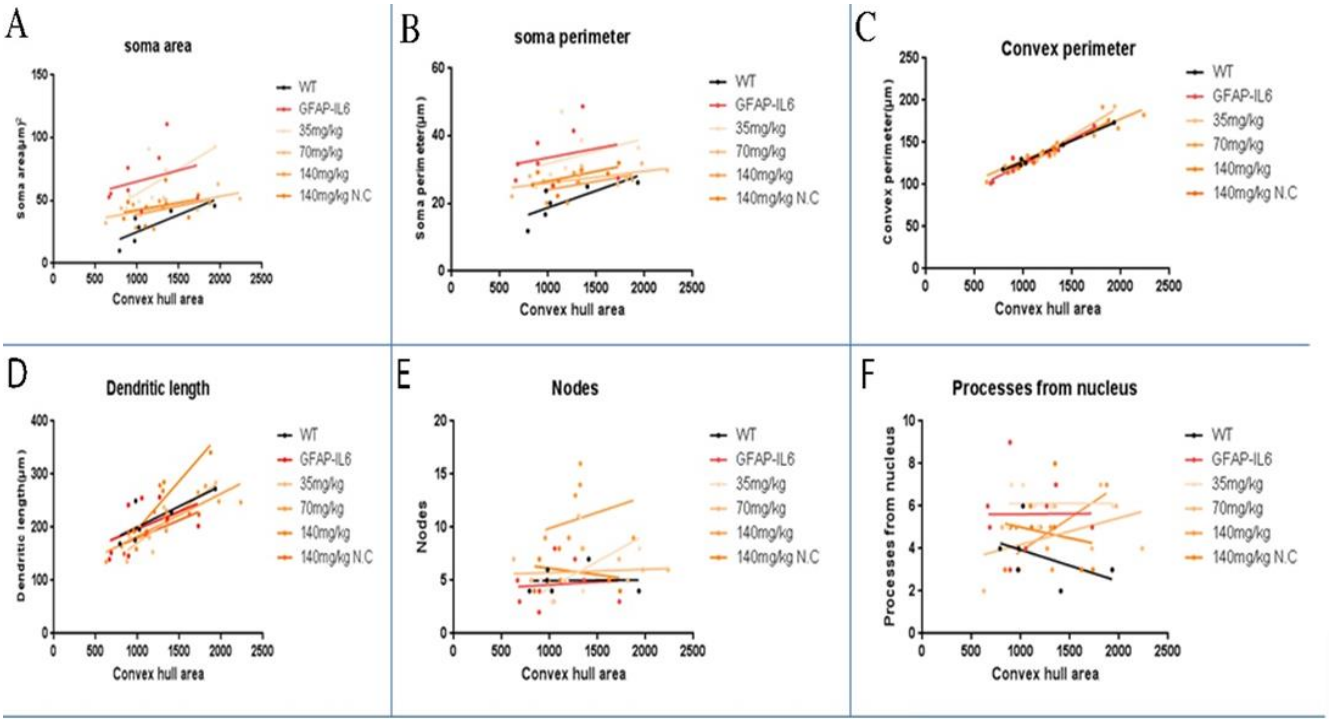

Figure 17. Bivariate correlation: MCP effects on morphology are dose-independent in the hippocampus. (A-F) Different morphological parameters have been plotted against the convex hull area to see the bivariate correlation between WT, GFAP-IL6 and between non-treated and treated ones. The statistical analysis has been summarized in tables S1. We found that the convex perimeter of both wild type and GFAP-IL6 are significantly correlated whereas, treatment with any dose of MCP gave significant correlation and change in the slope of linear correlation of convex perimeter and dendritic length in the hippocampus compared to GFAP-IL6 mice. ANCOVA and Sum-of-Square tests.

Table 5. Morphological analysis of Iba-1$^+$ microglia

Cohorts	Diet	Soma area(μm)^2 (Mean±SEM)		Soma perimeter (μm) (Mean ± SEM)		Convex 2D (area) (μm)^2(Mean ± SEM)		Convex perimeter (μm) Mean ± SEM)		Total length of dendrites (μm) (Mean± SEM)		Nodes (Mean ± SEM)		Dendrites (Mean ± SEM)	
		H	C	H	C	H	C	H	C	H	C	H	C	H	C
WT	Normal food	30.005±5.68	30.03±3.52	20.63±2.24	20.55±1.34	1183.93±171	1197.53±126.4	136.4±8.50	140.93±4.69	215.15±16.99	208.81±20.25	5±0.51	4.33±0.91	3.66±0.55	4.33±0.42
GFAP-IL6	Normal food	66.36±8.0	66.64±4.46	33.93±2.89	33.3±1.00	1067±128.8	1014.54±178.3	128.78±7.84	121.73±11.26	201.55±17.47	168.81±24.81	4.62±0.73	4.75±0.67	5.62±0.65	5.25±0.25
GFAP-IL6	MCP 140mg	42.55±3.34	42.48±4.48	25.47±1.21	26.3±1.60	1277.96±99.78	1617.23±218.1	139.21±5.97	156.31±12.2	247.0±20.44	235.22±23.6	10.75±1.23	7.37±1.08	4.75±0.49	6.87±0.58
GFAP-IL6	MCP 70mg	46.57±3.31	47.62±4.11	27.63±1.16	26.5±1.19	1446.16±205.5	1570.76±60.69	150.95±10.72	154.92±3.21	219.16±18.29	226.28±9.20	5.87±0.54	8.12±1.21	4.75±0.55	5.25±0.52
GFAP-IL6	MCP 35mg	63.82±6.89	55.34±5.30	33.43±2.52	31.11±2.54	1216.13±119.8	1040.06±33.3	137.88±8.59	126.73±1.87	196.47±16.59	172.06±14.33	5.37±1.01	5.62±1.14	6.12±0.29	4.5±0.5
GFAP-IL6	NC 140mg	45.46±4.13	43.66±4.25	28.08±1.08	25.4±1.08	1248.86±114	1150.19±146.9	139.51±6.37	131.67±8.18	196.88±8.60	195.38±16.33	5.75±0.59	6.37±0.90	4.75±0.61	5±0.46

H=Hippocampus, C= Cerebellum

Table 6. Bivariate correlation of morphological characteristics with overall microglial cell size in the hippocampus

	Soma area		Soma perimeter		Convex perimeter		Dendritic length		Nodes		Primary dendrites	
	R^2	Correlation	R^2	Correlation	R^2	Correlation	R^2	Correlation	R^2	Correlation	R^2	Correlation
WT	0.67	*0.0453	0.58	0.0756	0.98	****<0.0001	0.61	0.0665	0	0.9718	0.2	0.3629
GFAP-IL6	0.08	0.4881	0.05	0.5626	0.92	***0.0001	0.23	0.2200	0	0.8238	0	0.9851
GFAP-IL6+35mg	0.47	0.0586	0.12	0.3955	0.95	****<0.0001	0.72	**0.0075	0.35	0.1211	0	0.9949
GFAP-IL6+70mg	0.58	*0.0281	0.38	0.1032	0.87	***0.0006	0.8	**0.0023	0.01	0.7821	0.21	0.2502
GFAP-IL6+140 mg	0.16	0.3164	0.16	0.3178	0.95	****<0.0001	0.78	**0.0035	0.05	0.5621	0.4	0.0905
GFAP-IL6+140 mg NC	0.1	0.4366	0.37	0.1091	0.91	***0.0002	0.79	**0.0031	0.05	0.6100	0.03	0.6555

4.2.2.2 Effect of curcumin formulations on the morphological characteristics of microglial cells in the cerebellum

In the cerebellum, microglial cells of GFAP-IL6 mice fed with normal food displayed significantly larger soma areas (66.64 ± 12.62) and soma perimeters (33.3 ± 2.84) as compared to those of WT mice [microglial soma area (30.03 ± 8.64) and soma perimeter (20.55 ± 0.28)]. In MCP fed mice, 70mg/kg MCP also reduced the soma perimeter of the microglia while, 140mg/kg dose significantly reduced the soma area (42.48 ± 12.69) and soma perimeter (26.3 ± 6.52), whereas, it significantly increased the convex area (1617.23 ± 617.94), convex perimeter (156.31 ± 56.31), and dendritic length of microglia (235.22 ± 35.73) compared to GFAP-IL6 controls. The 140mg/kg normal curcumin significantly reduced the soma area (Fig. 18 A-H, Table 5). The rest of the lower MCP doses did not result in significant changes in any of the measured parameters.

Sholl analysis, of microglial cells from the cerebellum, revealed some further variations in morphology. In the cerebellum of GFAP-IL6 mice, the Iba-1^+ microglia have a significantly

smaller surface area, process volume (0.0008), and process diameter (0.001) compared to microglia of WT mice. In MCP fed mice, the 35mg dose significantly downregulated the surface area and process volume while, 140mg dose significantly reduced the surface area, process volume, and the processing diameter of the microglia compared to the microglia of non-fed GFAP-IL6 mice. The 140mg NC also reduced the surface area, process volume, and the diameter of the processes (Fig. 19A -F).

In the cerebellum, some significant correlations were observed between the soma area and dendritic length of GFAP-IL6 microglia whereas, additional significant correlations were observed in convex perimeter in each cohort, showing that soma area and dendritic length of microglia change with the overall cell size, while the convex perimeter increased with the overall increase in microglial cells. The remaining perimeter measures had no effect and remained consistent regardless of the cell size (Fig 20, Table 7).

A

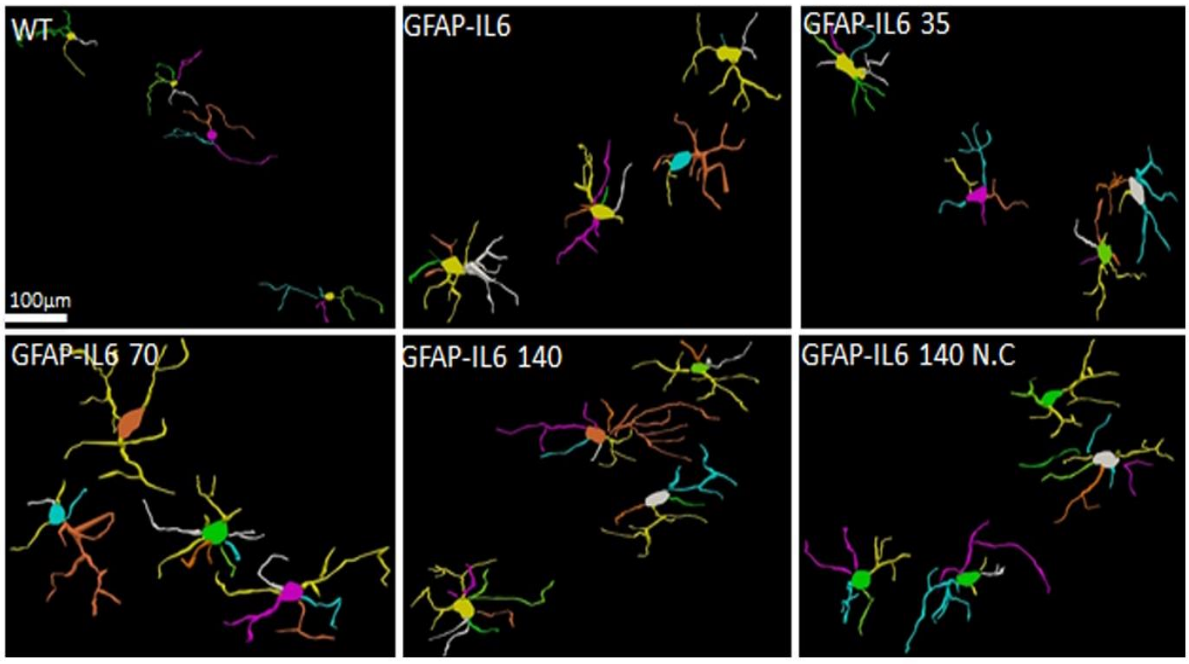

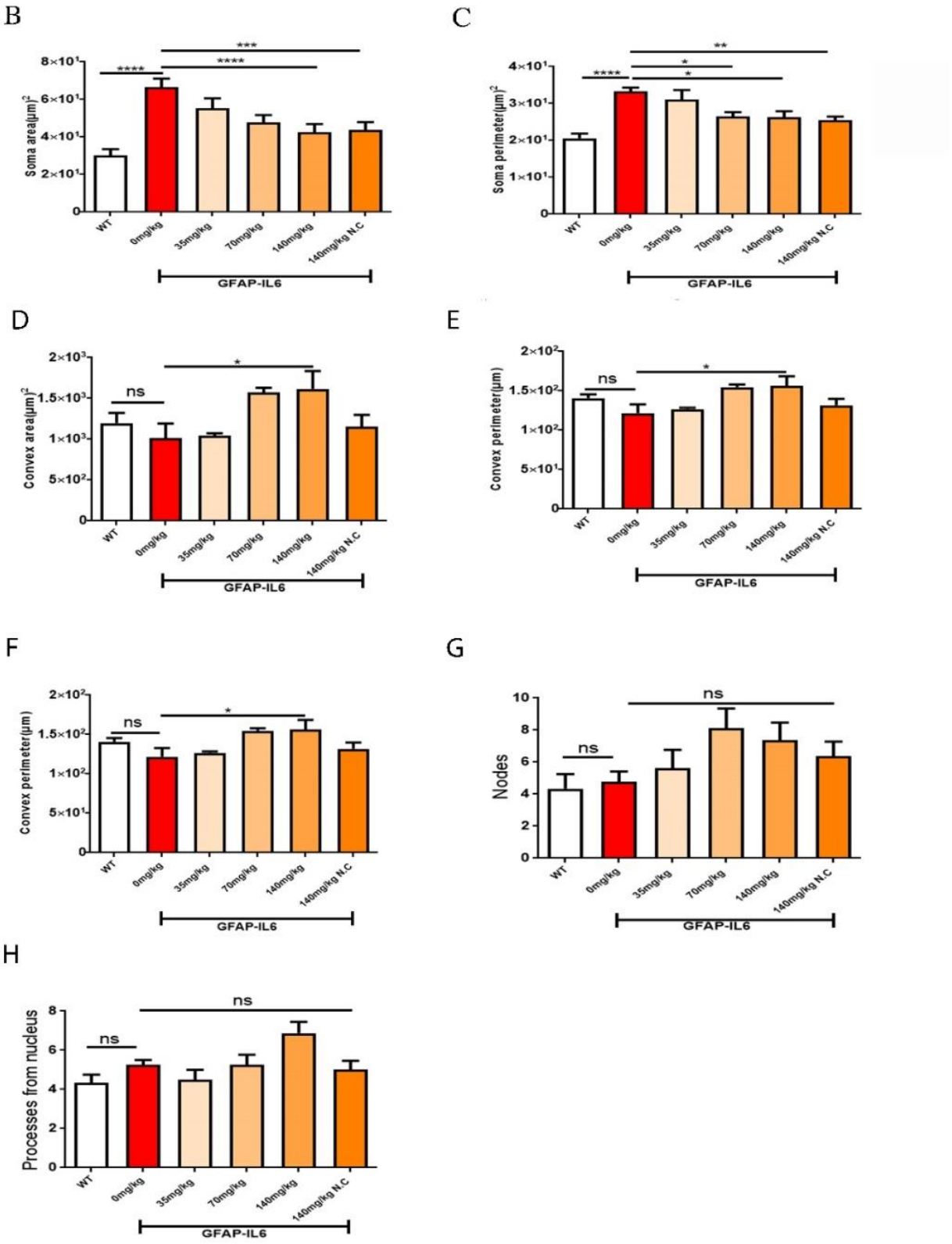
B
Soma area(µm)²
8×10¹
6×10¹
4×10¹
2×10¹
0
****
****
***
WT
0mg/kg
35mg/kg
70mg/kg
140mg/kg
140mg/kg N.C
GFAP-IL6
C
Soma perimeter(µm)²
4×10¹
3×10¹
2×10¹
1×10¹
0
****
*
*
**
WT
0mg/kg
35mg/kg
70mg/kg
140mg/kg
140mg/kg N.C
GFAP-IL6
D
Convex area(µm)²
2×10³
1.5×10³
1×10³
5×10²
0
ns
*
WT
0mg/kg
35mg/kg
70mg/kg
140mg/kg
140mg/kg N.C
GFAP-IL6
E
Convex perimeter(µm)
2×10²
1.5×10²
1×10²
5×10¹
0
ns
*
WT
0mg/kg
35mg/kg
70mg/kg
140mg/kg
140mg/kg N.C
GFAP-IL6
F
Convex perimeter(µm)
2×10²
1.5×10²
1×10²
5×10¹
0
ns
*
WT
0mg/kg
35mg/kg
70mg/kg
140mg/kg
140mg/kg N.C
GFAP-IL6
G
Nodes
10
8
6
4
2
0
ns
ns
WT
0mg/kg
35mg/kg
70mg/kg
140mg/kg
140mg/kg N.C
GFAP-IL6
H
Processes from nucleus
8
6
4
2
0
ns
ns
WT
0mg/kg
35mg/kg
70mg/kg
140mg/kg
140mg/kg N.C
GFAP-IL6

Figure 18. Effect of curcumin formulations on the morphological characteristics of microglial cells in the cerebellum. (A) Morphological assessment of reactive and nonreactive microglia in the cerebellum. (B-H) In the cerebellum, microglia in the inflamed mice have significantly high soma area and soma perimeter compared to the WT microglia. MCP and normal curcumin both significantly reduced the soma area while, CP high and medium dose with the normal curcumin significantly decreased the soma perimeter whereas, only the high dose MCP significantly increase the convex area, convex perimeter, and dendritic length compared to the GFAP-IL6 mice. One-way ANOVA, Tukey's post-test, Significance = **p* <0.01, ****p* < 0.001, *****p* < 0.0001. mean ± SEM)

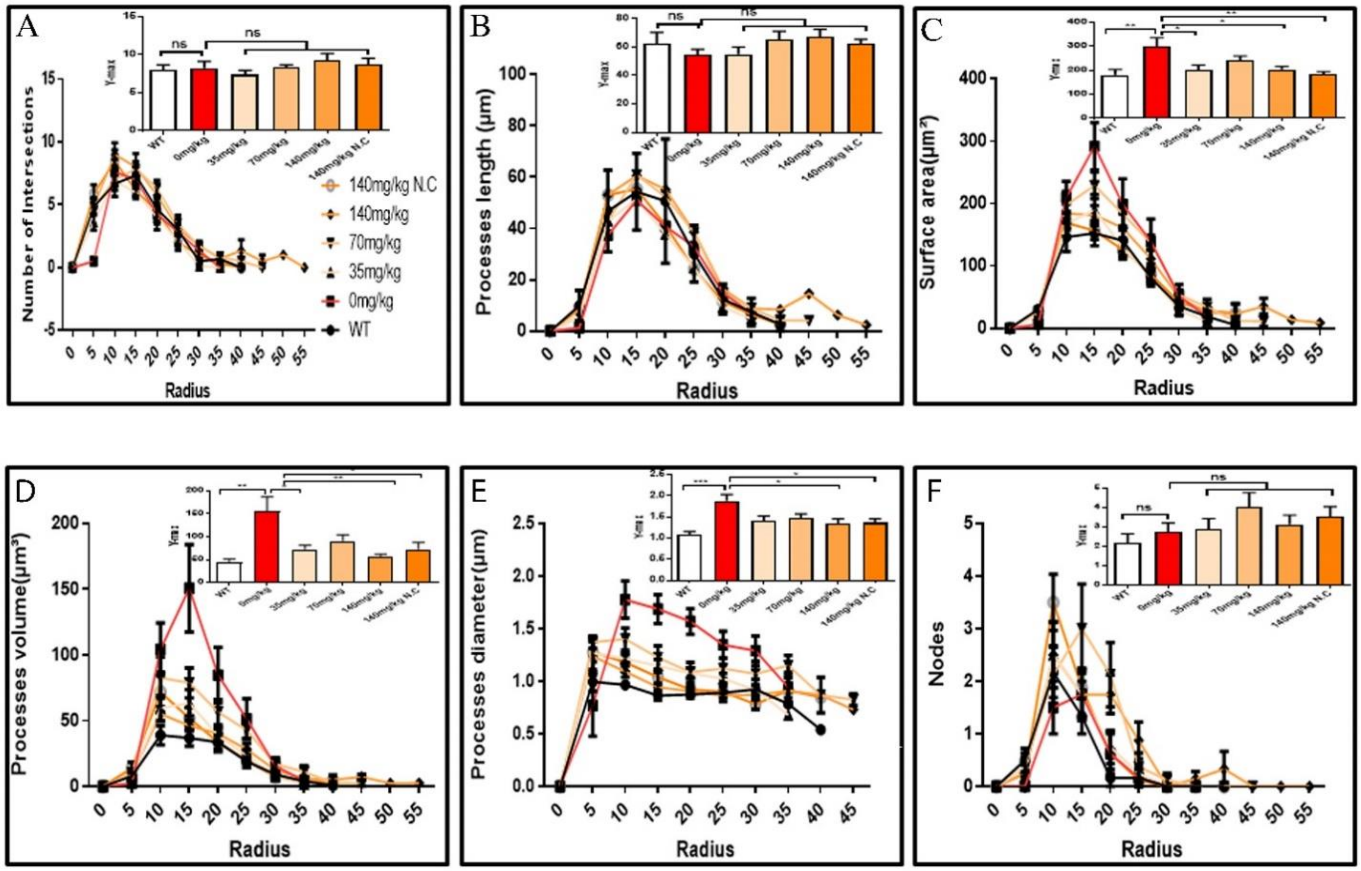

Figure 19: MCP and normal curcumin retract Iba-1^{+}microglia in the cerebellum. A Sholl analysis revealed a significant change in the surface area, processes volume and processes diameter of microglia between wild type and GFAP-IL6 inflamed microglia both in the cerebellum. (A-F) MCP and normal curcumin retracted surface area, processes volume and processes diameter compared to the inflamed microglia. this can be observed in the peaks of the distributions of different morphological features being closer to the center compared to wild-type and GFAP-IL6 mice, we call it X at Y_{max}. One-way ANOVA test.

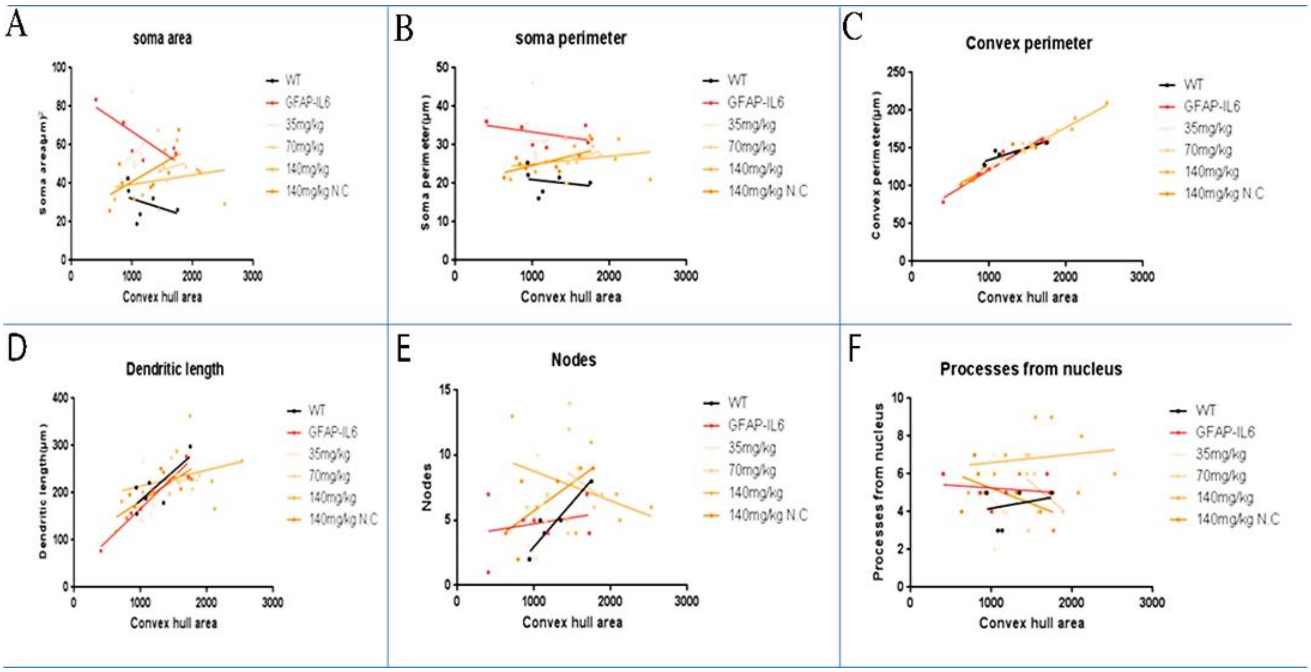

Figure 20. Bivariate correlation: MCP effects on morphology are dose-independent in the cerebellum. (A-F) Different morphological parameters have been plotted against the convex hull area to see the bivariate correlation between WT, GFAP-IL6 and between non-treated and treated ones. The statistical analysis has been summarized in tables. We found that medium and high doses of MCP showed a significant correlation in convex perimeter compared to the GFAP-IL6. ANCOVA and Sum-of-Square tests.

Table 7. Bivariate correlation of morphological characteristics with overall Iba-1$^+$ microglial cell size in the cerebellum

	Soma area		Soma perimeter		Convex perimeter		Dendritic length		Nodes		Primary dendrites	
	R^2	Correlation	R^2	Correlation	R^2	Correlation	R^2	Correlation	R^2	Correlation	R^2	Correlation
WT	0.13	0.4787	0.04	0.6975	0.77	*0.0204	0.59	0.0709	0.88	**0.0054	0.05	0.6602
GFAP-IL6	0.72	**0.0076	0.26	0.1937	0.95	****<0.0001	0.94	****<0.0001	0.06	0.5462	0.04	0.6103
GFAP-IL6+35 mg	0.04	0.6193	0	0.9659	0.46	0.0636	0	0.835	0.06	0.5371	0.08	0.4734
GFAP-IL6+70 mg	0.02	0.7305	0.08	0.471	0.78	**0.0035	0	0.9741	0.04	0.6067	0.17	0.2969
GFAP-IL6+140 mg	0.05	0.5692	0.07	0.5112	0.97	****<0.0001	0.09	0.4469	0.2	0.2572	0.02	0.6960
GFAP-IL6+140 mg NC	0.4	0.0877	0.46	0.0636	0.9	***0.0002	0.61	0.0205	0.48	0.0547	0.27	0.1787

4.2.2.3 Effect of curcumin formulations on the morphological characteristics of astrocytes in the hippocampus

During inflammation, astrocytes are thought to undergo cellular hypertrophy and increased the thickness of their main cellular processes. In order to investigate the difference in morphology of the astrocytes between WT and GFAP-IL6 normal food fed mice, GFAP-IL6 normal food and different doses of MCP food fed mice, the morphology of astrocytes was characterized in the hippocampus. Figure 21 A-F demonstrates the representative images of astrocytes immunostained for GFAP in the hippocampus. The astrocytes in the GFAP-IL6 normal food fed mice had significantly larger convex area (1247.74 ± 371.77μm^2), convex perimeter (142.27 ± 26.27μm), dendritic length (224.35 ± 66.24μm), and number of nodes (7.33 ± 2.49), when compared to astrocytes of WT mice [convex area (601.93 ± 201.46 μm^2), convex perimeter (95.04 ± 27.79 μm), dendritic length (107.68 ± 29.17 μm) and number of nodes (4.68 ± 1.0)]. In contrast, 70mg/kg dose significantly decreased the dendritic length (160.85 ± 30.96 μm) and the number of nodes (4.46 ± 1.94) whereas, 140mg fed MCP significantly decreased the convex area

(857.27 ± 200.79 µm^2) (p <0.02), dendritic length (139.72 ± 32.87µm), and the number of nodes (3.86 ± 2.61). (Table 8).

A

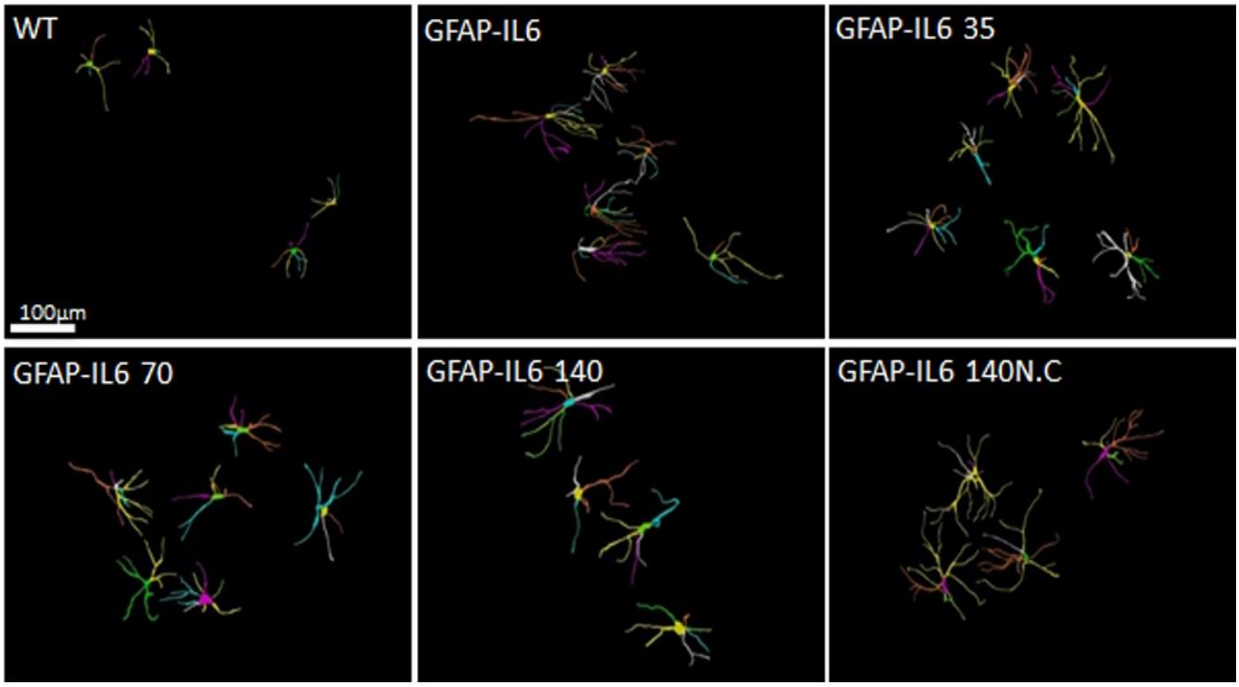

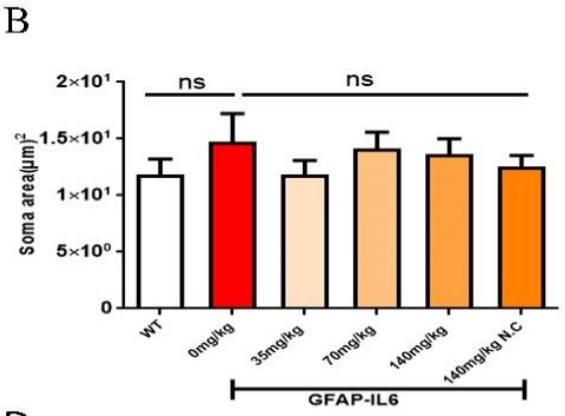
B
Soma area(µm)²
2×10¹
1.5×10¹
1×10¹
5×10⁰
0
ns
ns
WT
0mg/kg
35mg/kg
70mg/kg
140mg/kg
140mg/kg N.C
GFAP-IL6

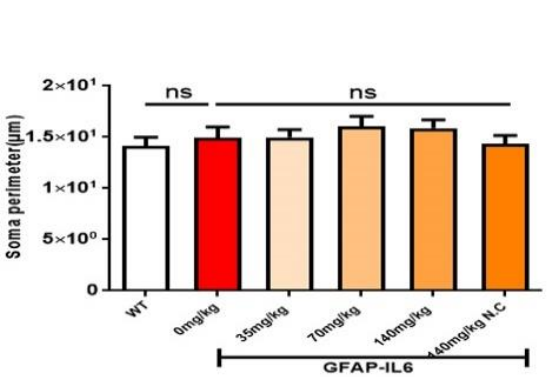
C
Soma perimeter(µm)
2×10¹
1.5×10¹
1×10¹
5×10⁰
0
ns
ns
WT
0mg/kg
35mg/kg
70mg/kg
140mg/kg
140mg/kg N.C
GFAP-IL6

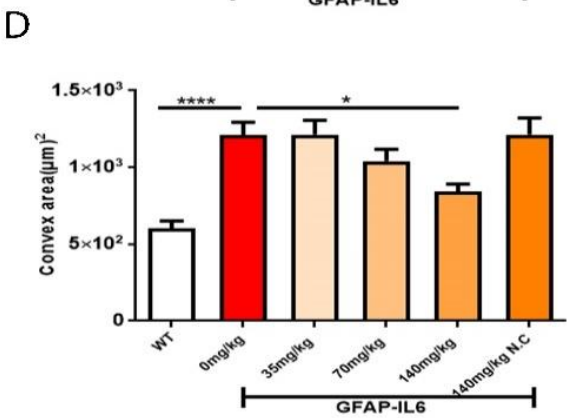
D
Convex area(µm)²
1.5×10³
1×10³
5×10²
0
****
*
WT
0mg/kg
35mg/kg
70mg/kg
140mg/kg
140mg/kg N.C
GFAP-IL6

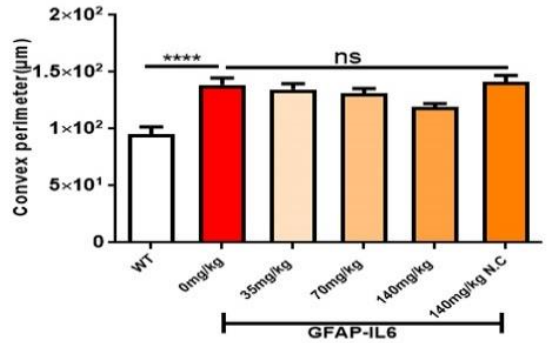
E
Convex perimeter(µm)
2×10²
1.5×10²
1×10²
5×10¹
0
****
ns
WT
0mg/kg
35mg/kg
70mg/kg
140mg/kg
140mg/kg N.C
GFAP-IL6

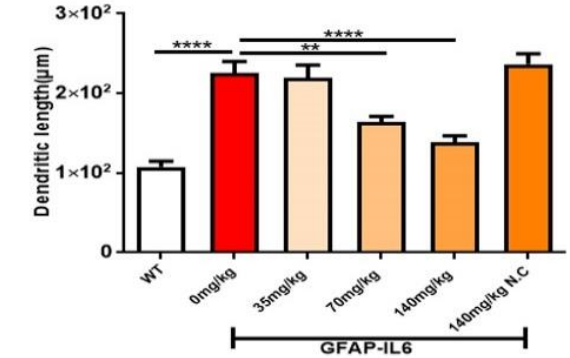
F
Dendritic length(µm)
3×10²
2×10²
1×10²
0
****
**
****
WT
0mg/kg
35mg/kg
70mg/kg
140mg/kg
140mg/kg N.C
GFAP-IL6

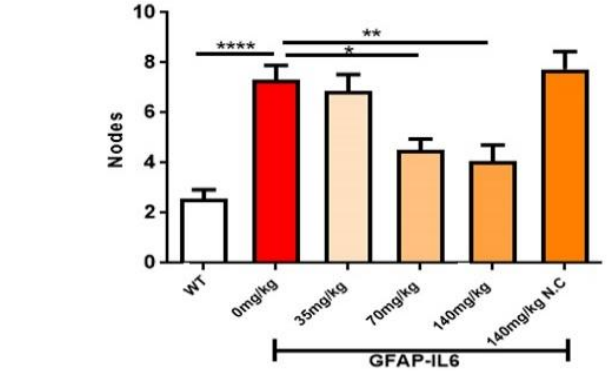
G
Nodes
10
8
6
4
2
0
****
*
**
WT
0mg/kg
35mg/kg
70mg/kg
140mg/kg
140mg/kg N.C
GFAP-IL6

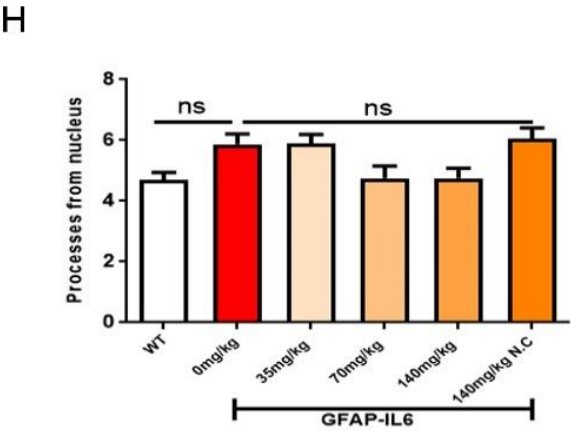
H
Processes from nucleus
8
6
4
2
0
ns
ns
WT
0mg/kg
35mg/kg
70mg/kg
140mg/kg
140mg/kg N.C
GFAP-IL6

Figure 21. Effect of curcumin formulations on the morphological characteristics of astrocytes in the hippocampus. (A) 3D reconstruction of astrocytes in WT and GFAP-IL6 in both treated and non-treated mice. (B-H) Astrocytes in the inflamed mice have a significantly high convex area, convex perimeter, dendritic length and nodes compared to WT. High dose MCP significantly decreased the convex area, dendritic length and nodes whereas, the medium dose also significantly decreased both the dendritic length and number of nodes compared to GFAP-IL6. One-way ANOVA, Tukey's post-test, Significance = *, **, **** p <0.02, 0.01,0.0001. mean ± SEM)

Furthermore, the morphology of astrocytes was quantified by Sholl analyses. This analysis revealed some phenotype differences in the number of intersections, processes length, surface area and a number of nodes, which were significantly larger in GFAP-IL6 mice compared to WT mice. In addition, it was found that 140mg/kg normal curcumin significantly reduced the number of intersections, and both 70mg/kg and 140mg/kg MCP significantly decreased the process length. Interestingly, 35mg/kg MCP and 140mg/kg normal curcumin increased the surface area, 35mg/kg, 70mg/kg and 140mg/kg and normal curcumin increased the process volume and length of the processes compared to the non-fed GFAP-IL6 mice. No effects of MCP were observed in the number of nodes (Fig 22 A-F).

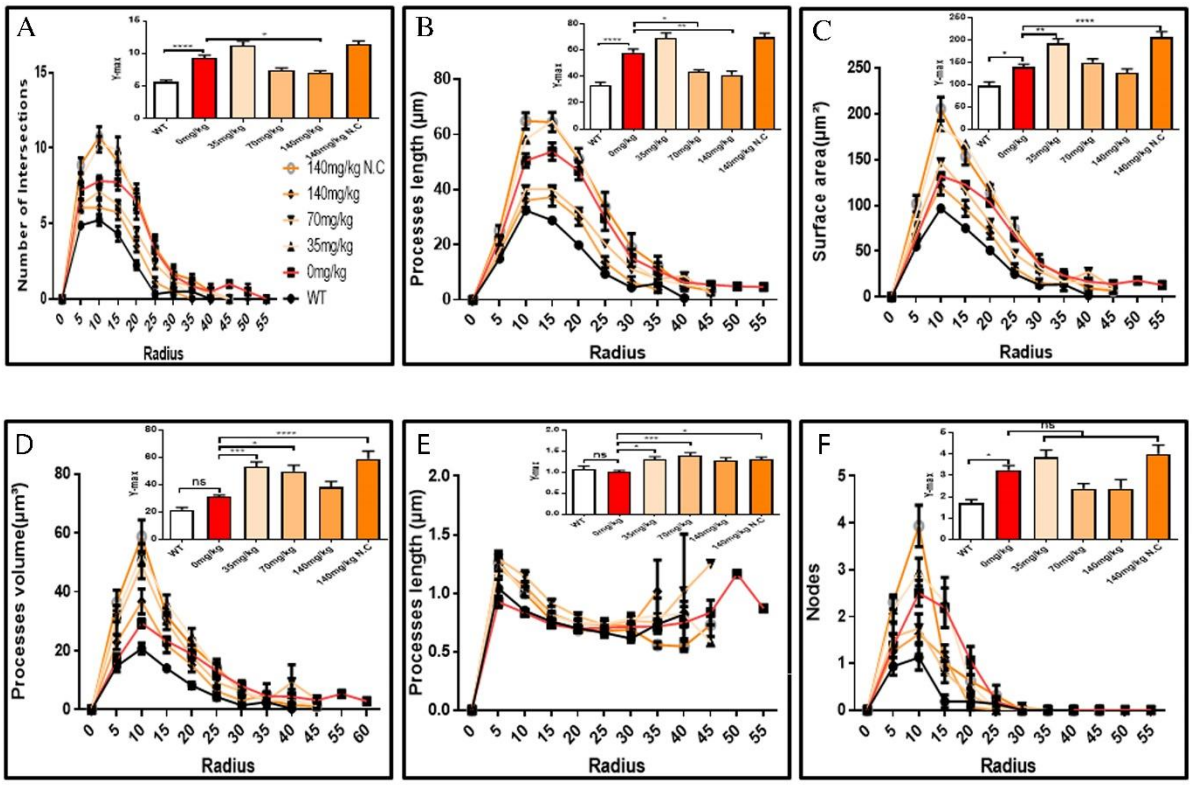

Figure 22: MCP and normal curcumin increase the ramification of astrocytes in the hippocampus region. (A-F) A Sholl analysis confirmed a significant increase in the number of the intersection, processes length, surface area,

and a number of nodes compared to wild type. In contrast, MCP significantly affects the inflamed astrocytes, which is observed in the peaks of the distributions of different morphological features being closer to the center compared to wild-type and GFAP-IL6 mice, we call it X at Y_{max}. One-way ANOVA test.

The bivariate correlations of morphological characteristics were performed with overall astroglial cell size to investigate the impact of the size of astroglial cells on the structural parameters. Some positive correlations of the astroglial cell size with morphological parameters were observed. Soma area and soma perimeter of astrocytes in the 35mg/kg CP group changed significantly with the overall change in the entire cells. The convex perimeter and dendritic length of all cohorts changed with the overall changes in astrocytes. It was also observed that the number of nodes in the astrocytes of 35mg/kg and 140mg/kg fed cohorts decreased when the overall size of the astrocytes decreased. In the case of primary dendrites, both the 70mg/kg and 140mg/kg doses positively decreased them with the decrease in the overall cell size of astrocytes (Fig 23, Table 9). Taken together, this study has revealed that the 140mg MCP decreased the activation and reduced the size of astrocytes, to a measure that is comparable to those seen in the WT brain.

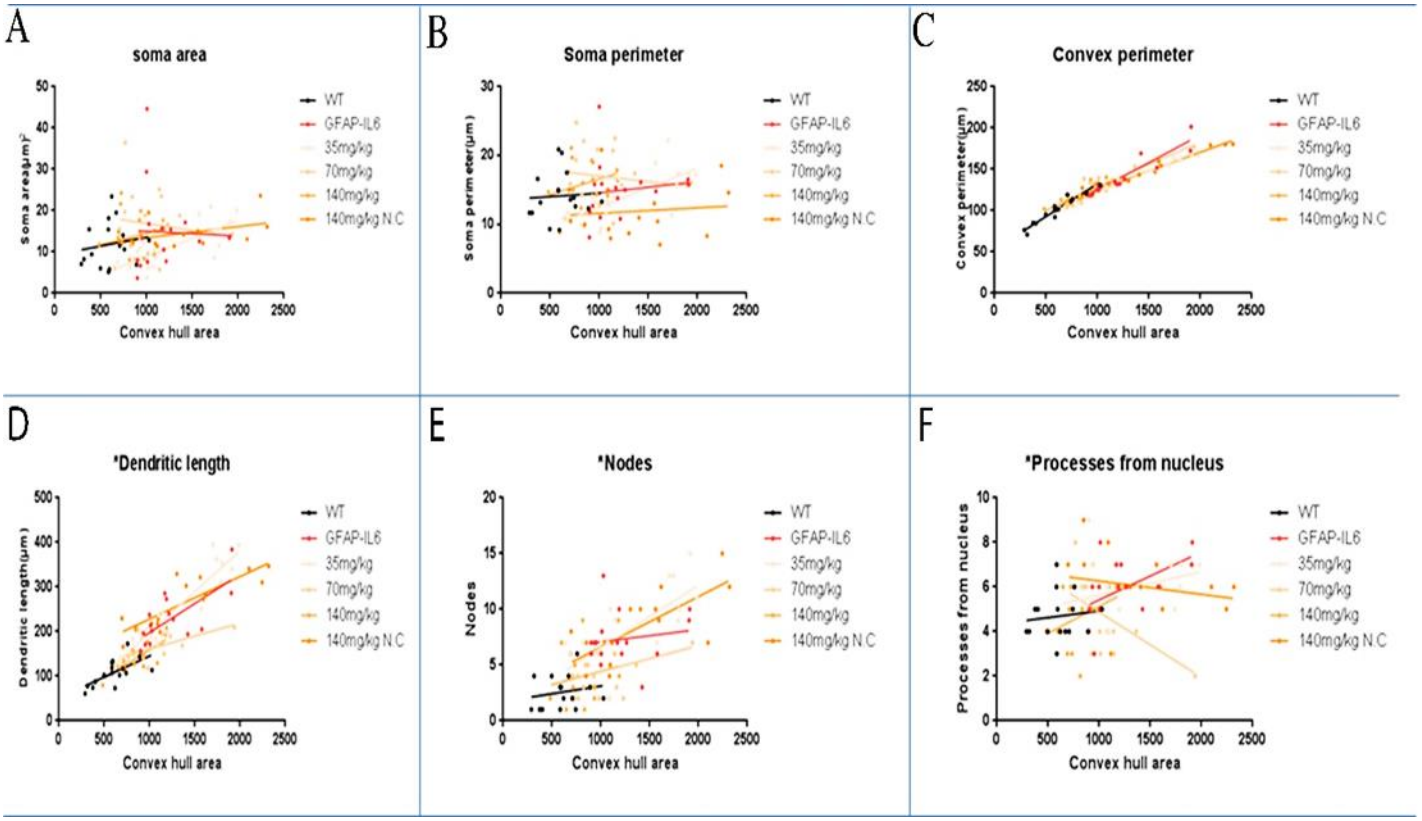

Figure 23. Bivariate correlation: MCP effects on astrocytes morphology are dose-independent in the hippocampus. (A-F) Different morphological parameters have been plotted against the convex hull area to see the bivariate correlation between WT, GFAP-IL6 and between non-treated and treated astrocytes which is summarized in Table S3. The analysis revealed that the convex perimeter and dendritic length are significantly correlated irrespective of the MCP dose. Whereas, in the case of a low dose of MCP, soma area, soma perimeter and nodes while the primary dendrites in medium dose, are significantly correlated compared to the GFAP-IL6 mice.

Table 8. Morphological analysis of GFAP$^+$ astrocytes in the hippocampus

Cohorts	Diet	Soma area $(\mu m)^2$ (Mean ± SEM)	Soma perimeter (µm) (Mean ± SEM)	Convex 2D (area) $(\mu m)^2$(Mean ± SEM)	Convex perimeter (µm) Mean ± SEM)	Total length (µm) (Mean ± SEM)	Nodes (Mean ± SEM)	Dendrites (Mean ± SEM)
WT	Normal food	16.84±1.36	14.13±0.84	601.93±50.37	95.04±6.94	107.68±7.29	2.56±0.36	4.68±0.25
GFAP-IL6	Normal food	13.96±2.48	13.93±1.04	1247.74±82.95	142.27±5.88	224.35±14.95	7.33±0.58	6.08±0.34
GFAP-IL6	MCP 35mg	11.20±1.23	13.86±0.76	1275.35±93.23	135.63±5.04	249.12±15.79	8.33±0.65	5.77±0.29
GFAP-IL6	MCP 70mg	18.67±1.48	18.10±0.99	1064.34±75.74	131.48±4.52	160.85±7.52	4.46±0.45	4.69±0.40
GFAP-IL6	MCP 140mg	14.16±1.39	16.34±0.82	857.27±51.17	120.36±3.20	139.72±7.98	3.86±0.66	4.8±0.33
GFAP-IL6	140mg NC	11.88±1.01	14.35±0.81	1347.6±107.9	141.11±6.03	261.31±13.01	8.18±0.70	6.06±0.34

Table 9. Bivariate correlation of morphological characteristics with overall astroglial cell size in the hippocampus

	Soma area		Soma perimeter		Convex perimeter		Dendritic length		Nodes		Primary dendrites	
	R^2	Correlation	R^2	Correlation	R^2	Correlation	R^2	Correlation	R^2	Correlation	R^2	Correlation
WT	0.02	0.5654	0	0.8276	0.93	****<0.0001	0.42	**0.0064	0.03	0.4794	0.01	0.6605
GFAP-IL6	0	0.8855	0.01	0.63	0.88	****<0.0001	0.52	**0.0014	0.02	0.561	0.27	*0.0375
GFAP-IL6+35mg	0.56	***0.0001	0.48	***0.0006	0.97	****<0.0001	0.88	****< 0.0001	0.53	***0.0003	0.11	0.139
GFAP-IL6+70mg	0.01	0.6311	0.01	0.6725	0.82	****<0.0001	0.33	*0.018	0.15	0.1357	0.3	*0.0272

4.2.3 Summary

Overall, our results indicate that the 140mg/kg dose of MCP is able to reverse microglial and astroglial activation. The healthy, diseased and MCP treated microglial morphology were characterized, which revealed certain characteristics of microglia not reported elsewhere. The present study has identified that the microglial soma area and soma perimeter significantly increased in both the hippocampus and cerebellum of GFAP-IL6 mice compared to those of the healthy controls. Additionally, there was a significantly larger number of processes in the microglia of the inflamed brains compared to normal brains. MCP altered the morphology of the microglial cells by reducing soma area and soma perimeter. The high dose MCP significantly reduced the soma area and soma perimeter, while it significantly increased the number of nodes in the hippocampus. In the cerebellum, the high dose MCP significantly reduced the soma area and soma perimeter while it increased the convex area, convex perimeter, and dendritic length compared to the non-fed control. Interestingly, the morphology of microglia in the 140mg NC GFAPIL6 mice was also affected, as soma area and soma perimeter was significantly decreased in the cerebellum of GFAP-IL6 mice. In short, the MCP modified morphology towards that of microglia in the normal mice.

Herein, morphological investigations of astrocytes in the hippocampus have shown that astrocytes of GFAP-IL6 mice have significantly longer dendritic length compared to that of WT mice, and the high and medium dose of MCP significantly decreased the dendritic length. Moreover, the convex area of the inflamed astrocytes was also significantly larger than that of WT type mice cells, and the high dose MCP significantly decreased the convex area. Astrocytes are activated in response to CNS challenges such as trauma, infections, and neuroinflammatory diseases, and this activation is considered as a hallmark of neurodegeneration. They have a bushy structure with tiny fine processes connected with synapses. Once they are activated, the reactive astrocytes undergo morphological changes relative to the resting cells, wherein cellular processes extend (Wilhelmsson et al. 2006; Grosche et al. 1999). Emerging studies have reported that curcumin can inhibit the hypertrophy of astrocytes in the CNS. One of the studies has reported that curcumin formulation has slightly decreased the astrocyte activation and the number of branches in the hippocampus. Similarly, another study conducted in rats using a trumatic brain

injury model reported a decrease in hypertrophy of astrocytes after been treated with curcumin (Ji et al. 2013; Maiti, Paladugu, and Dunbar 2018).

4.3. Effect of Longvida curcumin® on microglia and astrocyte numbers in the GFAP-IL6 mouse model

4.3.1 Introduction

Chronic microglial activation describes the chronic, CNS-specific, inflammation-like glial responses that do not reproduce the classic characteristics of inflammation but cause neurodegeneration (Block and Hong 2007). Microglia and astrocytes play a key role in the CNS's innate immunity. The role of microglia is to clear the damaged neurons and may control the pathological processes to maintain the homeostasis of the CNS (Suzumura 2017) while, astrocytes help to remove debris and toxins from the cerebrospinal fluid (Heneka, Golenbock, and Latz 2015). The inflammatory response is mediated by the activated microglia, which is considered as the hallmark of neuroinflammation. The chronic activation of microglia leads to neuronal damage through the release of various cytotoxic molecules such as cytokines, reactive oxygen intermediates, proteinases (Heneka et al. 2015). TSPO is a mitochondrial translocator protein predominantly expressed in the microglia, astrocytes, and macrophages in the blood vessels in the nervous system, specifically on the outer mitochondrial membrane (Chen and Guilarte 2008), (Kuhlmann and Guilarte 2000; Wilms et al. 2003).

Curcumin, obtained from the dry rhizome of *Curcuma longa Linn*, targets multiple chemotherapeutic and inflammatory pathways and has demonstrated safety and tolerability in animal and humans, supporting its potential as a therapeutic agent; however, the pre-clinical and clinical literature lacks conclusive evidence supporting its use as a therapeutic agent due to its low bioavailability in humans (Gota et al. 2010). Therefore, the SLCP preparation, LC, patented by Verdure Sciences (Noblesville, IN, USA) has the potential to enables the uptake of free curcumin to the blood and target tissues. It has been reported that LC has comparatively high bioavailability and absorption compared to the unformulated curcumin. A study conducted in mice which have revealed that LC has the to cross the blood-brain barrier when orally administered, where it was reported to reach concentrations four times greater than that of unformulated curcumin (Begum et al. 2008b). Clinical studies conducted to compare the pharmacokinetics and bioavailability of free curcumin and LC in humans. The study has confirmed that the mean peak concentration of curcumin achieved from dosing 650 mg of LC was 22.43 ng/mL, whereas plasma curcumin from dosing an equal quantity of unformulated 95%

curcuminoids extract was not detected (Gota et al. 2010). The present study sought to investigate the effects of LC on microglia and astroglia numbers in the GFAP-IL6 mouse.

4.3.2. Results

4.3.2.1. LC decreased the microglia numbers in the hippocampus

In order to test the genotype difference between wild type and GFAP-IL6 normal food fed mice, and the effect of LC on the microglial number in both wild type and GFAP-IL6, immunohistochemistry and stereological counting of Iba-1^+ microglia were performed in the hippocampus in control and LC fed cohorts.

Using two way ANOVA on our cohorts, a significant difference was found between the groups [$F(3,16) = 35.10$] in the hippocampus. In the hippocampus, the wild type mice had 184,706 ± 19,037 Iba-1^+ microglia, which was slightly decreased by (16.53%) in wild type LC fed mice (156,498 ± 10,762) (Fig 24 A-B, E). In contrast, the GFAP-IL6 mice had 383,588 ± 12,253 Iba-1^+ microglia, which was significantly reduced to 295,666 ± 31,017 (25.88%) in LC fed mice (Fig 24 C-E).

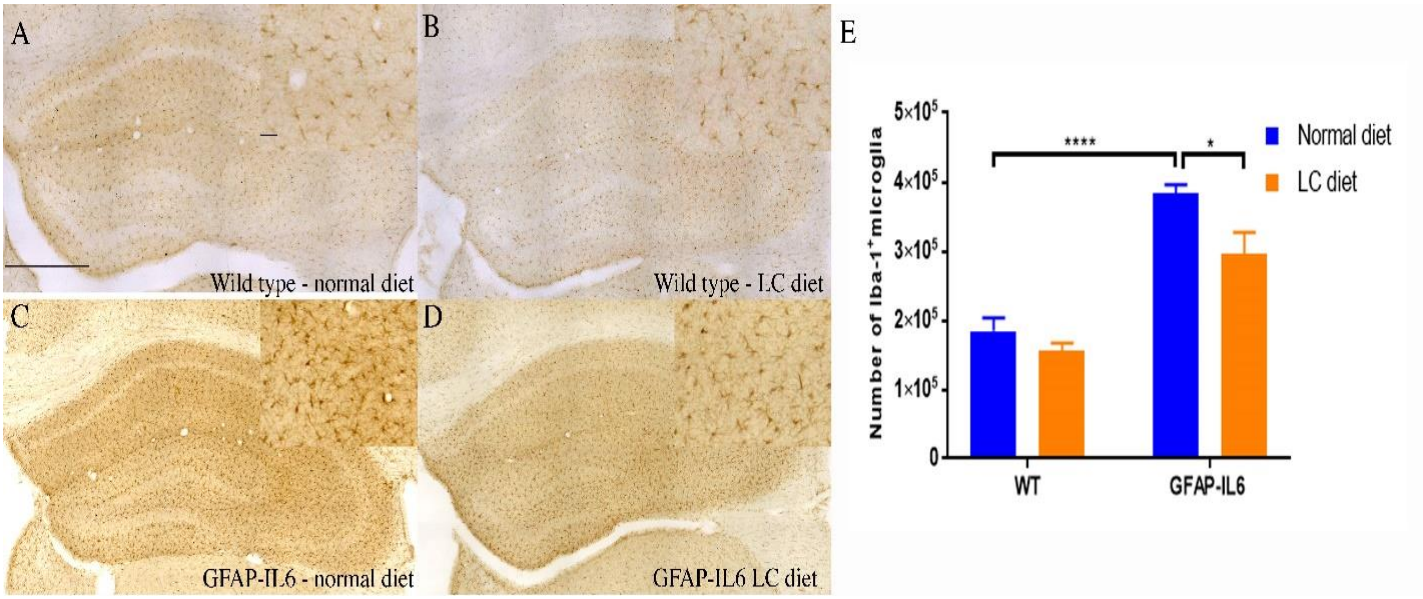

Figure 24. LC decreased the microglia numbers in the hippocampus. (A-D) Representative photomicrographs of immunohistochemical staining for the microglia (Iba-1$^+$ cells) of the hippocampus. (Magnification 10x objective field, scale bar = 500µm and 100µm in inserts). Images are representative of at least six animals per group (n=6). E. Graphical representation of total Iba-1$^+$ count in the hippocampus. The graph represents the mean ± SEM and significant differences were determined using a two-way analysis of variance (ANOVA). Significance = $^{**}p < 0.0015$

4.3.2.2. LC decreased the microglia numbers in the cerebellum

In order to test the genotype difference between wild type and GFAP-IL6 normal food fed mice, and the effect of LC on the microglial number in both wild type and GFAP-IL6, immunohistochemistry and stereological counting of Iba-1$^+$ microglia were performed in the cerebellum in control and LC fed cohorts.

In the cerebellum, using two-way ANOVA on our cohorts, a significant difference was found between the groups [$F(3,23) = 16.72$]. The wild type mice had 156,454 ± 33,721 Iba-1$^+$ microglia which was slightly, but not significantly increased in wild type LC fed mice (222,026 ± 75,55) (Fig 25 A-B, E). The GFAP-IL6 mice had 847,456 ± 46,120 Iba-1$^+$ microglia, which was significantly downregulated by (48%) in LC fed GFAP-IL6 mice (439,038 ± 49,423) (Fig 25 C-E).

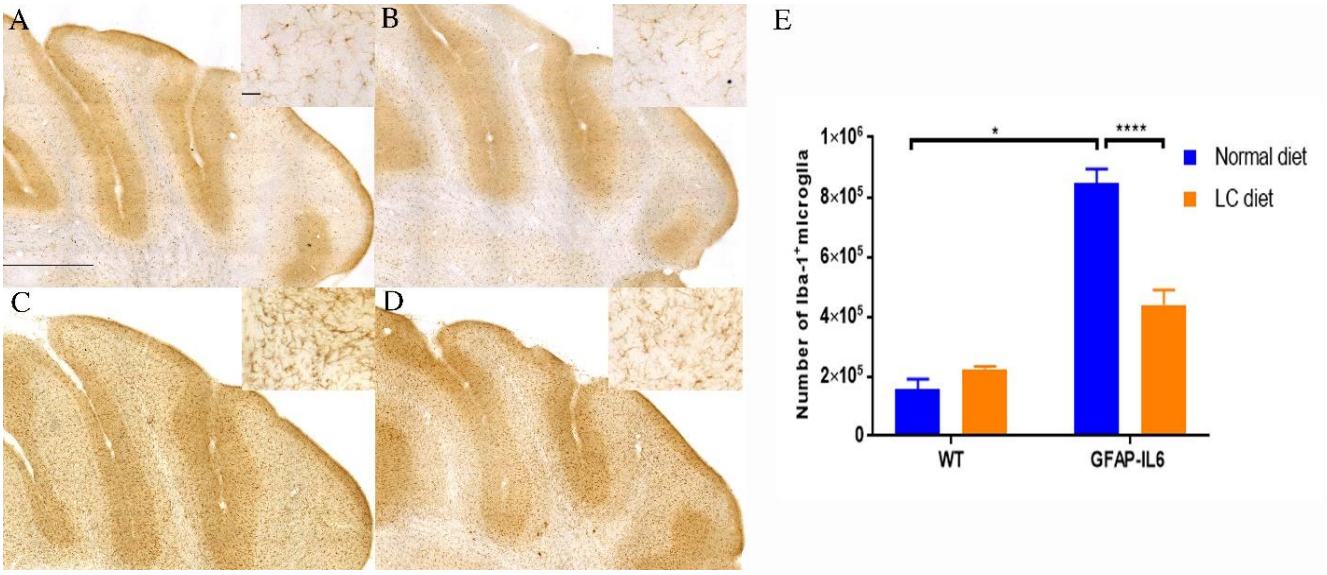

Figure 25. LC decreased the microglia numbers in the cerebellum. (A-D) Representative photomicrographs of immunohistochemical staining for the microglia (Iba-1$^+$ cells) of the cerebellum. (Magnification 10x objective field, scale bar = 500µm and 100µm in inserts). Images are representative of at least six animals per group (n=6). E. Graphical representation of total Iba-1$^+$ count in the cerebellum. The graph represents the mean ± SEM and statistical analyses were applied using a two-way analysis of variance (ANOVA).

4.3.2.3. LC downregulated the number of TSPO$^+$ cells in GFAP-IL6 mice in the hippocampus

In order to investigate the genotype difference between the wild type and GFAP-IL6 normal food fed mice, and to test the effect of LC on TSPO$^+$ microglia in both wild type and GFAP-IL6 mice, immunohistochemistry and stereological counting of the TSPO positive microglia/macrophages was performed.

In the hippocampus, using two-way ANOVA on our cohorts, a significant difference was observed between the groups.[$F(3,10) = 30.80$, $p < 0.0001$]. However, using multiple comparisons, the wild type mice had 6626 ± 3952 TSPO$^+$ microglia, which were slightly, but non-significantly increased by (1.92%) in LC fed wild type mice (6755 ± 1730) (Fig 26 A-B). In contrast, GFAP-IL6 had 236, 098 ± 28,005 TSPO$^+$ microglia, which were reduced by 24.46% in LC fed GFAP-IL6 mice (184,624 ± 23,174) (Fig 26 C-E).

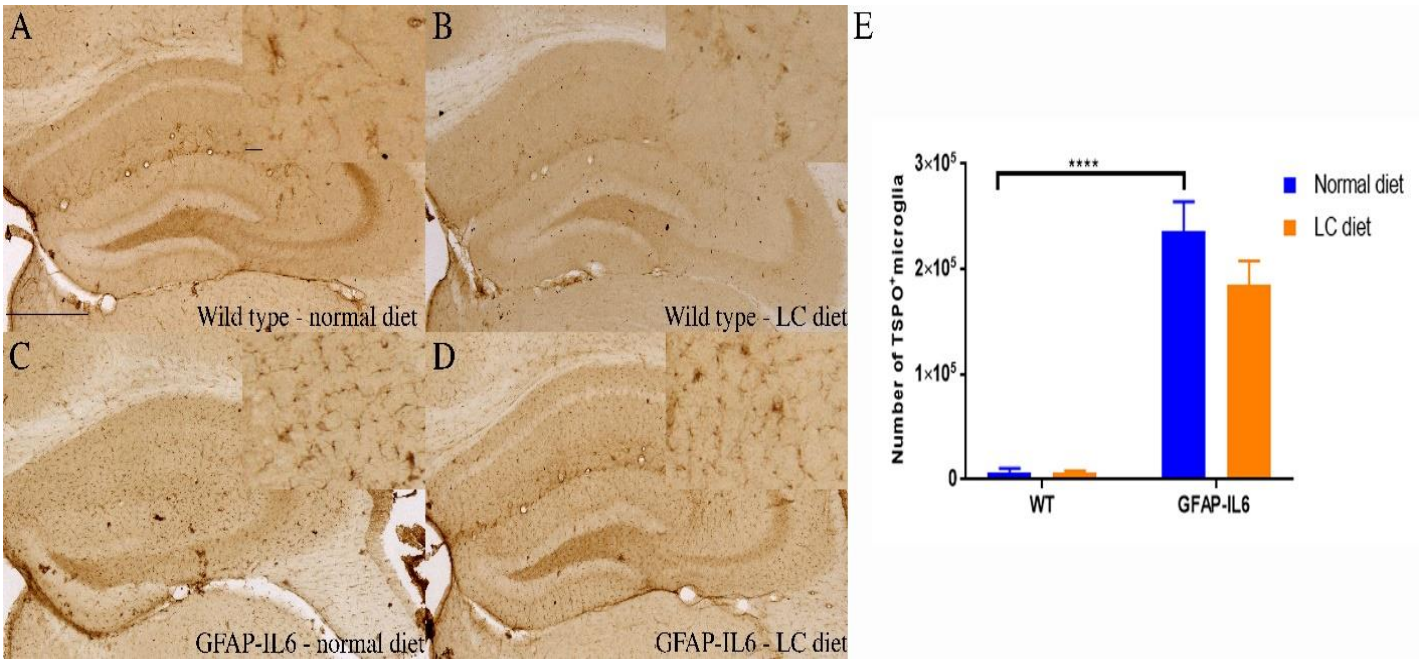

Figure 26. LC downregulated the number of TSPO$^+$ cells in GFAP-IL6 mice in the hippocampus. (A-D) Representative photomicrographs of immunohistochemical staining for the microglia (TSPO$^+$ cells) of the hippocampus. (Magnification 10x objective field, scale bar = 500µm and 100µm in inserts). Images are representative of at least six animals per group (n=6). E. Graphical representation of total TSPO$^+$ count in the hippocampus. The graph represents the mean ± SEM and the percentage differences were determined using a two-way analysis of variance (ANOVA), $p < 0.19$.

4.3.2.4. LC downregulated the number of TSPO$^+$ cells in GFAP-IL6 mice in the cerebellum

In order to investigate the genotype difference between the wild type and GFAP-IL6 normal food fed mice, and to test the effect of LC on TSPO$^+$ microglia in both wild type and GFAP-IL6 mice, immunohistochemistry and stereological counting of the TSPO positive microglia/macrophages was performed in the cerebellum.

In the cerebellum, using two-way ANOVA on our cohorts, a significant differenence were found between the groups. [F(3,10) = 23.89]. Using multiple comparisons, wild type mice had 18,108 ± 2933 TSPO$^+$ microglia, which were slightly decreased (by 5.73%) in LC fed wild type mice (17,098 ± 4161) (Fig 27 A-B). Whereas, GFAP-IL6 mice on normal diet had 364,942 ± 28,577 TSPO$^+$ cells, which was significantly downregulated by 31.37% in the LC fed GFAP-IL6 group (265,979 ± 55,791)) (Fig 27, C-E).

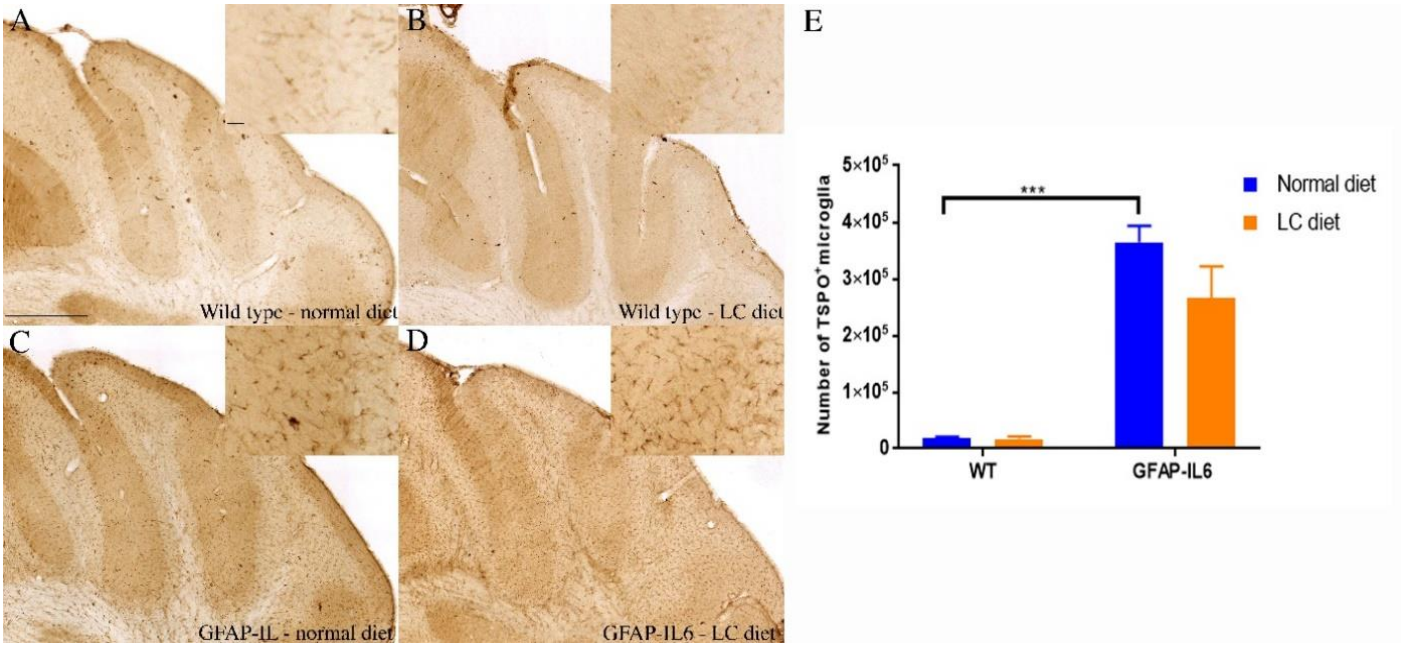

Figure 27. LC downregulated the number of TSPO$^+$ cells in GFAP-IL6 mice in the cerebellum. (A-D) Representative photomicrographs of immunohistochemical staining for the microglia (TSPO$^+$ cells) of the cerebellum. (Magnification 10x objective field, scale bar = 500µm and 100µm in inserts). Images are representative of at least six animals per group (n=6). E. Graphical representation of total TSPO$^+$ count in the cerebellum. The graph represents the mean ± SEM and significant differences were determined using a two-way analysis of variance (ANOVA). Significance = ***$p < 0.005$

4.3.2.5. LC decreased the number of GFAP$^+$ astrocytes in the hippocampus

In order to quantify the number of astrocytes, GFAP immunostaining and stereological quantification were performed to investigate the genotype difference between WT and GFAP-IL6 normal food fed mice. Furthermore, the effect of LC on the elevated number of GFAP$^+$ astrocytes in the wild type GFAP-IL6 mice was investigated in the hippocampus and cerebellum.

In the hippocampus, GFAP-IL6 mice had a significantly larger number of GFAP$^+$ astrocytes (372,850 ± 36,861) compared to WT mice (211,968 ± 11,730)) (Fig 28A-B). In LC fed WT mice, the astrocytes number reduced by 23% (161,441 ± 19,648) whereas, In LC fed GFAP-IL6

mice, a significant reduction in GFAP$^+$ astrocytes were observed by 30% (264,105 ± 24,115) compared to the GFAP-IL6 normal food fed mice (Fig 28, C-E).

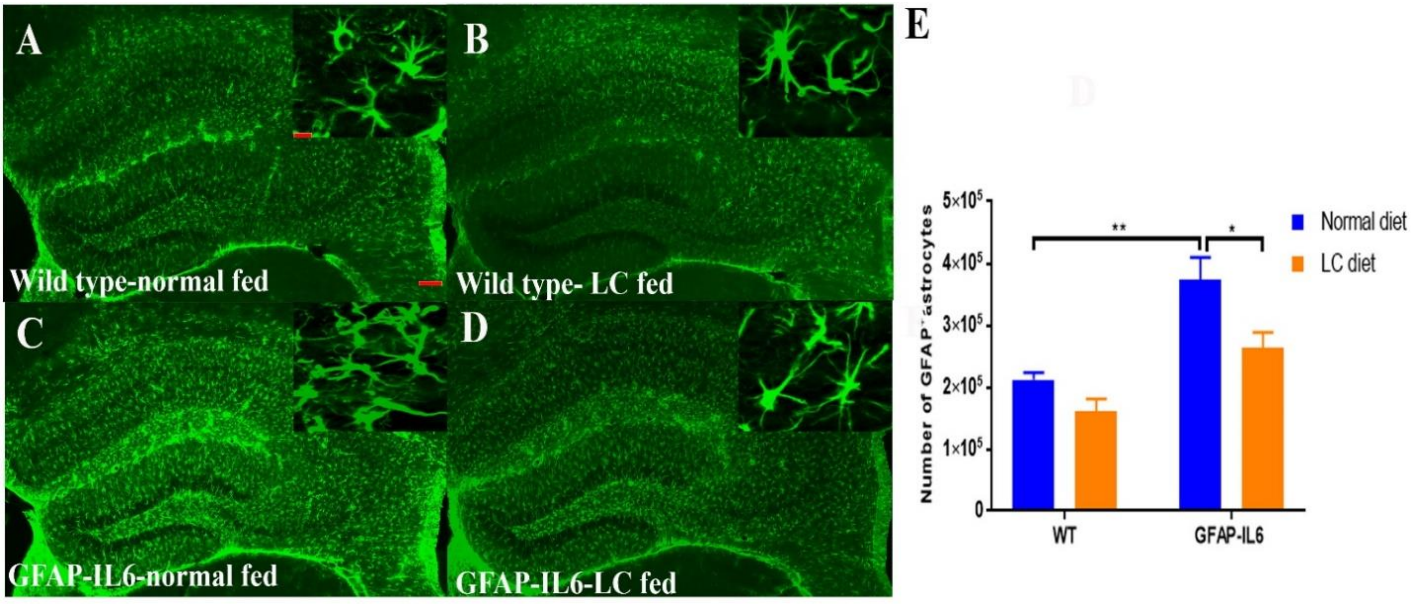

Figure 28. LC decreased the number of GFAP$^+$ astrocytes in the hippocampus. (A-D) Representative photomicrographs of immunofluorescence staining for the astrocytes (GFAP$^+$ cells) in the hippocampus. (Magnification 5x objective field, scale bar=100µm in 20x and 20µm). Images are representative of at least six animals per group (n=6). (E) Graphical representation of total GFAP count in the hippocampus. The Graph represents the mean± SEM and significant differences were determined using a two-way analysis of variance (ANOVA). Significance = *p <0.05, **p <0.001

4.3.2.6. Effect of LC on the number of GFAP$^+$ astrocytes in the cerebellum

In the cerebellum, the astrocytes and their processes were very closely packed, making stereological counting difficult, hence the numbers of GFAP$^+$ cells were not stereologically analyzed. However, high-level expression of GFAP protein was observed in GFAP-IL6 mice compared to WT mice, located mostly but not exclusively in the gray matter of the cerebellum, with a strong presence of elongated microglia in the white matter and molecular layer. The difference in the distribution of astrocytes between the WT and GFAP-IL6 animals was substantial. No conclusions could be drawn in the absence of quantitative stereology. (Fig 29 A-D).

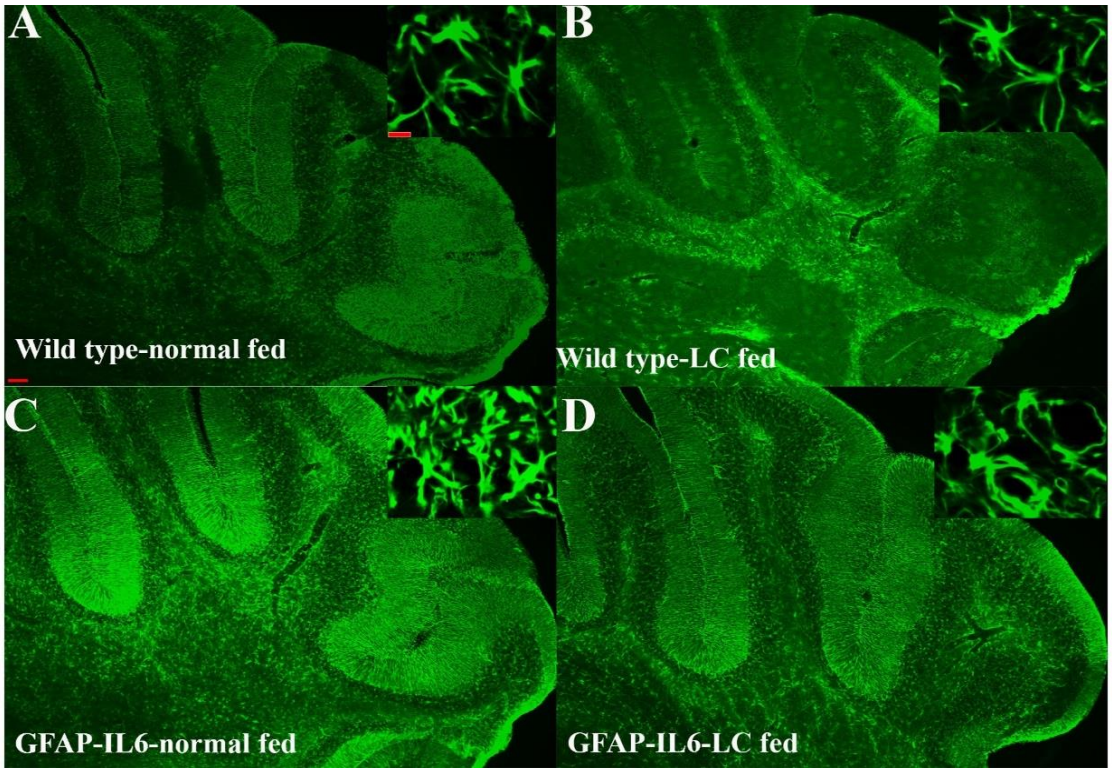

Figure 29. The effect of LC on the number of GFAP$^+$ astrocytes in the cerebellum. (A-D) Representative photomicrographs of immunofluorescence staining for the astrocytes (GFAP$^+$ cells) in the cerebellum. (Magnification 5x objective field, scale bar=100μm in 5x and 20μm in inserts). Images are representative of at least six animals per group (n=6).

Table 10. Stereological counting summary of the Iba-1, TSPO positive microglia in the hippocampus and the cerebellum and GFAP positive astrocytes in the hippocampus. All values are presented as mean ± SEM

Genotype	Diet	Iba-1 hippocampus	Iba-1 cerebellum	TSPO hippocampus	TSPO cerebellum	GFAP hippocampus
WT	Normal food	184706±19037	156454±33721	6626±3952	18108±2933	211968±11730
WT	LC 500ppm	156498±10762	222026±7555	6755±1730	17098±4161	161441±19648
GFAP-IL6	Normal food	383588±12253	847456±46120	236098±28005	364942±28577	372850±36861
GFAP-IL6	LC 500ppm	295666±31017	439038±49423	184624±23174	265979±55791	264105±24115

4.3.3. Summary

The purpose of the study was to investigate the therapeutic effects of LC in chronic glial activation in the central nervous system. In this study, we have assessed the anti-inflammatory effect of LC in GFAP-IL6 mice. The mice were fed for 4 months and the results were compared with normal diet fed animals, using both wild type and GFAP-IL6 animals on both diets.

In summary, our results revealed that LC decreased the $Iba1^{+}$ microglia numbers by 25.88% in the hippocampus and by 48% in the cerebellum, as well as the TSPO+ microglia numbers by 24.45% in the hippocampus and by 31% in the cerebellum. These reductions in these activated microglia numbers could indicate overall decreased levels of glial activation, meaning an improvement in the condition associated with the neuroinflammatory process (Sasaki 2017). Moreover, In LC fed GFAP-IL6 mice, a significant reduction in $GFAP^{+}$ astrocytes were observed in the hippocampus by 30% compared to the GFAP-IL6 normal food fed mice. In Cerebellum, using qualitative observation and analysis, LC fed groups appeared to have a comparatively low expression of GFAP protein compared to the GFAP-IL6 group.

In short, the long term LC feeding to the mice was able to reduce the chronic microglia and astroglial activation in GFAP-IL6 mice compared to the normal food fed mice.

4.4. Effect of Longvida® curcumin on the glial cell morphology in the hippocampus and the cerebellum in GFAP-IL6 mice

4.4.1 Introduction

The morphology of microglia and astrocytes is also considered as the key characteristic of the progress of neuroinflammation (Kirkley et al. 2017). Microglia are distributed throughout the brain in unequal fashion and shape which is evidence that microglial cells are sensitive to the surrounding microenvironment (Lawson et al. 1990). Under normal condition, the microglia are characterized by ramified morphology such as normal soma with long dendrites and bushy shape. However, they are never in a real resting state and constantly scan the surrounding environment (Nimmerjahn, Kirchhoff, and Helmchen 2005). During an injury or neuroinflammatory assaults, the resting microglial cells go into "activated state" characterized by swollen soma, shorter, thick processes and sometimes adopt amoeboid-like morphologies termed as "de-ramified microglia (Kirkley et al. 2017) (Sierra et al. 2013; Davis, Foster, and Thomas 1994).

Astrocytes are the most abundant cell type of the CNS, playing a major role in brain homeostasis, provide metabolites and growth support to neurons synapse formation and plasticity and regulate the extracellular balance of ions and fluids (Colombo and Farina 2016). The resting astrocytes are thought to exhibit an intricate bushy or spongiform morphology, and they have fine processes (Bushong et al. 2002). Astrocytes are activated in respond to neural insults, such as neuroinflammation release cytokines, ILs, NO, and other potentially cytotoxic molecules (Ahmad, Fatima, and Mondal 2019; Sofroniew 2009). Astrocytes respond to CNS challenges and the activated astrocytes are a hallmark of neuroinflammation which is characterized by high-level expression of the glial fibrillary acidic protein (GFAP) (Wilhelmsson et al. 2006). Astrocytes display a bushy or spongiform morphology with very fine processes (Bushong et al. 2002). When the astrocytes are activated, they exhibit striking increases in GFAP immunoreactivity and in the number and length of GFAP-positive processes (Kimelberg and Norenberg 1989).

The study investigates the effect of LC on the morphology of astroglial cells in the GFAP-IL6 mouse model. To determine how LC affects the morphology of activated (Iba-1^{+}) microglia and activated ($GFAP^{+}$) astroglia in the brain, 3D reconstruction techniques were applied to assess the

morphology of reactive and nonreactive microglia and astrocytes in the hippocampus and the cerebellum in an unbiased manner.

4.4.2. Results

4.4.2.1 Effect of LC on microglial morphology in the hippocampus

In neuroinflammation or after brain injury, a de-ramification of microglia has been observed. Thus, the microglia get into the "activated state" characterized by swollen ramified cells with larger some and short dendrites (Davis, Foster, and Thomas 1994). In order to investigate the genotype difference and the effect of the LC diet on Iba-1^+ microglial cells, we analyzed the morphological features of the Iba-1^+ microglia in the WT and GFAP-IL6 both normal fed and LC fed animals in the hippocampus.

In the hippocampus, a difference in few parameters between the genotypes was observed, as Iba-1^+ microglial cells of GFAP-IL6 mice normal fed had significantly larger soma areas (57.25 ± 4.03μm^2), small convex areas (1035.60 ± 79.12μm^2) and convex perimeter (127.68 ± 4.39μm) than those of WT [soma areas (42.57 ± 3.82μm^2), convex areas (1535.63 ± 139.68μm^2) and convex perimeter (155.83 ± 6.11μm)]. In addition, Iba-1^+ microglia in WT LC fed mice had a significantly larger dendritic length (281.94 ± 21.97μm) than that of the WT normal fed mice (212.90 ± 10.23μm). Whereas, Iba-1^+ microglial cells of GFAP-IL6 LC fed mice had significantly large dendritic length (266.83 ± 14.10) and number of nodes (9.25±0.59) than that of GFAP-IL6 normal fed mice [Dendritic length (192.16 ± 14.58), number of nodes (6.43 ± 0.70)] (Fig. 30 A-H, Table 11).

In order to further the morphological characteristics, of microglial cells from the hippocampus, a quantitative analysis termed as Sholl analysis was applied which revealed some further variation in morphology between WT and GFAP-IL6 normal fed and LC fed mice. In the hippocampus, there was no significant difference between WT and GFAP-IL6 normal fed mice Observed in any parameter. Although, the microglia of WT LC fed mice have a significantly larger surface area, process volume, and process diameter than that of WT normal fed mice. Whereas, the

microglia of LC fed GFAP-IL6 mice have significantly larger processes in length compared to GFAP-IL6 normal fed mice (Fig. 31 A-F).

In the hippocampus, correlation analysis of overall microglial cell size with each morphological characteristic revealed a significant correlation with soma area, soma perimeter, number of nodes and primary dendrites in LC fed GFAP-IL6 mice, which clearly revealed that the microglial cells of the GFAP-IL6 LC fed mice potentially increased the overall soma size and dendrites number. In addition, the convex perimeter and dendritic length of each cohort increased with the increasing size of the entire cell. Whereas, the rest of the parameters in the other cohorts remained consistent (Fig 32 A-F, Table 12).

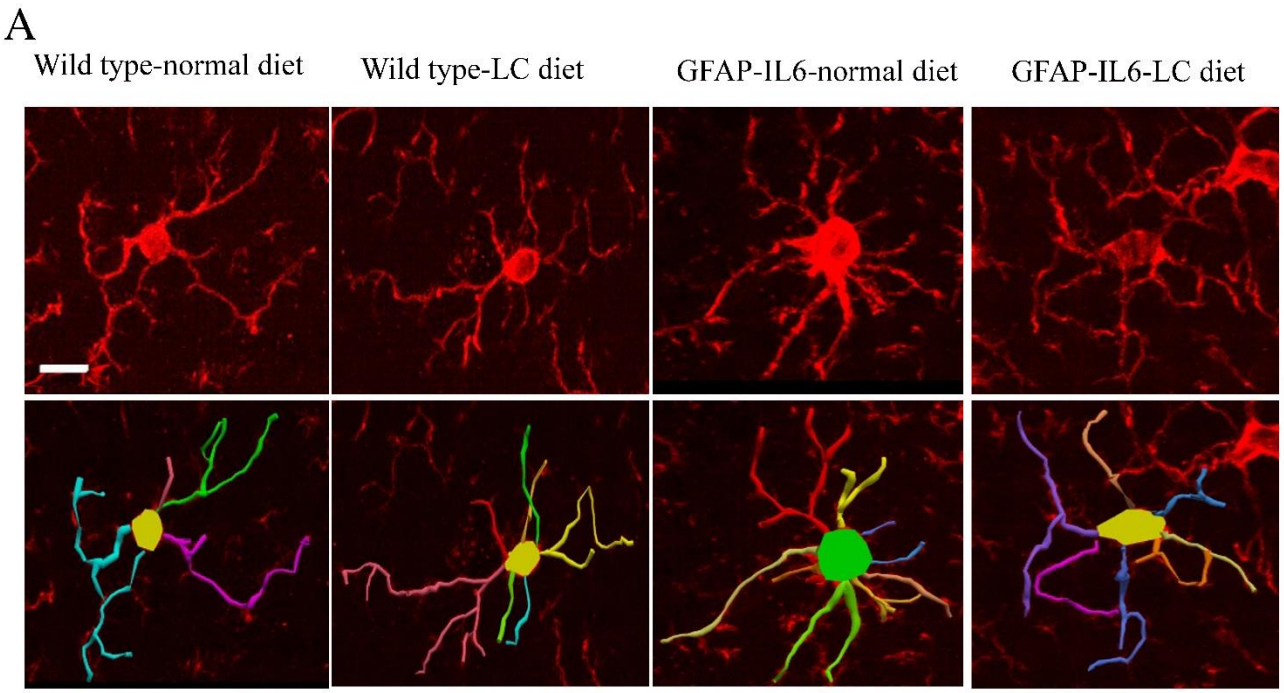

B

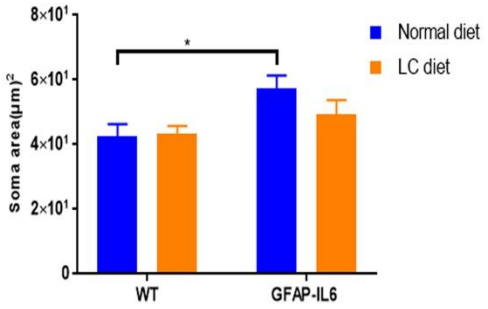
Soma area(µm)²
8×10¹
6×10¹
4×10¹
2×10¹
0
*
Normal diet
LC diet
WT
GFAP-IL6

C

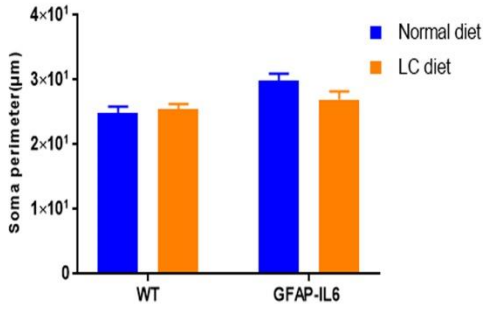
Soma perimeter(µm)
4×10¹
3×10¹
2×10¹
1×10¹
0
Normal diet
LC diet
WT
GFAP-IL6

D

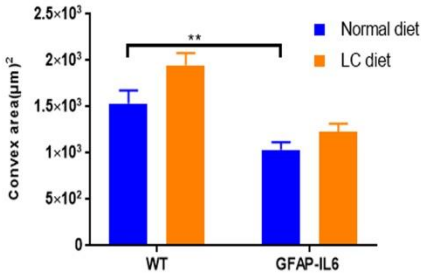
Convex area(µm)²
2.5×10³
2×10³
1.5×10³
1×10³
5×10²
0
**
Normal diet
LC diet
WT
GFAP-IL6

E

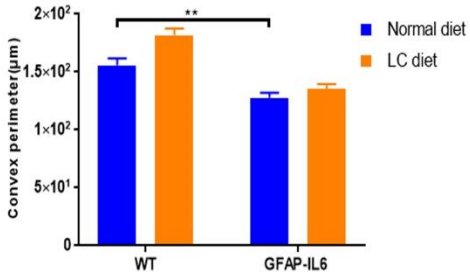
Convex perimeter(µm)
2×10²
1.5×10²
1×10²
5×10¹
0
**
Normal diet
LC diet
WT
GFAP-IL6

F

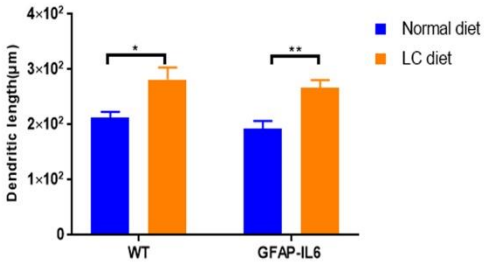
Dendritic length(µm)
4×10²
3×10²
2×10²
1×10²
0
*
**
Normal diet
LC diet
WT
GFAP-IL6

G

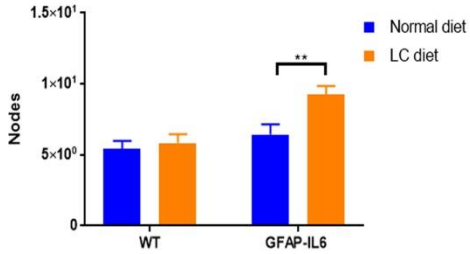
Nodes
1.5×10¹
1×10¹
5×10⁰
0
**
Normal diet
LC diet
WT
GFAP-IL6

H

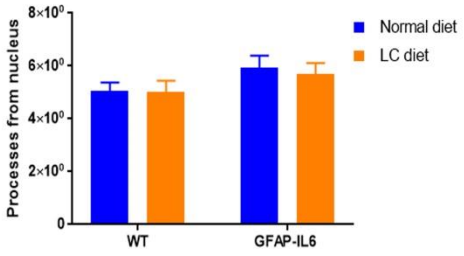
Processes from nucleus
8×10⁰
6×10⁰
4×10⁰
2×10⁰
0
Normal diet
LC diet
WT
GFAP-IL6

Figure 30. Effect of LC on microglial morphology in the hippocampus. (A) The representative images of microglia immunostained for Iba-1 in the hippocampus. Scale bar 10µm. (B-H) Graphs showing the morphological changes in Iba-1^{+} microglia. Two-way ANOVA, Tukey's post-test, mean ± SEM)

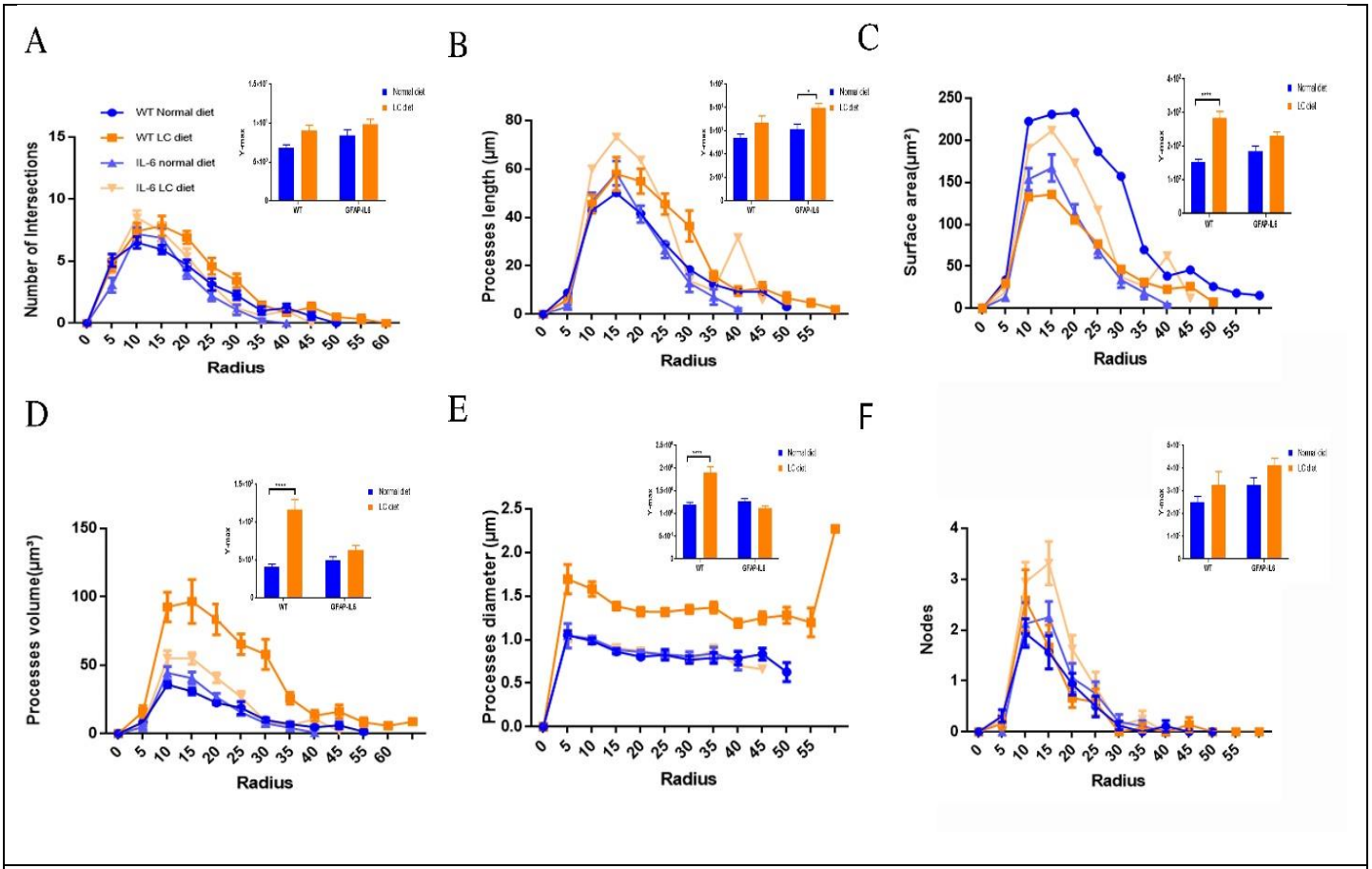

Figure 31. The effect of LC on microglial cells in sholl analysis in the hippocampus region. (A-F) There was no significant difference between WT and GFAP-IL6 normal fed mice in any parameter. WT LC fed mice have a significantly larger surface area, process volume, and process diameter than that of WT normal fed mice. Whereas the microglia of LC fed GFAP-IL6 mice have significantly larger processes in length, which is observed in the peaks of the distributions of different morphological features, we call it X at Y_{max}. Two-way ANOVA test.

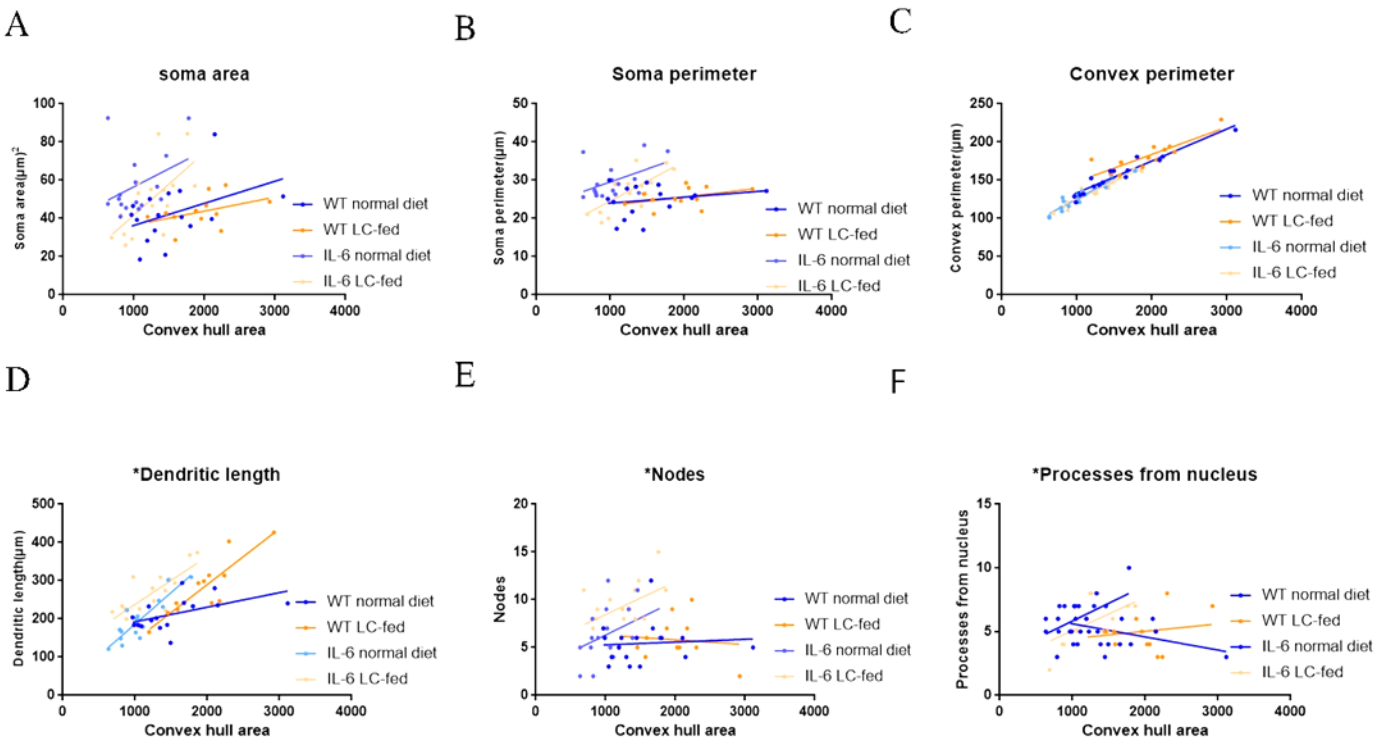

Figure 32. Bivariate correlation: LC effects on microglial morphology in the hippocampus. (A-F) Different morphological parameters have been plotted against the convex hull area to see the bivariate correlation between WT normal-diet, WT LC-diet GFAP-IL6 normal-diet, and GFAP-IL6 LC-diet.

4.4.2.2 Effect of LC on microglial morphology in the cerebellum

In order to investigate the genotype difference and the effect of the LC diet on Iba-1$^+$ microglial cells, we analyzed the morphological features of the Iba-1+ microglia in the WT and GFAP-IL6 both normal fed and LC fed animals in the cerebellum.

In cerebellum, a significant difference was observed in genotype as, Iba-1$^+$ microglial cells of GFAP-IL6 mice normal fed had significantly large soma area (77.68 ± 7.89µm^2), soma perimeter (37.21 ± 2.44µm) and small convex area (1087.96 ± 150µm^2) ($p < 0.015$), convex perimeter (137.57 ± 9.45µm) than those of the wild type non-fed mice [soma area (38.82±2.80µm^2), soma perimeter (24.10 ± 0.82µm) and small convex area (1750.71 ± 148.98µm^2), convex perimeter

(171.42 ± 7.98μm). Also, Iba-1^+ microglia in WT LC diet had a significantly large dendritic length (265.30 ± 21.52μm) than WT normal fed mice (199.55 ± 14.70). Whereas, Iba-1^+ microglial cells of GFAP-IL6 LC fed mice had significantly reduced soma area (50.18 ± 4.77μm^2), soma perimeter (28.10 ± 1.68μm) and more number of nodes (8.07±1.06) than that of GFAP-IL6 normal fed mice [soma area (77.68 ± 7.89μm^2), soma perimeter (37.21 ± 2.44μm) number of nodes (4.92 ± 0.65)] (Fig. 33 A-H, Table 11).

In order to further the morphological characteristics, of microglial cells from the cerebellum, a quantitative analysis termed as Sholl analysis was applied which revealed some further variation in morphology between WT and GFAP-IL6 normal fed and LC fed mice. In the cerebellum, there was not any genotype difference between WT and GFAP-IL6 normal fed mice. In WT fed mice, the microglial cells have a significantly larger surface area, process volume, and process diameter than that of WT normal fed mice (Fig. 34 A-F).

In the cerebellum, significant correlations were observed in all cohorts in convex perimeter and dendritic length with overall cell size, showing that the convex perimeter and the length of dendrites increased with the overall increase in microglial cells. Moreover, the numbers of nodes in GFAP-IL6 non fed cohorts were increased with the overall increase in microglial cells. The other parameter remained consistent across the cohort regardless of the cell size (Fig 35 A-F, Table 13).

A

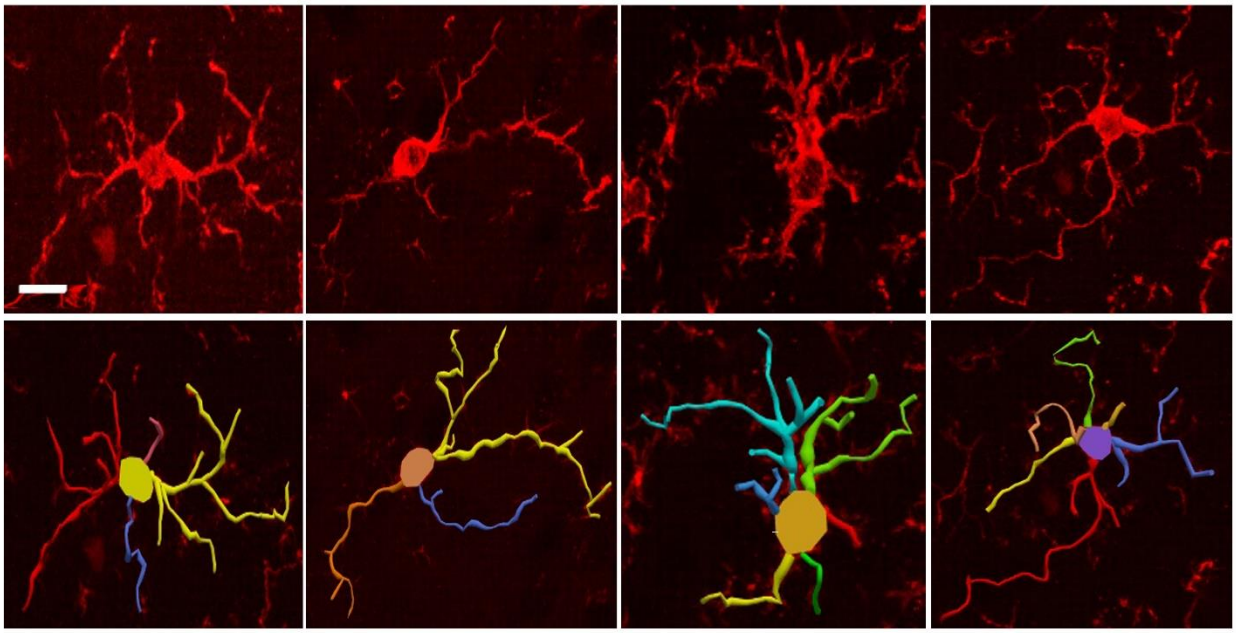
Wild type-normal diet
Wild type-LC diet
GFAP-IL6-normal diet
GFAP-IL6-LC diet

B

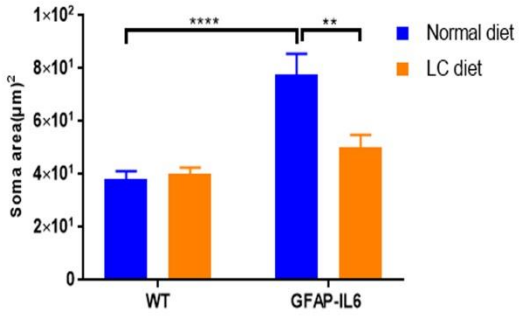
Soma area(μm)²
1×10²
8×10¹
6×10¹
4×10¹
2×10¹
0
****
**
Normal diet
LC diet
WT
GFAP-IL6

C

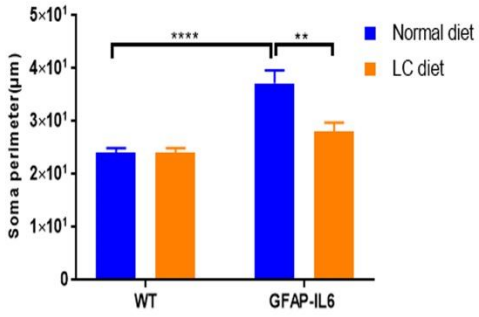
Soma perimeter(μm)
5×10¹
4×10¹
3×10¹
2×10¹
1×10¹
0
****
**
Normal diet
LC diet
WT
GFAP-IL6

D

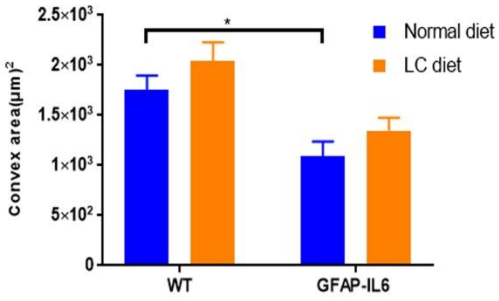
Convex area(μm)²
2.5×10³
2×10³
1.5×10³
1×10³
5×10²
0
*
Normal diet
LC diet
WT
GFAP-IL6

E

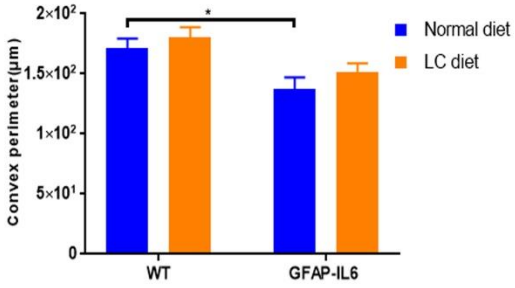
Convex perimeter(μm)
2×10²
1.5×10²
1×10²
5×10¹
0
*
Normal diet
LC diet
WT
GFAP-IL6

F

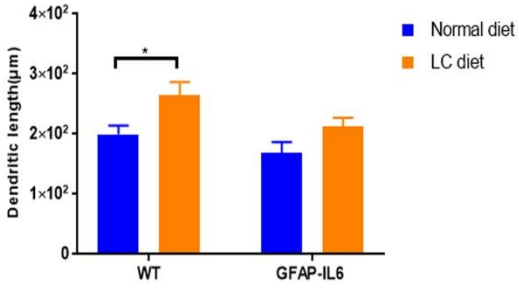
Dendritic length(μm)
4×10²
3×10²
2×10²
1×10²
0
*
Normal diet
LC diet
WT
GFAP-IL6

G

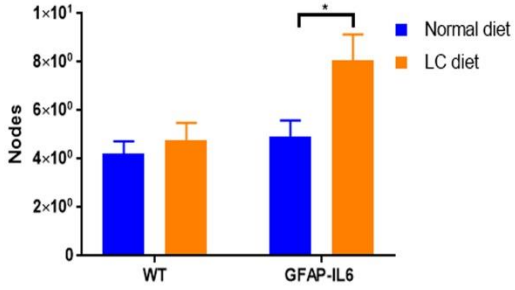
Nodes
1×10¹
8×10⁰
6×10⁰
4×10⁰
2×10⁰
0
*
Normal diet
LC diet
WT
GFAP-IL6

H

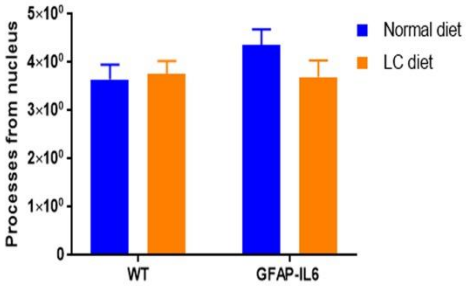
Processes from nucleus
5×10⁰
4×10⁰
3×10⁰
2×10⁰
1×10⁰
0
Normal diet
LC diet
WT
GFAP-IL6

Figure 33. Effect of LC on microglial morphology in the cerebellum. (A) The representative images of microglia immunostained for Iba^{+}-1 in the cerebellum. Scale bar 10µm. (B-H) Graphs showing the morphological changes in Iba-1^{+} microglia. Two-way ANOVA, Tukey's post-test, mean ± SEM)

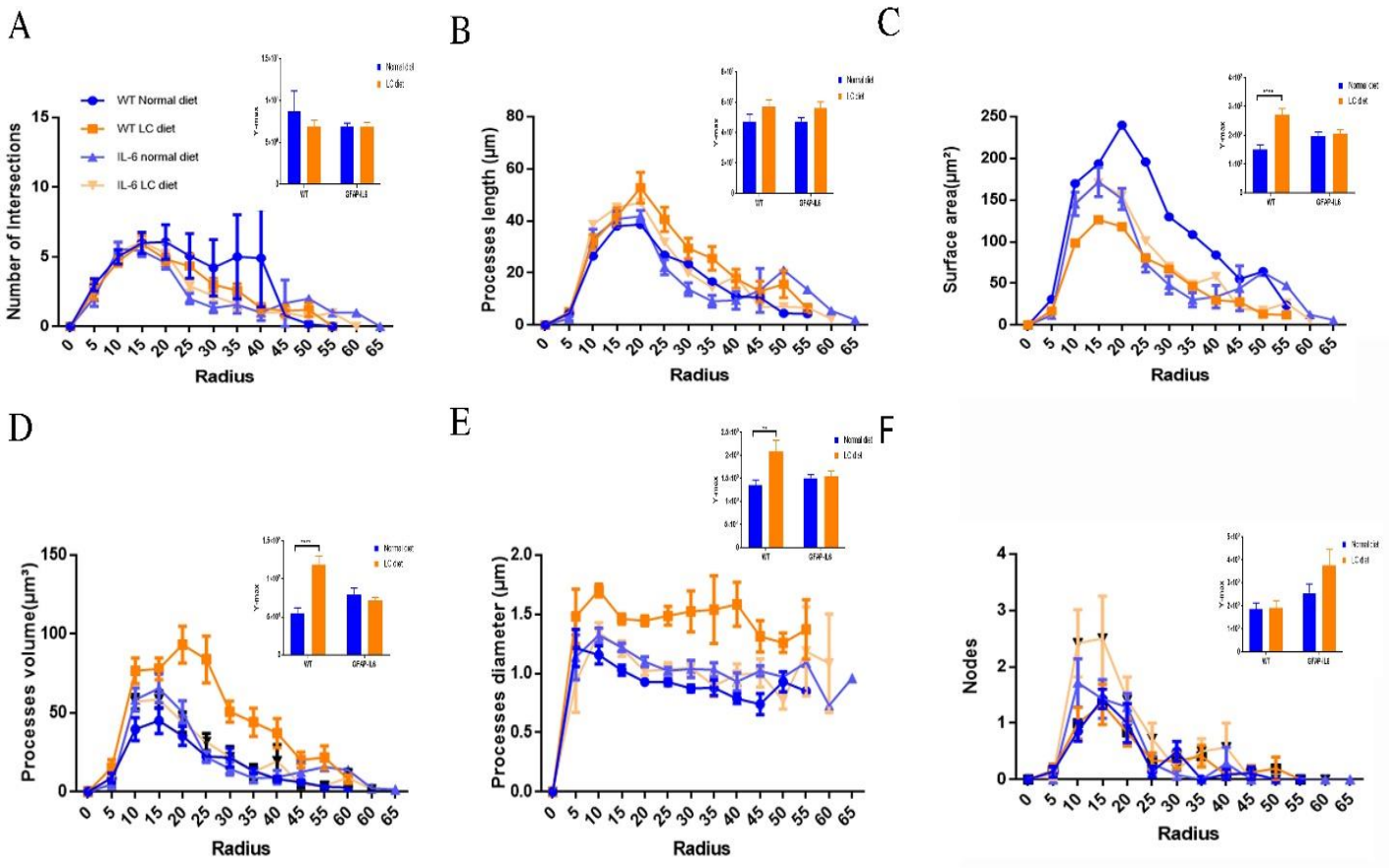

Figure 34. Effect of LC on microglial cells in sholl analysis in the cerebellum region (A-F) There was not any genotype difference between WT and GFAP-IL6 normal fed mice. The microglial cells have a significantly larger surface area, process volume, and process diameter than that of WT normal fed mice**,** Which was observed in the peaks of the distributions of different morphological features, we call it, X at Y_{max}. Two-way ANOVA test.

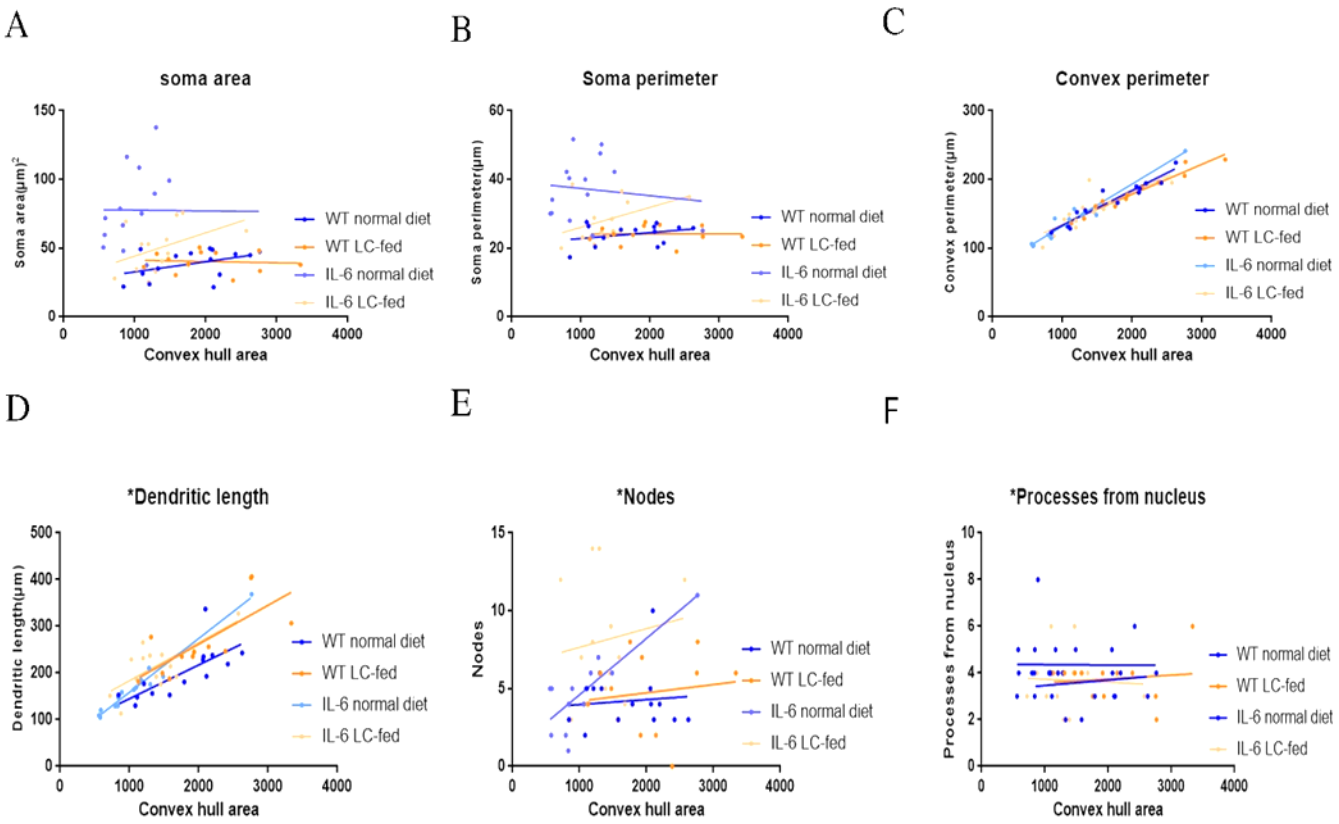

Figure 35. Bivariate correlation: LC effects on microglial morphology in the cerebellum. (A-F) Different morphological parameters have been plotted against the convex hull area to see the bivariate correlation between WT normal-diet, WT LC-diet GFAP-IL6 normal-diet, and GFAP-IL6 LC-diet.

Table 11. Morphological analysis of Iba-1$^+$ microglia

Genotype	Diet	Soma area (µm)^2 (Mean±SEM)		Soma perimeter (µm) (Mean ± SEM)		Convex 2D (area) (µm)^2(Mean ± SEM)		Convex perimeter (µm) Mean ± SEM)		Total length of dendrites (µm) (Mean± SEM)		Number of Nodes (Mean ± SEM)		Number of Dendrites (Mean ± SEM)	
		H	C	H	C	H	C	H	C	H	C	H	C	H	C
WT	Normal food	42.57 ±3.82	38.82 ±2.80	24.84± 1.02	24.10±0. 82	1535.63 ±139.6 8	1750.71 ±148.98	155.83 ±6.11	171.42± 7.98	212.90 ±10.23	199.55± 14.70	5.43±0 .55	4.21±0. 51	5.06±0 .30	3.64±0.3 0
WT	LC food	43.45 ±2.34	40.29 ±2.21	25.50± 0.72	24.15±0. 76	1946.17 ±132.5 1	2038.34 ±191.51	181.92 ±5.63	180.25± 8.56	281.94 ±21.97	265.30± 21.52	5.83±0 .62	4.75±0. 74	5±0.44	3.75±0.2 7
GFAP-IL6	Normal food	57.25 ±4.03	77.68 ±7.89	29.80± 1.13	37.21±2. 44	1035.60 ±79.12	1087.96 ±150	127.68 ±4.39	137.57± 9.45	192.16 ±14.58	169.17± 17.58	6.43±0 .70	4.92±0. 65	5.93±0 .45	4.35±0.3 2
GFAP-IL6	LC food	49.28 ±4.45	50.18 ±4.77	26.96± 1.24	28.10±1. 68	1230.88 ±86.08	1348.88 ±127.20	135.33 ±4.28	151.17± 7.55	266.83 ±14.10	212.36± 14.84	9.25±0 .59	8.07±1. 06	5.68±0 .42	3.69±0.3 4

H=Hippocampus, C= Cerebellum

Table 12. Bivariate correlation of morphological characteristics with overall microglial cell size in the hippocampus

	Soma area		Soma perimeter		Convex perimeter		Dendritic length		Nodes		Primary dendrites	
	R^2	Correlation	R^2	Correlation	R^2	Correlation	R^2	Correlation	R^2	Correlation	R^2	Correlation
WT NF	0.17	0.1037	0.04	0.44	0.91	****<0.0001	0.26	*0.0393	0.00	0.7869	0.21	0.0693
WT LC	0.17	0.1799	0.16	0.1878	0.70	***0.0006	0.77	***0.0001	0.01	0.7491	0.02	0.5932
IL-6 NF	0.13	0.1548	0.22	0.0646	0.90	****<0.0001	0.80	****<0.0001	0.16	0.1227	0.23	0.0552
IL-6 LC	0.40	**0.0084	0.51	**0.0019	0.92	****<0.0001	0.58	***0.0005	0.24	*0.0498	0.28	*0.0347

Table 13. Bivariate correlation of morphological characteristics with overall microglial cell size in the cerebellum

	Soma area		Soma perimeter		Convex perimeter		Dendritic length		Nodes		Primary dendrites	
	R^2	Correlation	R^2	Correlation	R^2	Correlation	R^2	Correlation	R^2	Correlation	R^2	Correlation
WT NF	0.15	0.1645	0.09	0.286	0.91	****<0.0001	0.53	**0.0028	0.00	0.7567	0.01	0.6987
WT LC	0.00	0.8008	0.08	0.9906	0.94	****<0.0001	0.54	**0.0059	0.01	0.6701	0.01	0.7196
IL-6 NF	0.00	0.9689	0.01	0.659	0.94	****<0.0001	0.96	****<0.0001	0.68	***0.0003	0.01	0.9854
IL-6 LC	0.20	0.1211	0.19	0.1331	0.62	**0.0014	0.49	**0.0075	0.02	0.6396	0.00	0.8734

4.4.2.3. Effect of LC curcumin on astrocytes morphology in the hippocampus

In inflammation, astrocytes are activated like microglial cells and undergo cellular hypertrophy which leads to altering their size and shape. We, therefore, characterized the morphology of astrocytes in the hippocampus of wild type normal diet, wild type LC diet, GFAP-IL6 normal-diet, and GFAP-IL6 LC-diet mice. Figure 36 A-H demonstrates the representative images of astrocytes immunostained for GFAP in the hippocampus. In both wild type normal diet and wild type LC diet, we observed almost similar astrocytes and there were no significant differences. Whereas the astrocytes in the GFAP-IL6 normal-diet mice had a significantly larger dendritic length (275 ± 17.8µm), a number of processes (6.06 ± 0.51), convex area (1418 ± 128.3µm^2), convex perimeter (147.9 ± 6.01µm) and a number of nodes (7.62 ± 0.77) compared to the wild types. The LC diet significantly decreased the dendritic length (175.2 ± 14.54µm), number of processes (4.06 ± 0.23), convex area (968.3 ± 74.04µm^2), convex perimeter (125.8 ± 4.24µm), and number of nodes (5.43 ± 0.56) (Fig 36 A-H, Table 14).

Furthermore, we quantified the astroglial cells by Sholl analyses. In the same manner, this analysis didn't reveal any significant changes between wild type normal-fed and LC fed mice.

We found that the LC significantly reduced the number of intersections and the length of processes compared to the normal-diet fed GFAP-IL6 mice. (Fig 37 A-H).

We performed the bivariate correlation of morphological characteristics with overall astroglial cell size to investigate the impact of the size of astroglial cells on the structural parameters. We observed some positive correlation of the astroglial cell size with some of the morphological parameters. The data revealed that the convex perimeter, dendritic length and the number of nodes increased significantly with the overall increase in the entire cell structure (Fig 38 A-H, Table 15).

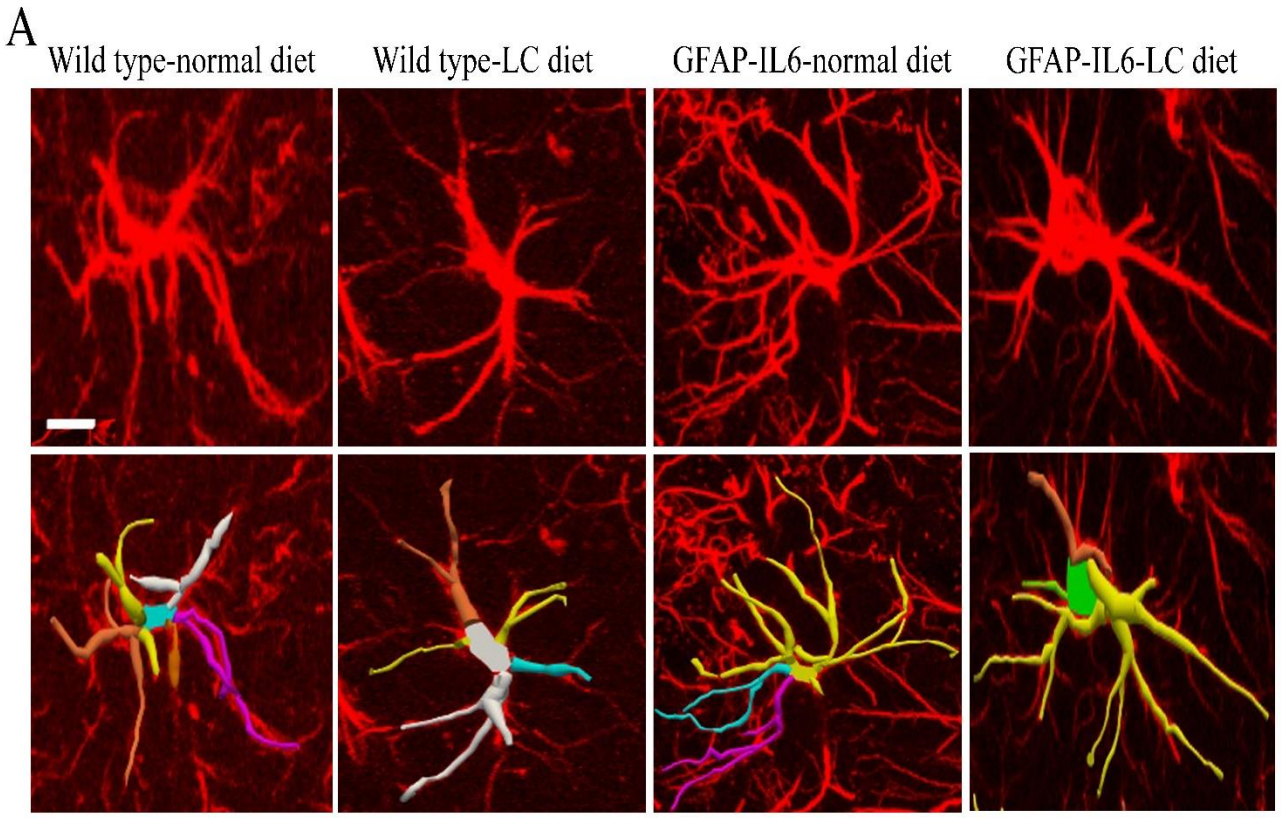

B

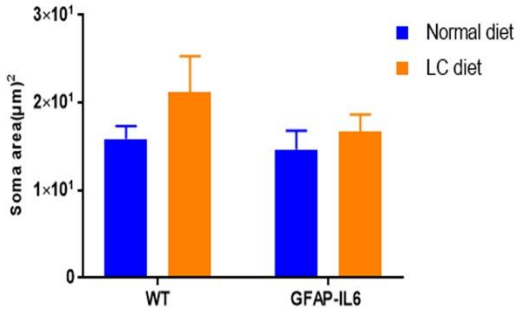
Soma area(µm)²
3×10¹
2×10¹
1×10¹
0
WT
GFAP-IL6
Normal diet
LC diet

C

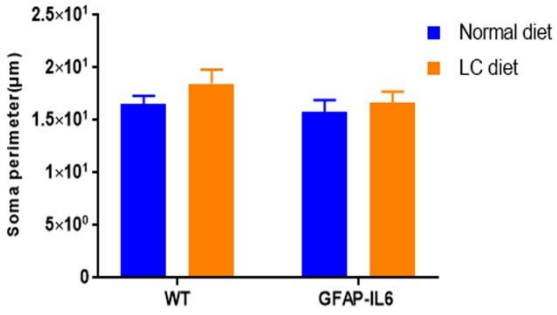
Soma perimeter(µm)
2.5×10¹
2×10¹
1.5×10¹
1×10¹
5×10⁰
0
WT
GFAP-IL6
Normal diet
LC diet

D

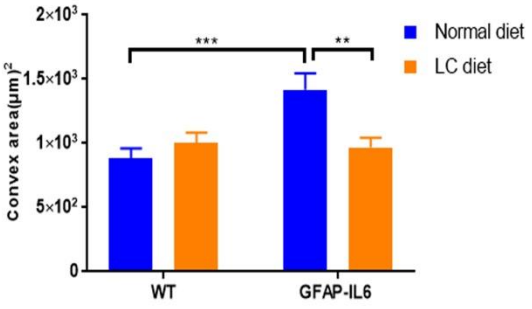
Convex area(µm)²
2×10³
1.5×10³
1×10³
5×10²
0
***
**
WT
GFAP-IL6
Normal diet
LC diet

E

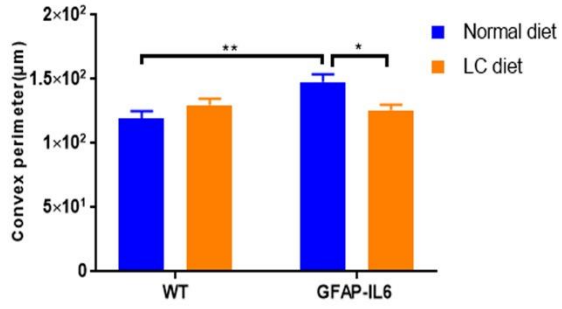
Convex perimeter(µm)
2×10²
1.5×10²
1×10²
5×10¹
0
**
*
WT
GFAP-IL6
Normal diet
LC diet

F

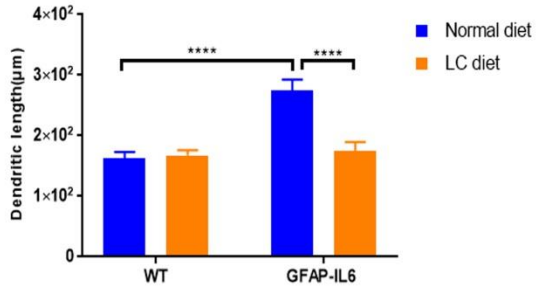
Dendritic length(µm)
4×10²
3×10²
2×10²
1×10²
0
****
****
WT
GFAP-IL6
Normal diet
LC diet

G

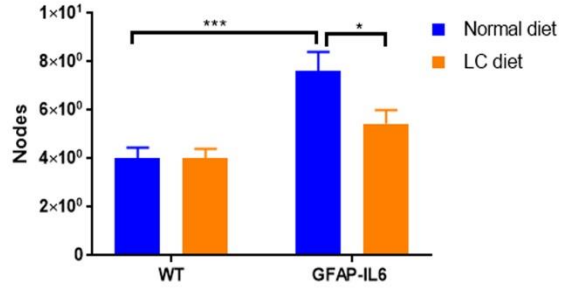
Nodes
1×10¹
8×10⁰
6×10⁰
4×10⁰
2×10⁰
0
***
*
WT
GFAP-IL6
Normal diet
LC diet

H

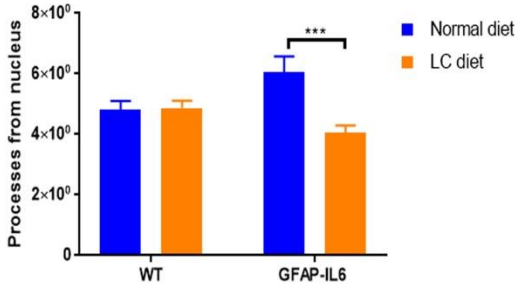
Processes from nucleus
8×10⁰
6×10⁰
4×10⁰
2×10⁰
0
***
WT
GFAP-IL6
Normal diet
LC diet

Figure 36. Effect of LC curcumin on astrocytes morphology in the hippocampus. (A) 3D reconstruction of astrocytes in wild type and GFAP-IL6 in both treated and non-treated mice Scale bar 10µm. (B-H) Graphs showing the morphological changes in Iba-1^{+} microglia. Two-way ANOVA, Tukey's post-test, mean ± SEM)

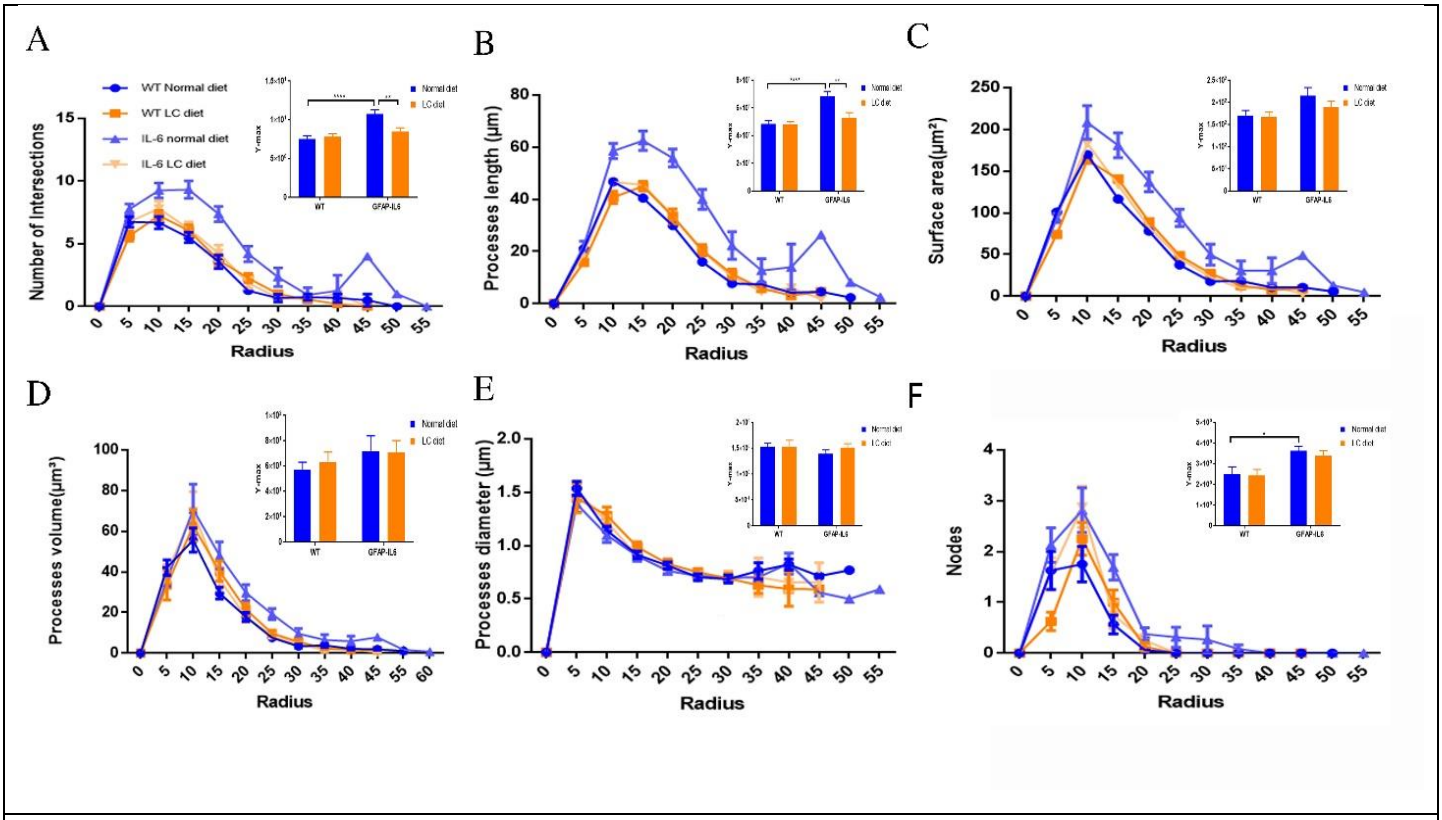

Fig 37. LC increased the ramification of astrocytes in the hippocampus region. (A-F) A Sholl analysis confirmed a significant decrease in a number of intersections and processes length in LC fed GFAP-IL6 mice compared to normal food-fed GFAP-IL6. Whereas, there were no significant changes occurred in wild type fed mice. LC significantly affects the inflamed astrocytes, which is observed in the peaks of the distributions of different morphological features being closer to the center compared to normal food-fed GFAP-IL6 mice, we call it X at Y_{max}. Two-way ANOVA test.

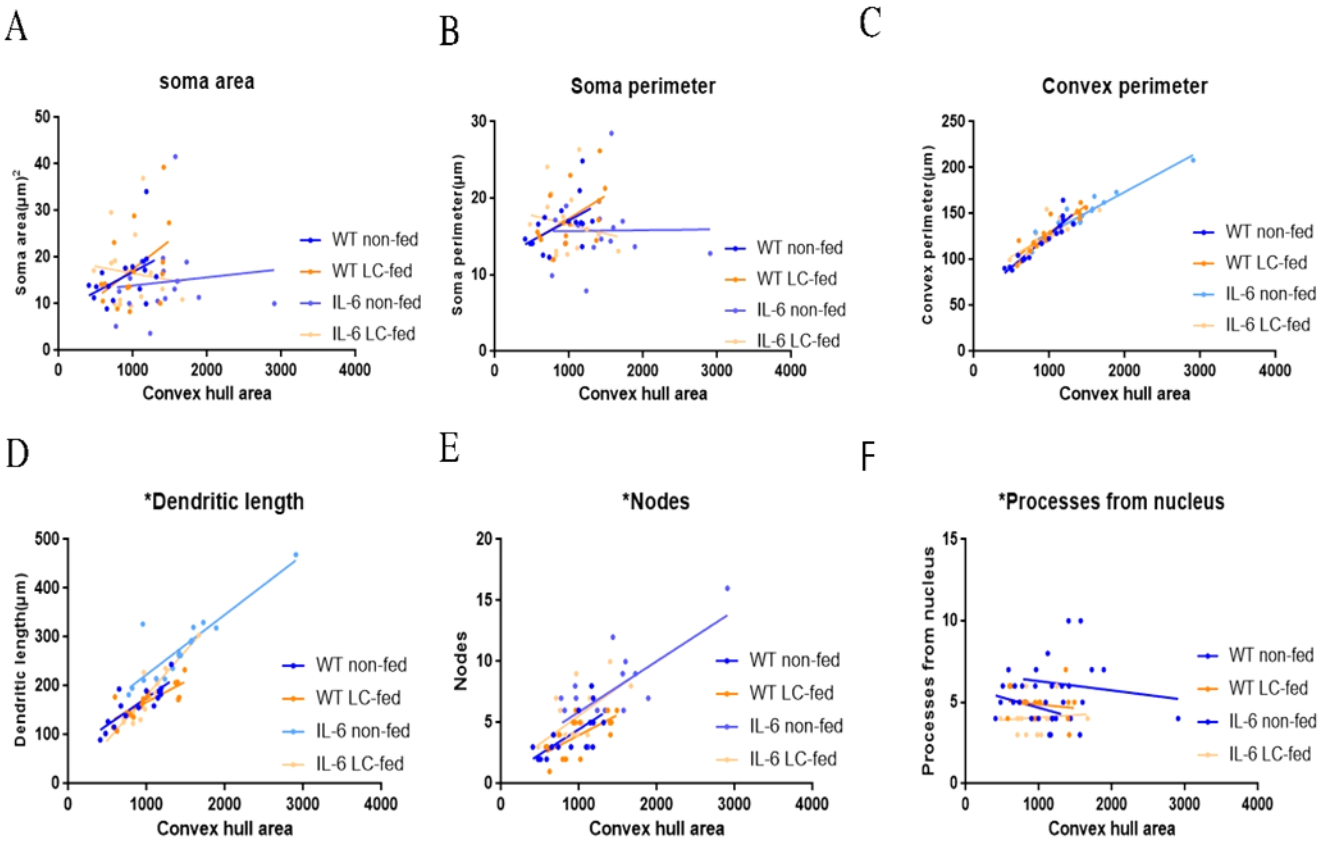

Figure 38. Bivariate correlation: Effect of LC on astrocytes morphology in the hippocampus. (A-F) Different morphological parameters have been plotted against the convex hull area to see the bivariate correlation between WT normal-diet, WT LC-diet GFAP-IL6 normal-diet, and GFAP-IL6 LC-diet.

Table 14. Morphological analysis of GFAP$^+$ astrocytes in the hippocampus

Cohorts	Diet	Soma area(µm)^2 (Mean± SEM)	Soma perimeter (µm) (Mean± SEM)	Convex 2D (area) (µm)^2(Mean± SEM)	Convex perimeter (µm) Mean± SEM)	Total length (µm) (Mean± SEM)	Number of nodes (Mean± SEM)	Number of dendrites (Mean± SEM)
WT	Normal food	15.88±1.46	16.52±0.79	885.3±76.14	119.3±5.82	163.2±10.07	4±0.45	4.81±0.29
WT	LC	21.22±4.13	18.46±1.35	1005±79.18	129.7±5.25	167.9±8.34	4±0.40	4.87±0.23
GFAP-IL6	Normal food	14.68±2.13	15.78±1.14	1418±128.3	147.9±6.01	275±17.8	7.62±0.77	6.06±0.51
GFAP-IL6	LC	16.66±1.99	16.66±1.07	968.3±74.04	125.8±4.24	175.2±14.54	5.43±0.56	4.06±0.23

Table 15. Bivariate correlation of morphological characteristics with overall astroglial cell size in the hippocampus

	Soma area		Soma perimeter		Convex perimeter		Dendritic length		Nodes		Primary dendrites	
	R^2	Correlation	R^2	Correlation	R^2	Correlation	R^2	Correlation	R^2	Correlation	R^2	Correlation
WT non-fed	0.19	0.0847	0.25	*0.0445	0.86	****<0.0001	0.70	****<0.0001	0.47	****<0.0001	0.11	0.2078
WT LC-fed	0.21	0.0825	0.25	0.0554	0.84	****<0.0001	0.63	****0.0002	0.41	***0.0002	0.02	0.5582
IL-6 non-fed	0.01	0.6979	0.00	0.9627	0.89	****<0.0001	0.78	****<0.0001	0.46	****<0.0001	0.02	0.5967
IL-6 LC-fed	0.01	0.6897	0.02	0.5403	0.69	****<0.0001	0.87	****<0.0001	0.36	****<0.0001	0.00	0.7341

4.4.3. Summary

In the present study, we have investigated some of the changes between ramified and non-ramifies microglia which is consistent with the previous reports. In the hippocampus, Iba-1^{+} microglial cells of GFAP-IL6 mice normal fed had significantly larger soma areas, small convex areas, and convex perimeter than those of WT. The LC significantly increased the dendritic length and number of nodes than that of GFAP-IL6 normal fed mice. Whereas, in the cerebellum, Iba-1^{+} microglial cells of GFAP-IL6 mice normal fed had significantly large soma area, soma perimeter, and small convex area, convex perimeter than those of the wild type non-fed mice. The LC significantly reduced soma area, soma perimeter and number of nodes Iba-1^{+} microglial cells of GFAP-IL6 LC fed mice than that of GFAP-IL6 normal fed mice.

Herein, morphological assessment of astrocytes in the hippocampus have shown that GFAP-IL6 normal-diet mice had a significantly larger dendritic length, a number of processes, convex area, convex perimeter and a number of nodes compared to the wild types. The LC diet significantly decreased the dendritic length number of processes, convex area, convex perimeter and number of nodes.

This study has investigated the impact of one of the curcumin formulation LC, against glial cell activation and chronic neuroinflammation. This study has provided a clue that LC has the potential to reduce and over-activation of microglia and astrocytes in the brain.

5. General Discussion

Chronic neuroinflammation is considered one of the major contributing factors in the progression of various neurodegenerative diseases. Chronic microglial and astroglial activation is a prominent feature of chronic neuroinflammation (Gyengesi et al. 2019). The neurons are surrounded by microglial cells in the brain. During neuroinflammation, the neurons get damaged and secrete various factors which activate the microglia to rescue neurons by upregulating phagocytosis and production of an anti-oxidant enzyme (Suzumura 2013). Few studies have claimed that chronic neuroinflammation may be an initiator in the cascade of events leading to the deficit in neuronal function which defines the disease (Lynch 2010), A study performed in hypoxia, ischemia and lipopolysaccharide (HIL) mouse model have reported the neuronal death induced in neuroinflammation. The HIL induce the neuronal injury within the hippocampus, periventricular white matter, and neocortex of mouse brain which further lead to neuronal death, enhanced HIF-1α expression, and numerous Iba-1 labelled, activated microglia. Rapamycin treatment significantly reduced neuronal death and neuroinflammation (Srivastava et al. 2016). Another study performed in hAPP-J20 AD mouse model by studying disease pathology at four different age points 6, 12, 24 and 36 weeks using stereological methods. The study has investigated that there is no neuron loss in the hippocampal CA3 region at any age and the extent of neuron loss increases with age with the number of activated microglia. However loss of neurons from the hippocampal CA1 region begins as early as 12 weeks of age, which suggest that the neuronal death and neuroinflammation are the key factors in various neurodegenerative diseases (Wright et al. 2013), Furthermore, a study performed in patients with Multiple scleroses to investigate the neuroinflammation and neuronal pathology, Chronic neuroinflammation followed by an axonal pathological features, correlating with the number of infiltrating immune cells, and focal cortical thinning seen on magnetic resonance imaging, indicating complete tissue loss and death of neuronal cell bodies (Peterson et al. 2001). These evidence suggest that neuroinflammation has a key impact on neuronal functions and neuronal survival.

In the present study, two different sets of groups were created, which were divided further into sub-cohorts for two different types of curcumin formulations. The two curcumin formulations MCP and LC have been fed to GFAP-IL6 mice for one month and six-months respectively in order to investigate the impact of these drugs on chronic neuroinflammation. In the case of MCP,

six cohorts were made and four cohorts were fed with different doses of MCP whereas; In the case of LC, four cohorts were made and only one dose of LC was fed to WT and GFAP-IL6 cohorts. We have applied an array of experimental methods, including immunohistochemistry on the brain, combined with stereology and morphological analysis to investigate the effects of these curcumin formulations.

Our results show that the number of Iba-1^+ microglia is significantly higher in the cerebellum and hippocampus of the brain in GFAP-IL6 normal fed mice compared to the WT normal fed mice in both age groups. Firstly, WT and GFAP-IL6 non-fed cohorts in these two age groups were compared. It was observed from the comparative analysis that the WTs in both age groups have very similar Iba-1^+ microglia, $TSPO^+$ microglia, and $GFAP^+$ astrocyte population numbers, with no significant differences. Similarly, the Iba-1^+ microglia in both the hippocampus and cerebellum and $TSPO^+$ microglia in the cerebellum in GFAP-IL6 groups in both age groups were similar. A previous study published by our group has estimated the number of $TSPO^+$ cells in two age groups for 8 months and 18 months. The study reported that the $TSPO^+$ cells in the 18 months age group has a significantly high number of $TSPO^+$ cells in the hippocampus whereas, the $TSPO^+$ cells in both age groups have a nearly close number in cerebellum region (Gyengesi et al. 2018) . In this study, $TSPO^+$ microglia in the cerebellum of the 4 month old group were significantly lower compared to the 8 month old group. Furthermore, $GFAP^+$ astrocytes in the hippocampus were significantly higher in 4 months old GFAP-IL6 mice compared to the 8 month cohort. The literature study has very limited information regarding the GFAP positive astrocytes. Some studies have suggested that aging in rodents brains show progressive increases in the levels of glial fibrillary acidic protein (GFAP) protein (Yoshida et al. 1996) Gyengesi et al have investigated the astrocytes number by measuring the GFAP positive cells intensity analysis. Intensity analysis for GFAP positive cells showed that GFAPIL6 mice had a significant increase in GFAP intensity in both age groups, while the cerebellum had a more prominent increase compared with the hippocampus (Gyengesi et al. 2018).

The high and medium doses of MCP significantly reduced the number of Iba-1^+ microglia in the cerebellum and the hippocampus, with the high dose of MCP resulting in the most significant decrease. Feeding LC significantly decreased the $Iba1^+$ microglia numbers by 25.88% in the hippocampus and by 48% in the cerebellum. Our results show a similar trend to a previous study

conducted in a mouse model of Alzheimer's disease (human APP and PSEN1 transgenes mice), that have compared the effect of solid lipid curcumin formulation (SLCP) and normal curcumin (Maiti, Paladugu, and Dunbar 2018). They reported that the SLCP leads to a greater reduction in Iba-1^+ microglial cells compared to the normal curcumin (Maiti, Paladugu, and Dunbar 2018). Previous studies have reported that the numbers of Iba-1^+ microglia in the mouse brain increase in chronic neuroinflammatory conditions, which were significantly reduced after being treated with anti-inflammatory drugs such as Tenilsetam and dexamethasone (Gyengesi et al. 2018; Claessens et al. 2012). A recent study conducted in a mouse model of AD has reported the protective effect of a curcumin formulation. These studies used Image-J software to count the number of the Iba-1^+ cell and reported that a solid lipid curcumin formulation was able to significantly downregulate the microglial numbers in different regions of the hippocampus in the mice brain (Maiti, Paladugu, and Dunbar 2018). Similarly, they claimed that the solid lipid curcumin has high permeability and potential effects against amyloid plaques relative to the normal curcumin (Maiti, Paladugu, and Dunbar 2018).

Microglia, as the brain immune macrophages, has a surveillance function characterized by the continuous scanning of their surrounding microenvironment in a ramified morphology (Nimmerjahn, Kirchhoff, and Helmchen 2005; Davalos et al. 2005). Resting and non-activated microglia are thought to rest in a dormant state, whereas, when activated, the microglia are then associated with structural changes (Nolte et al. 1996). A previous study performed in healthy adult mice has reported that ramified cells have small somas, long and thin processes, necessary for active surveillance of microglia microdomains (Lawson et al. 1990). However, microglial cells are activated in response to the neuronal assault, injury or inflammation, and undergo morphological transformations (Nimmerjahn, Kirchhoff, and Helmchen 2005). A recent study performed in a mouse model of AD has proved that curcumin can reduce the aggregation and de-ramification of microglial cells in the hippocampus (Maiti, Paladugu, and Dunbar 2018). Ramified microglia function in a highly dynamic manner, constantly surveying the neuronal environment for homeostatic and infective changes and protects hippocampal neurons under pathological conditions (Vinet et al. 2012). It has been reported that microglial cells are activated in response to many types of neuronal injury or inflammation, and undergo morphological transformations (Nimmerjahn, Kirchhoff, and Helmchen 2005). Moreover, resting microglia has the ability to facilitate prompt reactions to brain injury (Nolte et al. 1996). Studies have shown

that changes in microglial cell size can influence the entire morphology in response to different challenges to the CNS (Hinwood et al. 2013). A recent study conducted in mice has proved that curcumin can reduce the aggregation and de-ramification of microglial cells in the hippocampus. They reported that the microglia were more aggregated in the vehicle-treated group while, after injecting solid lipid curcumin to the mice for five days, they noticed a significant reduction in microglial aggregation, activation, and branches number (Maiti, Paladugu, and Dunbar 2018). In this study, microglial cells were reconstructed and quantitatively analyzed for changes in their morphology. It has been reported that microglial cells are activated in response to many types of neuronal injury or inflammation, and undergo morphological transformations (Nimmerjahn, Kirchhoff, and Helmchen 2005). Our results revealed that chronic neuroinflammation increased the aggregation and de-ramification of microglial cells and hypertrophy of astrocytes in GFAP-IL6 mice. The literature studies have very limited evidence about the specific mechanism of the morphological changes occurred in microglial cells in chronic neuroinflammation. In this study, the microglial soma area and soma perimeter significantly increased in both the hippocampus and cerebellum of GFAP-IL6 mice compared to those of the healthy ones. Additionally, there were a significantly larger number of processes in microglia of the inflamed brains compared to normal brains. While in the case of LC, Iba-1^{+} microglial cells of GFAP-IL6 mice normal fed had significantly larger soma areas, small convex areas, and convex perimeter than those of WT. A recent study conducted in mice has showed that curcumin formulation can reduce the aggregation and de-ramification of microglial cells in the hippocampus. They reported that the microglia were more aggregated in the vehicle-treated group while, after injecting solid lipid curcumin to the mice for five days, they noticed a significant reduction in microglial aggregation, activation, and branches number (Maiti, Paladugu, and Dunbar 2018). Our results indicated that the high dose MCP significantly reduced the soma area and soma perimeter, while it significantly increased the number of nodes in the hippocampus. In the cerebellum, the high dose MCP significantly reduced the soma area and soma perimeter while it increased the convex area, convex perimeter, and dendritic length compared to the non-fed control. Interestingly, the morphology of microglia in the 140mg NC, GFAPIL6 mice was also affected, as soma area and soma perimeter was significantly decreased in the cerebellum of GFAP-IL6 mice. In short, the MCP modified microglia morphology towards that of in the normal mice. Whereas, The LC significantly increased the dendritic length and number of nodes than that of GFAP-IL6 normal

fed mice in the hippocampus and significantly reduced soma area, soma perimeter and more number of nodes Iba-1^{+} microglial cells of GFAP-IL6 LC fed mice than that of GFAP-IL6 normal fed mice in the cerebellum.

The previous research study had mentioned that microglial size has an impact on the overall cellular morphology (Raivich 2005). One of the studies performed in rats has correlated the microglial cells with total processes length, branch point, and total branch volume. They found that larger cells tended to have larger, thicker and more branches (Kongsui et al. 2014). In the present study, the correlation analysis revealed some significant correlations. In the hippocampus, microglial cells of WT and 70 mg/kg fed groups tended to increase the size of the soma area and convex perimeter of the microglia of each cohort with the increasing size of the cells. Whereas, the dendritic length of the microglia of the fed cohorts were increased with the overall cell size. While, in the cerebellum, it showed that the soma area and dendritic length of the microglia changed with the overall cell size, while the convex perimeter increased with the overall increase in microglial cells. In case of LC, in the hippocampus, correlation analysis of overall microglial cell size with each morphological characteristic revealed that the microglial cells of the GFAP-IL6 LC fed mice potentially increased the overall soma size and dendrites number. In addition, the convex perimeter and dendritic length of each cohort increased with the increasing size of the entire cell. In the cerebellum, it shows that the convex perimeter and the length of dendrites increased with the overall increase in microglial cells and numbers of nodes in GFAP-IL6 non fed cohorts were increased with the overall increase in microglial cells.

The unique microglial morphology in human brains is more challenging. Postmortem studies have confirmed the existence of various morphological phenotypes (Sheng, Mrak, and Griffin 1997). Recent advances in neuroimaging techniques have made it possible to visualize microglial activation by positron emission tomography (PET) (Banati 2002). Using this approach, the presence of activated microglia has been reported in the brains of humans who suffer from brain disorders such as Alzheimer's disease and Parkinson's disease (Cagnin et al. 2001). There are a still much gap and the lack of detailed knowledge on the fine properties of microglia in the human brain, and how these properties could be compared to those of rodents. A study conducted on human brains having died with no history of inflammatory. The study found different microglial phenotypes in postmortem samples of the dorsal anterior cingulate cortex

(dACC) (Miller et al. 2013). One interesting finding emerged from this analysis is to relate to mouse and human microglia. One of the studies conducted on human microglia has reported ramified microglia in the human prefrontal cortex have an average 5.8 (±0.5) primary processes (Torres-Platas et al. 2014) and we have identified that there are around 5.06 (±0.30) in mice (Table 10), which turned out to be comparable.

TSPO exists in the outer mitochondrial membrane of the cell and it plays important roles in cell physiology (Papadopoulos et al. 1997). It has been reported in the literature studies that TSPO protein is expressed in microglia, astrocytes and at low levels in neurons in diseased brains (Cosenza-Nashat et al. 2009). In a study conducted in mice, it has been reported that the fluorescence intensity and the number of $TSPO^+$ per $0.1mm^2$, has elevated in the brain after exposure to an injury or inflammation (Bonsack, Alleyne, and Sukumari-Ramesh 2016). Another study conducted in our group in the same mouse model found that the number of $TSPO^+$ cells was increased in GFAP-IL6 mice and even more in drug (Tenilsetam) treated mice (Gyengesi et al. 2018). In the present study, we have investigated the $TSPO^+$ microglia cells only based on their morphology. Our study found that the total estimated number of $TSPO^+$ microglia cells was significantly larger in the GFAP-IL6 group than that of the WT group in the cerebellum and the hippocampus. In our study, the 140mg/kg of MCP significantly downregulated microglial cells number in GFAP-IL6 mice in both the hippocampus and the cerebellum compared to the non-fed group. While LC significantly reduced the $TSPO^+$ microglia numbers by 31% in the cerebellum and 24.45% in the hippocampus.

Like microglia, astrocytes are also activated in response to injury, trauma, neuroinflammation and various other CNS challenges. When activated, they adopt more bushy shape with an increase in their number and length of processes (Fawcett and Asher 1999; McGraw, Hiebert, and Steeves 2001; Sofroniew 2009). A study recently used curcumin formulation has reported that curcumin treatment has decreased the astrocyte activation (Maiti, Paladugu, and Dunbar 2018). Astrocytes are activated in response to neuroinflammation or injury. A study performed in a mouse model of Alzheimer's disease has reported inhibition of $GFAP^+$ astrocytes after being treated with curcumin and SLCP (Maiti, Paladugu, and Dunbar 2018). In our study, a significantly higher number of $GFAP^+$ astrocytes have been observed in GFAP-IL6 mice compared to WT mice in the hippocampus. All three doses of MCP significantly decreased the

number of reactive astrocytes in the hippocampus compared to the GPAP-IL6 control mice whereas, in the LC fed GFAP-IL6 mice, a significant reduction in $GFAP^{+}$ astrocytes were observed by 30% compared to the GFAP-IL6 normal food fed mice.

Astrocytes, as a part of the anti-inflammatory response, are also activated in response to injury, trauma, neuroinflammation and various other CNS challenges and adopt more bushy shape with an increase in their number and length of processes, when activated (Fawcett and Asher 1999; McGraw, Hiebert, and Steeves 2001; Sofroniew 2009). Once they are activated, the reactive astrocytes undergo morphological changes relative to the resting cells, wherein cellular processes extend (Wilhelmsson et al. 2006; Grosche et al. 1999). In the MCP case, morphological investigations of astrocytes in the hippocampus have shown that astrocytes of GFAP-IL6 mice have significantly longer dendritic length and convex area compared to that of WT mice cells. While, in LC case, GFAP-IL6 normal-diet mice had a significantly larger dendritic length, a number of processes, convex area, convex perimeter and a number of nodes compared to the wild types. A study conducted in rat injury models has reported a decrease in hypertrophy of astrocytes after been treated with curcumin formulations (Ji et al. 2013; Maiti, Paladugu, and Dunbar 2018). Therefore, high dose MCP has significantly reduced the dendritic length and convex area in GFAP-IL6 fed mice compared to the normal fed GFAP-IL6 mice. While, The LC diet significantly decreased the dendritic length number of processes, convex area, convex perimeter and number of nodes.

Furthermore, the bivariate correlations of morphological characteristics were performed with overall astroglial cell size to investigate the impact of the size of astroglial cells on the structural parameters. In MCP, it was observed that the number of nodes in the astrocytes of 35mg/kg and 140mg/kg fed cohorts decreased when the overall size of the astrocytes decreased. In the case of primary dendrites, both the 70mg/kg and 140mg/kg doses positively decreased them with the decrease in the overall cell size of astrocytes. This clearly showed that the 140mg MCP decrease the astrocytes activation and reduced its size like the astrocytes in the WT. Whereas, we observed some positive correlation of the astroglial cell size with the some of the morphological parameters, which revealed that the convex perimeter, dendritic length and the number of nodes increased significantly with the overall increase in the entire cell structure

In summary, our study has investigated that, the MCP short term feeding at a reasonable dose (highest dose: 140mg/kg bw, approx. 12mg/kg bw in humans) is able to significantly downregulate the chronic neuroinflammation in the GFAP-IL6 measured by various anatomical markers, which could be translated into human studies with patients with neuroinflammatory disorders. Whereas, long term feeding of LC (Dose: 500ppm, approx. 3.5mg/kg bw in humans) has the potential to reduce the chronic neuroinflammation and over-activation of microglia and astrocytes in the brain.

This study has investigated that, the MCP at a reasonable dose (highest dose: 140mg/kg bw, approx. 12mg/kg bw in humans) and LC (500ppm~60mg/kg bw, approx. 5.5mg/kg bw in humans) is able to significantly downregulate the microglial and astroglial activation in the GFAP-IL6 measured by various anatomical markers. It also has investigated that both formulations of curcumin have the potential to reverse the activation of microglial and astrocytes measured through morphological tools. Altogether this study did both answered some questions and opened a new window of possibilities in order to ameliorate the chronic neuroinflammation symptoms caused by over-activation of microglia and astrocytes in the brain.

Our results might also have clinical relevance if translated into human studies in patients with neuroinflammatory disorders following the progress of their treatment with curcumin using different imaging techniques such as PET imaging with TSPO ligands (Dupont et al. 2017). There are a number of curcumin formulations tested in human patients and volunteers to investigate its effects against chronic inflammation conditions. Curcumin C3 complex® (Sabinsa Corporation Piscataway, NJ, USA) is a curcumin formulation. In a study, this formulation was taken by patients with mild AD on 2 and 4 gm/day for 24-weeks to two different groups. No differences were detected between treatment groups and placebo due to the low bioavailability of the curcumin as the likely reason (Ringman et al. 2012). The major challenges to the therapeutic potential of curcumin, which are identified as a potential limitation in most CNS disorders, are its poor bioavailability and BBB permeability, therefore, controlled formulation of curcumin is required for effective therapeutic outcomes. In a study, preclinical investigations have been conducted in 60 healthy adults aged 60-85. This double-blind, randomized, placebo-controlled trial examined the acute (1 and 3 h after a single dose), chronic (4 weeks) and acute-on-chronic (1 and 3 h after single dose following chronic treatment) effects of solid

lipid curcumin formulation (400 mg as Longvida®) on cognitive function, mood and blood biomarkers in 60 healthy adults aged 60-85. The study has proved that curcumin significantly improved performance, memory, and mood compared with placebo in healthy human subjects (Cox, Pipingas, and Scholey 2015). Few studies have been performed in patients with Alzheimer's disease. Baum et al. (Baum et al. 2008) conducted a randomized, double-blind, placebo-controlled study 34 patients with Alzheimer's disease. Two different doses of curcumin mixed with food (1 g/day or 4 g/day) or placebo (4 g/day) were received by each subject for six months the Mini-Mental State Examination (MMSE) score change was measured between the baseline and the follow-up assessment. The authors did not observe any significant difference between curcumin and placebo and no reduction in serum Aβ40 levels were observed (Baum et al. 2008). Another double-blind, placebo-controlled was conducted in 36 patients with dementia which randomly received two different doses of Curcumin C3 Complex in two divided doses or placebo for 24 weeks which was extended to 48 weeks. The authors have stated some outcomes that the patients become better and a change at the Neuropsychiatric Inventory (NPI), the Alzheimer's disease Cooperative Study Activities of Daily Living (ADCS-ADL), and the MMSE were observed (Ringman et al. 2012). Another study conducted in 2012, has reported that three dementia patients treated with 100 mg/day of curcumin for 12 weeks reprted a decreased in NPI-questionnaire brief version (NPI-Q) score (particularly, reduction in agitation, irritability, anxiety, and apathy) (Hishikawa et al. 2012). Similarly, there are several ongoing clinical trials evaluating the efficacy of curcumin in AD patients and neuroinflammatory conditions with the Australian and New Zealand clinical trial (ANZCTR). According to ANZCTR, In Australia, a randomized double-blind placebo controlled trial has been started and is recruiting patients with dementia (sample size: 200) which will be treated with oral curcumin titrated up to 1500 mg/day. The expected outcome is the prevention of the cognitive decline in the curcumin treated group. Similarly, the two curcumin formulations used in this study have very positive outcomes in mouse models and these preparations could be used in diseases with neuroinflammatory responses in human patients in the future.

6. Future directions

Our study have reported some of the key investigations but some limitations of this study are there. In future, gene expression profiles study using RNA sequencing, flow cytometry, and the curcumin concentration in the brain would give some more understanding about the exact mechanism and effects of curcumin against neuroinflammation. Few studies in the literature have investigated the gene expression profiles in order to reveal the microglial or even astroglial activation. A study performed in transgenic mice expressing eGFP in CNS resident microglia and peripheral monocytes ($CX3CR1^{+/GFP}$) with spinal card injury (SCI). The study has investigated the molecular alterations in microglia, the potential involvement of DNA damage, the upregulation of tumor suppressor gene *breast cancer susceptibility gene 1* (*Brca1*) in microglia and increased expression of microglia and monocyte markers after SCI and neuroinflammation (Noristani et al. 2017). The same study has also used flow cytometry to study neuroinflammation after injury and reported eGFP high expressing cells (Noristani et al. 2017). Another study has shown that ramified microglia express $CD11b^{+}/CD45^{low}$ cells whereas fully activated microglia and infiltrating macrophages are $CD11b^{+}/CD45^{high}$ cells using flow cytometry (David and Kroner 2011). Similarly, a study conducted in aged C57BL/6J mice and mice lacking the microglial-secreted cytokines (IL-1α, TNF, and C1q) known to induce astrocyte activation have reported that the astrocytes gene is activated during aging and neuroinflammation which leads to astrocytes activation (Clarke et al. 2018). The difference in protein expression is difficult to reliably quantify histologically, but rather more accurate when microglia and macrophages are isolated from CNS tissue and analysed by flow cytometric. A study has discovered that in contrast to peripheral macrophages, parenchymal microglia expressed much lower levels of CD45, a protein tyrosine phosphatase expressed by all nucleated cells of hemopoietic lineage (Carson, Thrash, and Walter 2006). A cell-specific flow cytometry and gene expression study were performed in the Superoxide Dismutase 1 $(SOD1)^{G93A}$ transgenic mouse model of ALS. The study showed significant phenotypic changes in microglia and the expression of genes linked to neuroprotection and neuroinflammation (Chiu et al. 2008).In the future, it could be possible to determine the exact concentration of curcumin and its derivatives and metabolites in the brain. Moreover, the beneficial effects of MCP and LC on impairment in cognition and motor performance of GFAP-IL6 mice would be a worthwhile investigation.

7. References

Abdel-Rahman, A., M. S. Rao, and A. K. Shetty. 2004. 'Nestin expression in hippocampal astrocytes after injury depends on the age of the hippocampus', *Glia*, 47: 299-313.

Abe, Y., S. Hashimoto, and T. Horie. 1999. 'Curcumin inhibition of inflammatory cytokine production by human peripheral blood monocytes and alveolar macrophages', *Pharmacological research : the official journal of the Italian Pharmacological Society*, 39: 41-7.

Aggarwal, B. B., S. C. Gupta, and B. Sung. 2013. 'Curcumin: an orally bioavailable blocker of TNF and other pro-inflammatory biomarkers', *Br J Pharmacol*, 169: 1672-92.

Aggarwal, Bharat B, Young-Joon Surh, and Shishir Shishodia. 2007. *The molecular targets and therapeutic uses of curcumin in health and disease* (Springer Science & Business Media).

Agostinho, P., R. A. Cunha, and C. Oliveira. 2010. 'Neuroinflammation, oxidative stress and the pathogenesis of Alzheimer's disease', *Curr Pharm Des*, 16: 2766-78.

Ahmad, M. H., M. Fatima, and A. C. Mondal. 2019. 'Influence of microglia and astrocyte activation in the neuroinflammatory pathogenesis of Alzheimer's disease: Rational insights for the therapeutic approaches', *J Clin Neurosci*, 59: 6-11.

Akira, S., T. Hirano, T. Taga, and T. Kishimoto. 1990. 'Biology of multifunctional cytokines: IL 6 and related molecules (IL 1 and TNF)', *Faseb j*, 4: 2860-7.

Akira, S., K. Takeda, and T. Kaisho. 2001. 'Toll-like receptors: critical proteins linking innate and acquired immunity', *Nat Immunol*, 2: 675-80.

Akiyama, H., S. Barger, S. Barnum, B. Bradt, J. Bauer, G. M. Cole, N. R. Cooper, P. Eikelenboom, M. Emmerling, B. L. Fiebich, C. E. Finch, S. Frautschy, W. S. Griffin, H. Hampel, M. Hull, G. Landreth, L. Lue, R. Mrak, I. R. Mackenzie, P. L. McGeer, M. K. O'Banion, J. Pachter, G. Pasinetti, C. Plata-Salaman, J. Rogers, R. Rydel, Y. Shen, W. Streit, R. Strohmeyer, I. Tooyoma, F. L. Van Muiswinkel, R. Veerhuis, D. Walker, S. Webster, B. Wegrzyniak, G. Wenk, and T. Wyss-Coray. 2000. 'Inflammation and Alzheimer's disease', *Neurobiol Aging*, 21: 383-421.

Anand, P., A. B. Kunnumakkara, R. A. Newman, and B. B. Aggarwal. 2007. 'Bioavailability of curcumin: problems and promises', *Mol Pharm*, 4: 807-18.

Anand, P., S. G. Thomas, A. B. Kunnumakkara, C. Sundaram, K. B. Harikumar, B. Sung, S. T. Tharakan, K. Misra, I. K. Priyadarsini, K. N. Rajasekharan, and B. B. Aggarwal. 2008. 'Biological activities of curcumin and its analogues (Congeners) made by man and Mother Nature', *Biochem Pharmacol*, 76: 1590-611.

Arends, Y. M., C. Duyckaerts, J. M. Rozemuller, P. Eikelenboom, and J. J. Hauw. 2000. 'Microglia, amyloid and dementia in alzheimer disease. A correlative study', *Neurobiol Aging*, 21: 39-47.

Ballabh, P., A. Braun, and M. Nedergaard. 2004. 'The blood-brain barrier: an overview: structure, regulation, and clinical implications', *Neurobiol Dis*, 16: 1-13.

Barzaghi, N., F. Crema, G. Gatti, G. Pifferi, and E. Perucca. 1990. 'Pharmacokinetic studies on IdB 1016, a silybin- phosphatidylcholine complex, in healthy human subjects', *Eur J Drug Metab Pharmacokinet*, 15: 333-8.

Basnet, P, I Tho, and N Skalko-Basnet. 2010. "Curcumin, a wonder drug of 21st century: liposomal delivery system targeting vaginal inflammation." In *5th International Congress on Complementary Medicine Research, Tromsø, Norway*.

Bastide, M. F., S. Dovero, G. Charron, G. Porras, C. E. Gross, P. O. Fernagut, and E. Bezard. 2014. 'Immediate-early gene expression in structures outside the basal ganglia is associated to l-DOPA-induced dyskinesia', *Neurobiol Dis*, 62: 179-92.

Baum, L., C. W. Lam, S. K. Cheung, T. Kwok, V. Lui, J. Tsoh, L. Lam, V. Leung, E. Hui, C. Ng, J. Woo, H. F. Chiu, W. B. Goggins, B. C. Zee, K. F. Cheng, C. Y. Fong, A. Wong, H. Mok, M. S. Chow, P. C. Ho, S. P. Ip, C. S. Ho, X. W. Yu, C. Y. Lai, M. H. Chan, S. Szeto, I. H. Chan, and V. Mok. 2008. 'Six-month randomized, placebo-controlled, double-blind, pilot clinical trial of curcumin in patients with Alzheimer disease', *J Clin Psychopharmacol*, 28: 110-3.

Beggs, Simon, and Michael W. Salter. 2007. 'Stereological and somatotopic analysis of the spinal microglial response to peripheral nerve injury', *Brain, Behavior, and Immunity*, 21: 624-33.

Begum, A. N., M. R. Jones, G. P. Lim, T. Morihara, P. Kim, D. D. Heath, C. L. Rock, M. A. Pruitt, F. Yang, B. Hudspeth, S. Hu, K. F. Faull, B. Teter, G. M. Cole, and S. A. Frautschy. 2008a. 'Curcumin structure-function, bioavailability, and efficacy in models of neuroinflammation and Alzheimer's disease', *The Journal of pharmacology and experimental therapeutics*, 326: 196-208.

———. 2008b. 'Curcumin structure-function, bioavailability, and efficacy in models of neuroinflammation and Alzheimer's disease', *J Pharmacol Exp Ther*, 326: 196-208.

Bento-Torres, J., L. L. Sobral, R. R. Reis, R. B. de Oliveira, D. C. Anthony, P. F. C. Vasconcelos, Pican, #xe7, and Cristovam Wanderley o Diniz. 2017. 'Age and Environment Influences on Mouse Prion Disease Progression: Behavioral Changes and Morphometry and Stereology of Hippocampal Astrocytes', *Oxidative Medicine and Cellular Longevity*, 2017: 18.

Betlazar, C., M. Harrison-Brown, R. J. Middleton, R. Banati, and G. J. Liu. 2018. 'Cellular Sources and Regional Variations in the Expression of the Neuroinflammatory Marker Translocator Protein (TSPO) in the Normal Brain', *Int J Mol Sci*, 19.

Bharti, A. C., N. Donato, and B. B. Aggarwal. 2003. 'Curcumin (diferuloylmethane) inhibits constitutive and IL-6-inducible STAT3 phosphorylation in human multiple myeloma cells', *J Immunol*, 171: 3863-71.

Block, M. L., and J. S. Hong. 2007. 'Chronic microglial activation and progressive dopaminergic neurotoxicity', *Biochem Soc Trans*, 35: 1127-32.

Block, M. L., L. Zecca, and J. S. Hong. 2007a. 'Microglia-mediated neurotoxicity: uncovering the molecular mechanisms', *Nat Rev Neurosci*, 8: 57-69.

Block, Michelle L., Luigi Zecca, and Jau-Shyong Hong. 2007b. 'Microglia-mediated neurotoxicity: uncovering the molecular mechanisms', 8: 57.

Bobbo, V. C. D., C. P. Jara, N. F. Mendes, J. Morari, L. A. Velloso, and E. P. Araujo. 2019. 'Interleukin-6 Expression by Hypothalamic Microglia in Multiple Inflammatory Contexts: A Systematic Review', *Biomed Res Int*, 2019: 1365210.

Bombardelli, E, A Cristoni, and P Morazzoni. 1994. 'Phytosomes in functional cosmetics', *Fitoterapia*, 65: 387-401.

Bombardelli, E, SB Curri, LR Della, NP Del, A Tubaro, and P Gariboldi. 1989. 'Complexes between phospholipids and vegetal derivatives of biological interest', *Fitoterapia*, 60: 1-9.

Bonsack, Frederick, Cargill H. Alleyne, and Sangeetha Sukumari-Ramesh. 2016. 'Augmented expression of TSPO after intracerebral hemorrhage: a role in inflammation?', *Journal of Neuroinflammation*, 13: 151.

Bowman, Christal C, Amy Rasley, Susanne L Tranguch, and Ian Marriott. 2003. 'Cultured astrocytes express toll-like receptors for bacterial products', *Glia*, 43: 281-91.

Braak, H, and E Braak. 1998. 'Evolution of neuronal changes in the course of Alzheimer's disease.' in, *Ageing and Dementia* (Springer).

Breitner, J. C., L. D. Baker, T. J. Montine, C. L. Meinert, C. G. Lyketsos, K. H. Ashe, J. Brandt, S. Craft, D. E. Evans, R. C. Green, M. S. Ismail, B. K. Martin, M. J. Mullan, M. Sabbagh, and P. N. Tariot. 2011.

'Extended results of the Alzheimer's disease anti-inflammatory prevention trial', *Alzheimers Dement*, 7: 402-11.

Brett, Francesca M, Andrew P Mizisin, Henry C Powell, and Iain L Campbell. 1995. 'Evolution of neuropathologic abnormalities associated with blood-brain barrier breakdown in transgenic mice expressing interleukin-6 in astrocytes', *Journal of Neuropathology & Experimental Neurology*, 54: 766-75.

Bronson, R. T., R. D. Lipman, and D. E. Harrison. 1993. 'Age-related gliosis in the white matter of mice', *Brain Res*, 609: 124-8.

Bushong, E. A., M. E. Martone, Y. Z. Jones, and M. H. Ellisman. 2002. 'Protoplasmic astrocytes in CA1 stratum radiatum occupy separate anatomical domains', *J Neurosci*, 22: 183-92.

Campbell, I L, C R Abraham, E Masliah, P Kemper, J D Inglis, M B Oldstone, and L Mucke. 1993a. 'Neurologic disease induced in transgenic mice by cerebral overexpression of interleukin 6', *Proceedings of the National Academy of Sciences*, 90: 10061-65.

Campbell, I. L. 1998. 'Structural and functional impact of the transgenic expression of cytokines in the CNS', *Ann N Y Acad Sci*, 840: 83-96.

Campbell, I. L., C. R. Abraham, E. Masliah, P. Kemper, J. D. Inglis, M. B. Oldstone, and L. Mucke. 1993b. 'Neurologic disease induced in transgenic mice by cerebral overexpression of interleukin 6', *Proc Natl Acad Sci U S A*, 90: 10061-5.

Campbell, I. L., M. Erta, S. L. Lim, R. Frausto, U. May, S. Rose-John, J. Scheller, and J. Hidalgo. 2014. 'Trans-signaling is a dominant mechanism for the pathogenic actions of interleukin-6 in the brain', *J Neurosci*, 34: 2503-13.

Campbell, I. L., M. V. Hobbs, J. Dockter, M. B. Oldstone, and J. Allison. 1994. 'Islet inflammation and hyperplasia induced by the pancreatic islet-specific overexpression of interleukin-6 in transgenic mice', *Am J Pathol*, 145: 157-66.

Campbell, I. L., M. J. Hofer, and A. Pagenstecher. 2010. 'Transgenic models for cytokine-induced neurological disease', *Biochim Biophys Acta*, 1802: 903-17.

Cardona, A. E., E. P. Pioro, M. E. Sasse, V. Kostenko, S. M. Cardona, I. M. Dijkstra, D. Huang, G. Kidd, S. Dombrowski, R. Dutta, J. C. Lee, D. N. Cook, S. Jung, S. A. Lira, D. R. Littman, and R. M. Ransohoff. 2006. 'Control of microglial neurotoxicity by the fractalkine receptor', *Nat Neurosci*, 9: 917-24.

Carson, M. J., J. C. Thrash, and B. Walter. 2006. 'The cellular response in neuroinflammation: The role of leukocytes, microglia and astrocytes in neuronal death and survival', *Clin Neurosci Res*, 6: 237-45.

Casellas, P., S. Galiegue, and A. S. Basile. 2002. 'Peripheral benzodiazepine receptors and mitochondrial function', *Neurochem Int*, 40: 475-86.

Castano, A., A. J. Herrera, J. Cano, and A. Machado. 2002. 'The degenerative effect of a single intranigral injection of LPS on the dopaminergic system is prevented by dexamethasone, and not mimicked by rh-TNF-alpha, IL-1beta and IFN-gamma', *J Neurochem*, 81: 150-7.

Chan, M. M., H. I. Huang, M. R. Fenton, and D. Fong. 1998. 'In vivo inhibition of nitric oxide synthase gene expression by curcumin, a cancer preventive natural product with anti-inflammatory properties', *Biochem Pharmacol*, 55: 1955-62.

Chattopadhyay, Ishita, Kaushik Biswas, Uday Bandyopadhyay, and Ranajit K Banerjee. 2004. 'Turmeric and curcumin: Biological actions and medicinal applications', *Curr Sci*, 87: 44-53.

Chen, M. K., and T. R. Guilarte. 2008. 'Translocator protein 18 kDa (TSPO): molecular sensor of brain injury and repair', *Pharmacol Ther*, 118: 1-17.

Cheng, Ann-Lii, Chih-Hung Hsu, Jen-Kun Lin, Mow-Ming Hsu, Yunn-Fang Ho, Tzung-Shiahn Shen, Jenq-Yuh Ko, Jaw-Town Lin, Bor-Ru Lin, and W Ming-Shiang. 2001. 'Phase I clinical trial of curcumin, a chemopreventive agent, in patients with high-risk or pre-malignant lesions', *Anticancer Res*, 21: 2895-900.

Chiang, C. S., A. Stalder, A. Samimi, and I. L. Campbell. 1994. 'Reactive gliosis as a consequence of interleukin-6 expression in the brain: studies in transgenic mice', *Dev Neurosci*, 16: 212-21.

Chiu, Isaac M., Adam Chen, Yi Zheng, Bela Kosaras, Stefanos A. Tsiftsoglou, Timothy K. Vartanian, Robert H. Brown, and Michael C. Carroll. 2008. 'T lymphocytes potentiate endogenous neuroprotective inflammation in a mouse model of ALS', *Proceedings of the National Academy of Sciences*, 105: 17913-18.

Chiu, S. S., E. Lui, M. Majeed, J. K. Vishwanatha, A. P. Ranjan, A. Maitra, D. Pramanik, J. A. Smith, and L. Helson. 2011. 'Differential distribution of intravenous curcumin formulations in the rat brain', *Anticancer Res*, 31: 907-11.

Choi, Moonseok, Sangzin Ahn, Eun-Jeong Yang, Hyunju Kim, Young Hae Chong, and Hye-Sun Kim. 2016. 'Hippocampus-based contextual memory alters the morphological characteristics of astrocytes in the dentate gyrus', *Molecular Brain*, 9: 72.

Citernesi, U, and M Sciacchitano. 1995. 'Phospholipid/active ingredient complexes', *Cosmetics and toiletries*, 110: 57-68.

Claessens, Sanne E. F., Joseph K. Belanoff, Sofia Kanatsou, Paul J. Lucassen, Danielle L. Champagne, and E. Ronald de Kloet. 2012. 'Acute effects of neonatal dexamethasone treatment on proliferation and astrocyte immunoreactivity in hippocampus and corpus callosum: Towards a rescue strategy', *Brain Research*, 1482: 1-12.

Clarke, Laura E., Shane A. Liddelow, Chandrani Chakraborty, Alexandra E. Münch, Myriam Heiman, and Ben A. Barres. 2018. 'Normal aging induces A1-like astrocyte reactivity', *Proceedings of the National Academy of Sciences*, 115: E1896-E905.

Colombo, E., and C. Farina. 2016. 'Astrocytes: Key Regulators of Neuroinflammation', *Trends Immunol*, 37: 608-20.

Cornago, Pilar, Rosa M. Claramunt, Latifa Bouissane, Ibon Alkorta, and José Elguero. 2008. 'A study of the tautomerism of β-dicarbonyl compounds with special emphasis on curcuminoids', *Tetrahedron*, 64: 8089-94.

Cosenza-Nashat, M., M. L. Zhao, H. S. Suh, J. Morgan, R. Natividad, S. Morgello, and S. C. Lee. 2009. 'Expression of the translocator protein of 18 kDa by microglia, macrophages and astrocytes based on immunohistochemical localization in abnormal human brain', *Neuropathol Appl Neurobiol*, 35: 306-28.

Cox, K. H., A. Pipingas, and A. B. Scholey. 2015. 'Investigation of the effects of solid lipid curcumin on cognition and mood in a healthy older population', *J Psychopharmacol*, 29: 642-51.

Cuomo, J., G. Appendino, A. S. Dern, E. Schneider, T. P. McKinnon, M. J. Brown, S. Togni, and B. M. Dixon. 2011. 'Comparative absorption of a standardized curcuminoid mixture and its lecithin formulation', *J Nat Prod*, 74: 664-9.

Dadhaniya, P., C. Patel, J. Muchhara, N. Bhadja, N. Mathuria, K. Vachhani, and M. G. Soni. 2011. 'Safety assessment of a solid lipid curcumin particle preparation: acute and subchronic toxicity studies', *Food Chem Toxicol*, 49: 1834-42.

Dantzer, R., J. C. O'Connor, G. G. Freund, R. W. Johnson, and K. W. Kelley. 2008. 'From inflammation to sickness and depression: when the immune system subjugates the brain', *Nat Rev Neurosci*, 9: 46-56.

Das, L., and M. Vinayak. 2014. 'Long-term effect of curcumin down-regulates expression of tumor necrosis factor-alpha and interleukin-6 via modulation of E26 transformation-specific protein and nuclear factor-kappaB transcription factors in livers of lymphoma bearing mice', *Leuk Lymphoma*, 55: 2627-36.

Davalos, D., J. Grutzendler, G. Yang, J. V. Kim, Y. Zuo, S. Jung, D. R. Littman, M. L. Dustin, and W. B. Gan. 2005. 'ATP mediates rapid microglial response to local brain injury in vivo', *Nat Neurosci*, 8: 752-8.

David, Samuel, and Antje Kroner. 2011. 'Repertoire of microglial and macrophage responses after spinal cord injury', *Nature Reviews Neuroscience*, 12: 388-99.
Davis, E. J., T. D. Foster, and W. E. Thomas. 1994. 'Cellular forms and functions of brain microglia', *Brain Res Bull*, 34: 73-8.
Davis, S., and S. Laroche. 2003. 'What can rodent models tell us about cognitive decline in Alzheimer's disease?', *Mol Neurobiol*, 27: 249-76.
Dempe, Julia, Erika Pfeiffer, and Manfred Metzler. 2007. 'Curcumin accumulates in membrane structures of human Ishikawa and HT-29 cells', *Cancer Epidemiology Biomarkers & Prevention*, 16: A122-A22.
Devi, Y. S., M. DeVine, J. DeKuiper, S. Ferguson, and A. T. Fazleabas. 2015. 'Inhibition of IL-6 signaling pathway by curcumin in uterine decidual cells', *PLoS One*, 10: e0125627.
DiSilvestro, R. A., E. Joseph, S. Zhao, and J. Bomser. 2012. 'Diverse effects of a low dose supplement of lipidated curcumin in healthy middle aged people', *Nutr J*, 11: 79.
Drion, C. M., J. van Scheppingen, A. Arena, K. W. Geijtenbeek, L. Kooijman, E. A. van Vliet, E. Aronica, and J. A. Gorter. 2018. 'Effects of rapamycin and curcumin on inflammation and oxidative stress in vitro and in vivo — in search of potential anti-epileptogenic strategies for temporal lobe epilepsy', *Journal of Neuroinflammation*, 15: 212.
Dupont, A. C., B. Largeau, M. J. Santiago Ribeiro, D. Guilloteau, C. Tronel, and N. Arlicot. 2017. 'Translocator Protein-18 kDa (TSPO) Positron Emission Tomography (PET) Imaging and Its Clinical Impact in Neurodegenerative Diseases', *Int J Mol Sci*, 18.
Farina, C., F. Aloisi, and E. Meinl. 2007. 'Astrocytes are active players in cerebral innate immunity', *Trends Immunol*, 28: 138-45.
Fawcett, J. W., and R. A. Asher. 1999. 'The glial scar and central nervous system repair', *Brain Res Bull*, 49: 377-91.
Gabay, C., and I. Kushner. 1999. 'Acute-phase proteins and other systemic responses to inflammation', *N Engl J Med*, 340: 448-54.
Garcia-Alloza, M., L. A. Borrelli, A. Rozkalne, B. T. Hyman, and B. J. Bacskai. 2007. 'Curcumin labels amyloid pathology in vivo, disrupts existing plaques, and partially restores distorted neurites in an Alzheimer mouse model', *J Neurochem*, 102: 1095-104.
Glass, Christopher K., Kaoru Saijo, Beate Winner, Maria Carolina Marchetto, and Fred H. Gage. 2010. 'Mechanisms Underlying Inflammation in Neurodegeneration', *Cell*, 140: 918-34.
Goel, A., and B. B. Aggarwal. 2010. 'Curcumin, the golden spice from Indian saffron, is a chemosensitizer and radiosensitizer for tumors and chemoprotector and radioprotector for normal organs', *Nutr Cancer*, 62: 919-30.
Goel, A., A. B. Kunnumakkara, and B. B. Aggarwal. 2008. 'Curcumin as "Curecumin": from kitchen to clinic', *Biochem Pharmacol*, 75: 787-809.
Gota, V. S., G. B. Maru, T. G. Soni, T. R. Gandhi, N. Kochar, and M. G. Agarwal. 2010. 'Safety and pharmacokinetics of a solid lipid curcumin particle formulation in osteosarcoma patients and healthy volunteers', *J Agric Food Chem*, 58: 2095-9.
Grosche, J., V. Matyash, T. Moller, A. Verkhratsky, A. Reichenbach, and H. Kettenmann. 1999. 'Microdomains for neuron-glia interaction: parallel fiber signaling to Bergmann glial cells', *Nat Neurosci*, 2: 139-43.
Gruol, D. L., and T. E. Nelson. 1997. 'Physiological and pathological roles of interleukin-6 in the central nervous system', *Mol Neurobiol*, 15: 307-39.
Guerreiro, R. J., I. Santana, J. M. Bras, B. Santiago, A. Paiva, and C. Oliveira. 2007. 'Peripheral inflammatory cytokines as biomarkers in Alzheimer's disease and mild cognitive impairment', *Neurodegener Dis*, 4: 406-12.

Gulbransen, B. D., and K. A. Sharkey. 2012. 'Novel functional roles for enteric glia in the gastrointestinal tract', *Nat Rev Gastroenterol Hepatol*, 9.

Gunawardena, D., N. Karunaweera, S. Lee, F. van Der Kooy, D. G. Harman, R. Raju, L. Bennett, E. Gyengesi, N. J. Sucher, and G. Munch. 2015. 'Anti-inflammatory activity of cinnamon (C. zeylanicum and C. cassia) extracts - identification of E-cinnamaldehyde and o-methoxy cinnamaldehyde as the most potent bioactive compounds', *Food Funct*, 6: 910-9.

Gyengesi, E., H. Liang, C. Millington, S. Sonego, D. Sirijovski, D. Gunawardena, K. Dhananjayan, M. Venigalla, G. Niedermayer, and G. Munch. 2018. 'Investigation Into the Effects of Tenilsetam on Markers of Neuroinflammation in GFAP-IL6 Mice', *Pharm Res*, 35: 22.

Gyengesi, E., A. Rangel, F. Ullah, H. Liang, G. Niedermayer, R. Asgarov, M. Venigalla, D. Gunawardena, T. Karl, and G. Munch. 2019. 'Chronic Microglial Activation in the GFAP-IL6 Mouse Contributes to Age-Dependent Cerebellar Volume Loss and Impairment in Motor Function', *Front Neurosci*, 13: 303.

Hama, T., Y. Kushima, M. Miyamoto, M. Kubota, N. Takei, and H. Hatanaka. 1991. 'Interleukin-6 improves the survival of mesencephalic catecholaminergic and septal cholinergic neurons from postnatal, two-week-old rats in cultures', *Neuroscience*, 40: 445-52.

Hanai, H., T. Iida, K. Takeuchi, F. Watanabe, Y. Maruyama, A. Andoh, T. Tsujikawa, Y. Fujiyama, K. Mitsuyama, M. Sata, M. Yamada, Y. Iwaoka, K. Kanke, H. Hiraishi, K. Hirayama, H. Arai, S. Yoshii, M. Uchijima, T. Nagata, and Y. Koide. 2006. 'Curcumin maintenance therapy for ulcerative colitis: randomized, multicenter, double-blind, placebo-controlled trial', *Clin Gastroenterol Hepatol*, 4: 1502-6.

He, P., Z. Zhong, K. Lindholm, L. Berning, W. Lee, C. Lemere, M. Staufenbiel, R. Li, and Y. Shen. 2007. 'Deletion of tumor necrosis factor death receptor inhibits amyloid beta generation and prevents learning and memory deficits in Alzheimer's mice', *J Cell Biol*, 178: 829-41.

Hefendehl, J. K., J. J. Neher, R. B. Suhs, S. Kohsaka, A. Skodras, and M. Jucker. 2014. 'Homeostatic and injury-induced microglia behavior in the aging brain', *Aging Cell*, 13: 60-9.

Heinrich, P. C., I. Behrmann, S. Haan, H. M. Hermanns, G. Muller-Newen, and F. Schaper. 2003. 'Principles of interleukin (IL)-6-type cytokine signalling and its regulation', *Biochem J*, 374: 1-20.

Heneka, M. T., M. J. Carson, J. El Khoury, G. E. Landreth, F. Brosseron, D. L. Feinstein, A. H. Jacobs, T. Wyss-Coray, J. Vitorica, R. M. Ransohoff, K. Herrup, S. A. Frautschy, B. Finsen, G. C. Brown, A. Verkhratsky, K. Yamanaka, J. Koistinaho, E. Latz, A. Halle, G. C. Petzold, T. Town, D. Morgan, M. L. Shinohara, V. H. Perry, C. Holmes, N. G. Bazan, D. J. Brooks, S. Hunot, B. Joseph, N. Deigendesch, O. Garaschuk, E. Boddeke, C. A. Dinarello, J. C. Breitner, G. M. Cole, D. T. Golenbock, and M. P. Kummer. 2015. 'Neuroinflammation in Alzheimer's disease', *Lancet Neurol*, 14: 388-405.

Heneka, M. T., D. T. Golenbock, and E. Latz. 2015. 'Innate immunity in Alzheimer's disease', *Nature Immunology*, 16: 229-36.

Heneka, M. T., M. P. Kummer, and E. Latz. 2014. 'Innate immune activation in neurodegenerative disease', *Nat Rev Immunol*, 14: 463-77.

Henry, C. J., Y. Huang, A. Wynne, M. Hanke, J. Himler, M. T. Bailey, J. F. Sheridan, and J. P. Godbout. 2008. 'Minocycline attenuates lipopolysaccharide (LPS)-induced neuroinflammation, sickness behavior, and anhedonia', *J Neuroinflammation*, 5: 15.

Hinwood, Madeleine, Ross J. Tynan, Janine L. Charnley, Sarah B. Beynon, Trevor A. Day, and F. Rohan Walker. 2013. 'Chronic Stress Induced Remodeling of the Prefrontal Cortex: Structural Re-Organization of Microglia and the Inhibitory Effect of Minocycline', *Cerebral Cortex*, 23: 1784-97.

Hirano, T., S. Akira, T. Taga, and T. Kishimoto. 1990. 'Biological and clinical aspects of interleukin 6', *Immunol Today*, 11: 443-9.

Hirano, T., T. Taga, N. Nakano, K. Yasukawa, S. Kashiwamura, K. Shimizu, K. Nakajima, K. H. Pyun, and T. Kishimoto. 1985. 'Purification to homogeneity and characterization of human B-cell differentiation factor (BCDF or BSFp-2)', *Proc Natl Acad Sci U S A*, 82: 5490-4.

Hirano, T., K. Yasukawa, H. Harada, T. Taga, Y. Watanabe, T. Matsuda, S. Kashiwamura, K. Nakajima, K. Koyama, A. Iwamatsu, and et al. 1986. 'Complementary DNA for a novel human interleukin (BSF-2) that induces B lymphocytes to produce immunoglobulin', *Nature*, 324: 73-6.

Hirsch, E. C., and S. Hunot. 2009. 'Neuroinflammation in Parkinson's disease: a target for neuroprotection?', *Lancet Neurol*, 8: 382-97.

Hishikawa, N., Y. Takahashi, Y. Amakusa, Y. Tanno, Y. Tuji, H. Niwa, N. Murakami, and U. K. Krishna. 2012. 'Effects of turmeric on Alzheimer's disease with behavioral and psychological symptoms of dementia', *Ayu*, 33: 499-504.

Honda, M., S. Yamamoto, M. Cheng, K. Yasukawa, H. Suzuki, T. Saito, Y. Osugi, T. Tokunaga, and T. Kishimoto. 1992. 'Human soluble IL-6 receptor: its detection and enhanced release by HIV infection', *J Immunol*, 148: 2175-80.

Hoppe, J. B., K. Coradini, R. L. Frozza, C. M. Oliveira, A. B. Meneghetti, A. Bernardi, E. S. Pires, R. C. Beck, and C. G. Salbego. 2013. 'Free and nanoencapsulated curcumin suppress beta-amyloid-induced cognitive impairments in rats: involvement of BDNF and Akt/GSK-3beta signaling pathway', *Neurobiol Learn Mem*, 106: 134-44.

Iliff, J. J., M. Wang, Y. Liao, B. A. Plogg, W. Peng, G. A. Gundersen, H. Benveniste, G. E. Vates, R. Deane, S. A. Goldman, E. A. Nagelhus, and M. Nedergaard. 2012. 'A paravascular pathway facilitates CSF flow through the brain parenchyma and the clearance of interstitial solutes, including amyloid beta', *Sci Transl Med*, 4: 147ra11.

Indena SA. 'Indena SA Human pharmacokinetic study with curcumin. Unpublished.'.

Jager, R., R. P. Lowery, A. V. Calvanese, J. M. Joy, M. Purpura, and J. M. Wilson. 2014. 'Comparative absorption of curcumin formulations', *Nutr J*, 13: 11.

Jayaprakasha, G. K., L. Jagan Mohan Rao, and K. K. Sakariah. 2005. 'Chemistry and biological activities of C. longa', *Trends in Food Science & Technology*, 16: 533-48.

Ji, F. T., J. J. Liang, L. Liu, M. H. Cao, and F. Li. 2013. 'Curcumin exerts antinociceptive effects by inhibiting the activation of astrocytes in spinal dorsal horn and the intracellular extracellular signal-regulated kinase signaling pathway in rat model of chronic constriction injury', *Chin Med J (Engl)*, 126: 1125-31.

Jin, C. Y., J. D. Lee, C. Park, Y. H. Choi, and G. Y. Kim. 2007. 'Curcumin attenuates the release of pro-inflammatory cytokines in lipopolysaccharide-stimulated BV2 microglia', *Acta Pharmacol Sin*, 28: 1645-51.

Johnston, H., H. Boutin, and S. M. Allan. 2011. 'Assessing the contribution of inflammation in models of Alzheimer's disease', *Biochem Soc Trans*, 39: 886-90.

Jung, K. K., H. S. Lee, J. Y. Cho, W. C. Shin, M. H. Rhee, T. G. Kim, J. H. Kang, S. H. Kim, S. Hong, and S. Y. Kang. 2006. 'Inhibitory effect of curcumin on nitric oxide production from lipopolysaccharide-activated primary microglia', *Life Sci*, 79: 2022-31.

Kang, G., P. J. Kong, Y. J. Yuh, S. Y. Lim, S. V. Yim, W. Chun, and S. S. Kim. 2004. 'Curcumin suppresses lipopolysaccharide-induced cyclooxygenase-2 expression by inhibiting activator protein 1 and nuclear factor kappab bindings in BV2 microglial cells', *J Pharmacol Sci*, 94: 325-8.

Kettenmann, H., F. Kirchhoff, and A. Verkhratsky. 2013. 'Microglia: new roles for the synaptic stripper', *Neuron*, 77: 10-8.

Kidd, P. . 2009. 'Bioavailability and activity of phytosome complexes from botanical polyphenols: the silymarin, curcumin, green tea, and grape seed extracts', *Altern Med Rev*, 14: 226-46.

Kidd, P., and K. Head. 2005. 'A review of the bioavailability and clinical efficacy of milk thistle phytosome: a silybin-phosphatidylcholine complex (Siliphos)', *Altern Med Rev*, 10: 193-203.

Kigerl, K. A., J. C. Gensel, D. P. Ankeny, J. K. Alexander, D. J. Donnelly, and P. G. Popovich. 2009. 'Identification of two distinct macrophage subsets with divergent effects causing either neurotoxicity or regeneration in the injured mouse spinal cord', *J Neurosci*, 29: 13435-44.

Kim, H. Y., E. J. Park, E. H. Joe, and I. Jou. 2003. 'Curcumin suppresses Janus kinase-STAT inflammatory signaling through activation of Src homology 2 domain-containing tyrosine phosphatase 2 in brain microglia', *J Immunol*, 171: 6072-9.

Kim, J. B., A. R. Han, E. Y. Park, J. Y. Kim, W. Cho, J. Lee, E. K. Seo, and K. T. Lee. 2007. 'Inhibition of LPS-induced iNOS, COX-2 and cytokines expression by poncirin through the NF-kappaB inactivation in RAW 264.7 macrophage cells', *Biol Pharm Bull*, 30: 2345-51.

Kimelberg, H. K., and M. D. Norenberg. 1989. 'Astrocytes', *Sci Am*, 260: 66-72, 74, 76.

Kirkley, Kelly S., Katriana A. Popichak, Maryam F. Afzali, Marie E. Legare, and Ronald B. Tjalkens. 2017. 'Microglia amplify inflammatory activation of astrocytes in manganese neurotoxicity', *J Neuroinflammation*, 14: 99.

Kishimoto, T. 2010. 'IL-6: from its discovery to clinical applications', *Int Immunol*, 22: 347-52.

Kongsui, R., S. B. Beynon, S. J. Johnson, and F. R. Walker. 2014. 'Quantitative assessment of microglial morphology and density reveals remarkable consistency in the distribution and morphology of cells within the healthy prefrontal cortex of the rat', *J Neuroinflammation*, 11: 182.

Kraska, A., M. D. Santin, O. Dorieux, N. Joseph-Mathurin, E. Bourrin, F. Petit, C. Jan, M. Chaigneau, P. Hantraye, P. Lestage, and M. Dhenain. 2012. 'In vivo cross-sectional characterization of cerebral alterations induced by intracerebroventricular administration of streptozotocin', *PLoS One*, 7: e46196.

Kuhlmann, A. C., and T. R. Guilarte. 2000. 'Cellular and subcellular localization of peripheral benzodiazepine receptors after trimethyltin neurotoxicity', *J Neurochem*, 74: 1694-704.

Lawson, L. J., V. H. Perry, P. Dri, and S. Gordon. 1990. 'Heterogeneity in the distribution and morphology of microglia in the normal adult mouse brain', *Neuroscience*, 39: 151-70.

Like, A. A., and A. A. Rossini. 1976. 'Streptozotocin-induced pancreatic insulitis: new model of diabetes mellitus', *Science*, 193: 415-7.

Lim, G. P., T. Chu, F. Yang, W. Beech, S. A. Frautschy, and G. M. Cole. 2001. 'The curry spice curcumin reduces oxidative damage and amyloid pathology in an Alzheimer transgenic mouse', *J Neurosci*, 21: 8370-7.

Liu, G. J., R. J. Middleton, C. R. Hatty, W. W. Kam, R. Chan, T. Pham, M. Harrison-Brown, E. Dodson, K. Veale, and R. B. Banati. 2014. 'The 18 kDa translocator protein, microglia and neuroinflammation', *Brain Pathol*, 24: 631-53.

Liu, Zun-Jing, Zhong-Hao Li, Lei Liu, Wen-Xiong Tang, Yu Wang, Ming-Rui Dong, and Cheng Xiao. 2016. 'Curcumin Attenuates Beta-Amyloid-Induced Neuroinflammation via Activation of Peroxisome Proliferator-Activated Receptor-Gamma Function in a Rat Model of Alzheimer's Disease', *Frontiers in Pharmacology*, 7.

Loddick, S. A., A. V. Turnbull, and N. J. Rothwell. 1998. 'Cerebral interleukin-6 is neuroprotective during permanent focal cerebral ischemia in the rat', *J Cereb Blood Flow Metab*, 18: 176-9.

Lust, J. A., K. A. Donovan, M. P. Kline, P. R. Greipp, R. A. Kyle, and N. J. Maihle. 1992. 'Isolation of an mRNA encoding a soluble form of the human interleukin-6 receptor', *Cytokine*, 4: 96-100.

Lynch, Marina. 2010. 'Age-related neuroinflammatory changes negatively impact on neuronal function', *Frontiers in Aging Neuroscience*, 1.

Ma, Q. L., X. Zuo, F. Yang, O. J. Ubeda, D. J. Gant, M. Alaverdyan, E. Teng, S. Hu, P. P. Chen, P. Maiti, B. Teter, G. M. Cole, and S. A. Frautschy. 2013a. 'Curcumin suppresses soluble tau dimers and corrects molecular chaperone, synaptic, and behavioral deficits in aged human tau transgenic mice', *J Biol Chem*, 288: 4056-65.

———. 2013b. 'Curcumin suppresses soluble tau dimers and corrects molecular chaperone, synaptic, and behavioral deficits in aged human tau transgenic mice', *The Journal of biological chemistry*, 288: 4056-65.
Maiti K, Mukherjee k, Gantait A, Ahamed H.N, Saha B.P, Mukherjee P.K. 2005. 'Enhanced therapeutic benefit of quercetin–phospholipid complex in carbon tetrachloride-induced acute liver injury in rats: a comparative study', *Iran J Pharmacol Ther* 4: 84–90.
Maiti, Panchanan, Leela Paladugu, and Gary L. Dunbar. 2018. 'Solid lipid curcumin particles provide greater anti-amyloid, anti-inflammatory and neuroprotective effects than curcumin in the 5xFAD mouse model of Alzheimer's disease', *BMC Neuroscience*, 19: 7.
Manach, C., A. Scalbert, C. Morand, C. Remesy, and L. Jimenez. 2004. 'Polyphenols: food sources and bioavailability', *Am J Clin Nutr*, 79: 727-47.
Mandybur, T. I., I. Ormsby, and F. P. Zemlan. 1989. 'Cerebral aging: a quantitative study of gliosis in old nude mice', *Acta Neuropathol*, 77: 507-13.
Marczylo, T. H., R. D. Verschoyle, D. N. Cooke, P. Morazzoni, W. P. Steward, and A. J. Gescher. 2007. 'Comparison of systemic availability of curcumin with that of curcumin formulated with phosphatidylcholine', *Cancer Chemotherapy and Pharmacology*, 60: 171-77.
Mathew, A. , and S. Pushpanath. 2005. 'Indian Spices, ' *DEE BEE Info Publications*.
Mauri, P., P. Simonetti, C. Gardana, M. Minoggio, P. Morazzoni, E. Bombardelli, and P. Pietta. 2001. 'Liquid chromatography/atmospheric pressure chemical ionization mass spectrometry of terpene lactones in plasma of volunteers dosed with Ginkgo biloba L. extracts', *Rapid Commun Mass Spectrom*, 15: 929-34.
McGraw, J., G. W. Hiebert, and J. D. Steeves. 2001. 'Modulating astrogliosis after neurotrauma', *J Neurosci Res*, 63: 109-15.
Meager. 2004. 'Cytokines: interleukins,' *R. Meyers, Ed*, Encyclopedia of Molecular Cell Biology and Molecular Medicine

115–51.
Meda, L., P. Baron, and G. Scarlato. 2001. 'Glial activation in Alzheimer's disease: the role of Abeta and its associated proteins', *Neurobiol Aging*, 22: 885-93.
Meda, L., M. A. Cassatella, G. I. Szendrei, L. Otvos, Jr., P. Baron, M. Villalba, D. Ferrari, and F. Rossi. 1995. 'Activation of microglial cells by beta-amyloid protein and interferon-gamma', *Nature*, 374: 647-50.
Mendes, N. F., Y. B. Kim, L. A. Velloso, and E. P. Araujo. 2018. 'Hypothalamic Microglial Activation in Obesity: A Mini-Review', *Front Neurosci*, 12: 846.
Menon, V. P., and A. R. Sudheer. 2007. 'Antioxidant and anti-inflammatory properties of curcumin', *Adv Exp Med Biol*, 595: 105-25.
Milanski, M., G. Degasperi, A. Coope, J. Morari, R. Denis, D. E. Cintra, D. M. Tsukumo, G. Anhe, M. E. Amaral, H. K. Takahashi, R. Curi, H. C. Oliveira, J. B. Carvalheira, S. Bordin, M. J. Saad, and L. A. Velloso. 2009. 'Saturated fatty acids produce an inflammatory response predominantly through the activation of TLR4 signaling in hypothalamus: implications for the pathogenesis of obesity', *J Neurosci*, 29: 359-70.
Miller, A. H., E. Haroon, C. L. Raison, and J. C. Felger. 2013. 'Cytokine targets in the brain: impact on neurotransmitters and neurocircuits', *Depress Anxiety*, 30: 297-306.
Milobedzka J, Kostanecki V, Lampe V 1910. 'Structure of curcumin', *Ber. Dtsch. Chem*: 2163-70.
Minogue, A. M., J. P. Barrett, and M. A. Lynch. 2012. 'LPS-induced release of IL-6 from glia modulates production of IL-1beta in a JAK2-dependent manner', *J Neuroinflammation*, 9: 126.
Mirzaei, Nazanin, Sac Pham Tang, Sharon Ashworth, Christopher Coello, Christophe Plisson, Jan Passchier, Vimal Selvaraj, Robin J. Tyacke, David J. Nutt, and Magdalena Sastre. 2016. 'In vivo

imaging of microglial activation by positron emission tomography with [11C]PBR28 in the 5XFAD model of Alzheimer's disease', *Glia*, 64: 993-1006.
Morazzoni, P., M. J. Magistretti, C. Giachetti, and G. Zanolo. 1992. 'Comparative bioavailability of Silipide, a new flavanolignan complex, in rats', *Eur J Drug Metab Pharmacokinet*, 17: 39-44.
Morgan, J. T., N. Barger, D. G. Amaral, and C. M. Schumann. 2014. 'Stereological study of amygdala glial populations in adolescents and adults with autism spectrum disorder', *PLoS One*, 9: e110356.
Mouton, P. R., J. M. Long, D. L. Lei, V. Howard, M. Jucker, M. E. Calhoun, and D. K. Ingram. 2002. 'Age and gender effects on microglia and astrocyte numbers in brains of mice', *Brain Res*, 956: 30-5.
Munch, G., R. Schinzel, C. Loske, A. Wong, N. Durany, J. J. Li, H. Vlassara, M. A. Smith, G. Perry, and P. Riederer. 1998. 'Alzheimer's disease--synergistic effects of glucose deficit, oxidative stress and advanced glycation endproducts', *J Neural Transm (Vienna)*, 105: 439-61.
Munoz-Fernandez, M. A., and M. Fresno. 1998. 'The role of tumour necrosis factor, interleukin 6, interferon-gamma and inducible nitric oxide synthase in the development and pathology of the nervous system', *Prog Neurobiol*, 56: 307-40.
Murata, M., A. Takahashi, I. Saito, and S. Kawanishi. 1999. 'Site-specific DNA methylation and apoptosis: induction by diabetogenic streptozotocin', *Biochem Pharmacol*, 57: 881-7.
Nahar, P. P., A. L. Slitt, and N. P. Seeram. 2015. 'Anti-Inflammatory Effects of Novel Standardized Solid Lipid Curcumin Formulations', *J Med Food*, 18: 786-92.
Nazem, A., R. Sankowski, M. Bacher, and Y. Al-Abed. 2015. 'Rodent models of neuroinflammation for Alzheimer's disease', *J Neuroinflammation*, 12: 74.
Nimmerjahn, A., F. Kirchhoff, and F. Helmchen. 2005. 'Resting microglial cells are highly dynamic surveillants of brain parenchyma in vivo', *Science*, 308: 1314-8.
Noble, F., E. Rubira, M. Boulanouar, B. Palmier, M. Plotkine, J. M. Warnet, C. Marchand-Leroux, and F. Massicot. 2007. 'Acute systemic inflammation induces central mitochondrial damage and mnesic deficit in adult Swiss mice', *Neurosci Lett*, 424: 106-10.
Nolte, C., T. Moller, T. Walter, and H. Kettenmann. 1996. 'Complement 5a controls motility of murine microglial cells in vitro via activation of an inhibitory G-protein and the rearrangement of the actin cytoskeleton', *Neuroscience*, 73: 1091-107.
Noristani, Harun N., Yannick N. Gerber, Jean-Charles Sabourin, Marine Le Corre, Nicolas Lonjon, Nadine Mestre-Frances, Hélène E. Hirbec, and Florence E. Perrin. 2017. 'RNA-Seq Analysis of Microglia Reveals Time-Dependent Activation of Specific Genetic Programs following Spinal Cord Injury', *Frontiers in Molecular Neuroscience*, 10.
Norman, J. . 1991. 'The Complete Book of Spices', *Viking Studio Books, Penguin Books USA Inc*, Viking Studio Books, Penguin Books USA Inc.
Novick, D., H. Engelmann, D. Wallach, and M. Rubinstein. 1989. 'Soluble cytokine receptors are present in normal human urine', *J Exp Med*, 170: 1409-14.
Ohsawa, K., Y. Imai, Y. Sasaki, and S. Kohsaka. 2004. 'Microglia/macrophage-specific protein Iba1 binds to fimbrin and enhances its actin-bundling activity', *J Neurochem*, 88: 844-56.
Olivera, A., T. W. Moore, F. Hu, A. P. Brown, A. Sun, D. C. Liotta, J. P. Snyder, Y. Yoon, H. Shim, A. I. Marcus, A. H. Miller, and T. W. Pace. 2012. 'Inhibition of the NF-kappaB signaling pathway by the curcumin analog, 3,5-Bis(2-pyridinylmethylidene)-4-piperidone (EF31): anti-inflammatory and anti-cancer properties', *Int Immunopharmacol*, 12: 368-77.
Palsson-McDermott, E. M., and L. A. O'Neill. 2004. 'Signal transduction by the lipopolysaccharide receptor, Toll-like receptor-4', *Immunology*, 113: 153-62.
Paolicelli, R. C., G. Bolasco, F. Pagani, L. Maggi, M. Scianni, P. Panzanelli, M. Giustetto, T. A. Ferreira, E. Guiducci, L. Dumas, D. Ragozzino, and C. T. Gross. 2011. 'Synaptic pruning by microglia is necessary for normal brain development', *Science*, 333: 1456-8.

Papadopoulos, V., H. Amri, N. Boujrad, C. Cascio, M. Culty, M. Garnier, M. Hardwick, H. Li, B. Vidic, A. S. Brown, J. L. Reversa, J. M. Bernassau, and K. Drieu. 1997. 'Peripheral benzodiazepine receptor in cholesterol transport and steroidogenesis', *Steroids*, 62: 21-8.

Parpura, V., T. A. Basarsky, F. Liu, K. Jeftinija, S. Jeftinija, and P. G. Haydon. 1994. 'Glutamate-mediated astrocyte-neuron signalling', *Nature*, 369: 744-7.

Payton, F., P. Sandusky, and W. L. Alworth. 2007. 'NMR study of the solution structure of curcumin', *J Nat Prod*, 70: 143-6.

Pekny, M., and M. Nilsson. 2005. 'Astrocyte activation and reactive gliosis', *Glia*, 50: 427-34.

Peterson, J. W., L. Bo, S. Mork, A. Chang, and B. D. Trapp. 2001. 'Transected neurites, apoptotic neurons, and reduced inflammation in cortical multiple sclerosis lesions', *Ann Neurol*, 50: 389-400.

Pocock, J. M., and H. Kettenmann. 2007. 'Neurotransmitter receptors on microglia', *Trends Neurosci*, 30: 527-35.

Priyadarsini, K. I. 2013. 'Chemical and structural features influencing the biological activity of curcumin', *Curr Pharm Des*, 19: 2093-100.

Quintana, Albert, Marcus Müller, Ricardo F. Frausto, Raquel Ramos, Daniel R. Getts, Elisenda Sanz, Markus J. Hofer, Marius Krauthausen, Nicholas J. C. King, Juan Hidalgo, and Iain L. Campbell. 2009. 'Site-Specific Production of IL-6 in the Central Nervous System Retargets and Enhances the Inflammatory Response in Experimental Autoimmune Encephalomyelitis', *The Journal of Immunology*, 183: 2079-88.

Raivich, G. 2005. 'Like cops on the beat: the active role of resting microglia', *Trends Neurosci*, 28: 571-3.

Ransohoff, R. M. 2016. 'A polarizing question: do M1 and M2 microglia exist?', *Nat Neurosci*, 19: 987-91.

Ray, B., and D. K. Lahiri. 2009. 'Neuroinflammation in Alzheimer's disease: different molecular targets and potential therapeutic agents including curcumin', *Curr Opin Pharmacol*, 9: 434-44.

Ringman, J. M., S. A. Frautschy, E. Teng, A. N. Begum, J. Bardens, M. Beigi, K. H. Gylys, V. Badmaev, D. D. Heath, L. G. Apostolova, V. Porter, Z. Vanek, G. A. Marshall, G. Hellemann, C. Sugar, D. L. Masterman, T. J. Montine, J. L. Cummings, and G. M. Cole. 2012. 'Oral curcumin for Alzheimer's disease: tolerability and efficacy in a 24-week randomized, double blind, placebo-controlled study', *Alzheimers Res Ther*, 4: 43.

Rinwa, P., A. Kumar, and S. Garg. 2013. 'Suppression of neuroinflammatory and apoptotic signaling cascade by curcumin alone and in combination with piperine in rat model of olfactory bulbectomy induced depression', *PLoS One*, 8: e61052.

Rogers, J. T., L. M. Leiter, J. McPhee, C. M. Cahill, S. S. Zhan, H. Potter, and L. N. Nilsson. 1999. 'Translation of the alzheimer amyloid precursor protein mRNA is up-regulated by interleukin-1 through 5'-untranslated region sequences', *J Biol Chem*, 274: 6421-31.

Rosenblat, J. D., D. S. Cha, R. B. Mansur, and R. S. McIntyre. 2014. 'Inflamed moods: A review of the interactions between inflammation and mood disorders', *Prog Neuropsychopharmacol Biol Psychiatry*, 53C: 23-34.

Roughley, Peter J., and Donald A. Whiting. 1973. 'Experiments in the biosynthesis of curcumin', *Journal of the Chemical Society, Perkin Transactions 1*: 2379-88.

Salvi, V., F. Sozio, S. Sozzani, and A. Del Prete. 2017. 'Role of Atypical Chemokine Receptors in Microglial Activation and Polarization', *Front Aging Neurosci*, 9: 148.

Sasaki, A. 2017. 'Microglia and brain macrophages: An update', *Neuropathology*, 37: 452-64.

Satoh, T., S. Nakamura, T. Taga, T. Matsuda, T. Hirano, T. Kishimoto, and Y. Kaziro. 1988. 'Induction of neuronal differentiation in PC12 cells by B-cell stimulatory factor 2/interleukin 6', *Mol Cell Biol*, 8: 3546-9.

Semalty, A., M. Semalty, M. S. Rawat, and F. Franceschi. 2010. 'Supramolecular phospholipids-polyphenolics interactions: the PHYTOSOME strategy to improve the bioavailability of phytochemicals', *Fitoterapia*, 81: 306-14.

Seyedzadeh, M. H., Z. Safari, A. Zare, J. Gholizadeh Navashenaq, S. A. Razavi, G. A. Kardar, and M. R. Khorramizadeh. 2014. 'Study of curcumin immunomodulatory effects on reactive astrocyte cell function', *Int Immunopharmacol*, 22: 230-5.

Sharma, R. A., A. J. Gescher, and W. P. Steward. 2005. 'Curcumin: the story so far', *Eur J Cancer*, 41: 1955-68.

Sheng, J. G., R. E. Mrak, and W. S. Griffin. 1997. 'Neuritic plaque evolution in Alzheimer's disease is accompanied by transition of activated microglia from primed to enlarged to phagocytic forms', *Acta Neuropathol*, 94: 1-5.

Shigemoto-Mogami, Y., S. Koizumi, M. Tsuda, K. Ohsawa, S. Kohsaka, and K. Inoue. 2001. 'Mechanisms underlying extracellular ATP-evoked interleukin-6 release in mouse microglial cell line, MG-5', *J Neurochem*, 78: 1339-49.

Sholl, D. A. 1956. 'The measurable parameters of the cerebral cortex and their significance in its organization', *Prog Neurobiol*: 324-33.

Shrikant, P., E. Weber, T. Jilling, and E. N. Benveniste. 1995. 'Intercellular adhesion molecule-1 gene expression by glial cells. Differential mechanisms of inhibition by IL-10 and IL-6', *J Immunol*, 155: 1489-501.

Sierra, A., O. Abiega, A. Shahraz, and H. Neumann. 2013. 'Janus-faced microglia: beneficial and detrimental consequences of microglial phagocytosis', *Front Cell Neurosci*, 7: 6.

Sierra, A., J. M. Encinas, J. J. Deudero, J. H. Chancey, G. Enikolopov, L. S. Overstreet-Wadiche, S. E. Tsirka, and M. Maletic-Savatic. 2010. 'Microglia shape adult hippocampal neurogenesis through apoptosis-coupled phagocytosis', *Cell Stem Cell*, 7: 483-95.

Silver, J., and J. H. Miller. 2004. 'Regeneration beyond the glial scar', *Nat Rev Neurosci*, 5: 146-56.

Singh, S., and B. B. Aggarwal. 1995. 'Activation of transcription factor NF-kappa B is suppressed by curcumin (diferuloylmethane) [corrected]', *J Biol Chem*, 270: 24995-5000.

Sofroniew, Michael V. 2009. 'Molecular dissection of reactive astrogliosis and glial scar formation', *Trends in Neurosciences*, 32: 638-47.

Song, C., and B. E. Leonard. 2005. 'The olfactory bulbectomised rat as a model of depression', *Neurosci Biobehav Rev*, 29: 627-47.

Sorrenti, V., G. Contarini, S. Sut, S. Dall'Acqua, F. Confortin, A. Pagetta, P. Giusti, and M. Zusso. 2018. 'Curcumin Prevents Acute Neuroinflammation and Long-Term Memory Impairment Induced by Systemic Lipopolysaccharide in Mice', *Front Pharmacol*, 9: 183.

Şovrea, A., and A. Boşca. 2013. 'Astrocytes reassessment - an evolving concept part one: embryology, biology, morphology and reactivity', *Journal of Molecular Psychiatry*, 1.

Spooren, A., K. Kolmus, G. Laureys, R. Clinckers, J. De Keyser, G. Haegeman, and S. Gerlo. 2011. 'Interleukin-6, a mental cytokine', *Brain Res Rev*, 67: 157-83.

Srivastava, I. N., J. Shperdheja, M. Baybis, T. Ferguson, and P. B. Crino. 2016. 'mTOR pathway inhibition prevents neuroinflammation and neuronal death in a mouse model of cerebral palsy', *Neurobiol Dis*, 85: 144-54.

Steinman, L. 2007. 'A brief history of T(H)17, the first major revision in the T(H)1/T(H)2 hypothesis of T cell-mediated tissue damage', *Nat Med*, 13: 139-45.

Stranahan, A. M., T. V. Arumugam, R. G. Cutler, K. Lee, J. M. Egan, and M. P. Mattson. 2008. 'Diabetes impairs hippocampal function through glucocorticoid-mediated effects on new and mature neurons', *Nat Neurosci*, 11: 309-17.

Streit, W. J., S. D. Hurley, T. S. McGraw, and S. L. Semple-Rowland. 2000. 'Comparative evaluation of cytokine profiles and reactive gliosis supports a critical role for interleukin-6 in neuron-glia signaling during regeneration', *J Neurosci Res*, 61: 10-20.

Sturrock, R. R. 1980. 'A comparative quantitative and morphological study of ageing in the mouse neostriatum, indusium griseum and anterior commissure', *Neuropathol Appl Neurobiol*, 6: 51-68.

Suresha, B. S., and K. Srinivasan. 2013. 'Antioxidant properties of fungal metabolite nigerloxin in vitro', *Prikl Biokhim Mikrobiol*, 49: 587-91.

Suzumura, A. 2013. 'Neuron-microglia interaction in neuroinflammation', *Curr Protein Pept Sci*, 14: 16-20.

———. 2017. '[The Role of Microglia in Neuroinflammation]', *Brain Nerve*, 69: 975-84.

Swardfager, W., K. Lanctot, L. Rothenburg, A. Wong, J. Cappell, and N. Herrmann. 2010. 'A meta-analysis of cytokines in Alzheimer's disease', *Biol Psychiatry*, 68: 930-41.

Swomley, A. M., and D. A. Butterfield. 2015. 'Oxidative stress in Alzheimer disease and mild cognitive impairment: evidence from human data provided by redox proteomics', *Arch Toxicol*, 89: 1669-80.

Takasu, N., I. Komiya, T. Asawa, Y. Nagasawa, and T. Yamada. 1991. 'Streptozocin- and alloxan-induced H2O2 generation and DNA fragmentation in pancreatic islets. H2O2 as mediator for DNA fragmentation', *Diabetes*, 40: 1141-5.

Tan, Z. S., and S. Seshadri. 2010. 'Inflammation in the Alzheimer's disease cascade: culprit or innocent bystander?', *Alzheimers Res Ther*, 2: 6.

Tannahill, G. M., A. M. Curtis, J. Adamik, E. M. Palsson-McDermott, A. F. McGettrick, G. Goel, C. Frezza, N. J. Bernard, B. Kelly, N. H. Foley, L. Zheng, A. Gardet, Z. Tong, S. S. Jany, S. C. Corr, M. Haneklaus, B. E. Caffrey, K. Pierce, S. Walmsley, F. C. Beasley, E. Cummins, V. Nizet, M. Whyte, C. T. Taylor, H. Lin, S. L. Masters, E. Gottlieb, V. P. Kelly, C. Clish, P. E. Auron, R. J. Xavier, and L. A. O'Neill. 2013. 'Succinate is an inflammatory signal that induces IL-1beta through HIF-1alpha', *Nature*, 496: 238-42.

Thaler, J. P., C. X. Yi, E. A. Schur, S. J. Guyenet, B. H. Hwang, M. O. Dietrich, X. Zhao, D. A. Sarruf, V. Izgur, K. R. Maravilla, H. T. Nguyen, J. D. Fischer, M. E. Matsen, B. E. Wisse, G. J. Morton, T. L. Horvath, D. G. Baskin, M. H. Tschop, and M. W. Schwartz. 2012. 'Obesity is associated with hypothalamic injury in rodents and humans', *J Clin Invest*, 122: 153-62.

Tiwari, S. K., S. Agarwal, B. Seth, A. Yadav, S. Nair, P. Bhatnagar, M. Karmakar, M. Kumari, L. K. Chauhan, D. K. Patel, V. Srivastava, D. Singh, S. K. Gupta, A. Tripathi, R. K. Chaturvedi, and K. C. Gupta. 2014. 'Curcumin-loaded nanoparticles potently induce adult neurogenesis and reverse cognitive deficits in Alzheimer's disease model via canonical Wnt/beta-catenin pathway', *ACS Nano*, 8: 76-103.

Tonnesen, H. H. 1989. 'Studies on curcumin and curcuminoids. XVI. Effect of curcumin analogs on hyaluronic acid degradation in vitro', *Int. J. Pharm*: 259–61.

———. 2002. 'Solubility, chemical and photochemical stability of curcumin in surfactant solutions. Studies of curcumin and curcuminoids, XXVIII', *Pharmazie*, 57: 820-4.

Torres-Platas, S. G., S. Comeau, A. Rachalski, G. D. Bo, C. Cruceanu, G. Turecki, B. Giros, and N. Mechawar. 2014. 'Morphometric characterization of microglial phenotypes in human cerebral cortex', *J Neuroinflammation*, 11: 12.

Torres-Platas, S. G., C. Hercher, M. A. Davoli, G. Maussion, B. Labonte, G. Turecki, and N. Mechawar. 2011. 'Astrocytic hypertrophy in anterior cingulate white matter of depressed suicides', *Neuropsychopharmacology*, 36: 2650-8.

Tremblay, M. E., R. L. Lowery, and A. K. Majewska. 2010. 'Microglial interactions with synapses are modulated by visual experience', *PLoS Biol*, 8: e1000527.

Tsai, Y. M., C. F. Chien, L. C. Lin, and T. H. Tsai. 2011. 'Curcumin and its nano-formulation: the kinetics of tissue distribution and blood-brain barrier penetration', *Int J Pharm*, 416: 331-8.

Ullah, F., T. Ali, N. Ullah, and M. O. Kim. 2015. 'Caffeine prevents d-galactose-induced cognitive deficits, oxidative stress, neuroinflammation and neurodegeneration in the adult rat brain', *Neurochem Int*, 90: 114-24.

Ullah, F., A. Liang, A. Rangel, E. Gyengesi, G. Niedermayer, and G. Munch. 2017. 'High bioavailability curcumin: an anti-inflammatory and neurosupportive bioactive nutrient for neurodegenerative diseases characterized by chronic neuroinflammation', *Arch Toxicol*, 91: 1623-34.

Vallieres, L., I. L. Campbell, F. H. Gage, and P. E. Sawchenko. 2002. 'Reduced hippocampal neurogenesis in adult transgenic mice with chronic astrocytic production of interleukin-6', *J Neurosci*, 22: 486-92.

Van Wagoner, N. J., and E. N. Benveniste. 1999. 'Interleukin-6 expression and regulation in astrocytes', *J Neuroimmunol*, 100: 124-39.

Vela, J. M., I. Dalmau, B. Gonzalez, and B. Castellano. 1995. 'Morphology and distribution of microglial cells in the young and adult mouse cerebellum', *J Comp Neurol*, 361: 602-16.

Vergoni, A. V., G. Tosi, R. Tacchi, M. A. Vandelli, A. Bertolini, and L. Costantino. 2009. 'Nanoparticles as drug delivery agents specific for CNS: in vivo biodistribution', *Nanomedicine*, 5: 369-77.

Vinet, Jonathan, Hilmar RJ van Weering, Annette Heinrich, Roland E. Kälin, Anja Wegner, Nieske Brouwer, Frank L. Heppner, Nico van Rooijen, Hendrikus WGM Boddeke, and Knut Biber. 2012. 'Neuroprotective function for ramified microglia in hippocampal excitotoxicity', *Journal of Neuroinflammation*, 9: 27.

Walsh, D. M., I. Klyubin, J. V. Fadeeva, M. J. Rowan, and D. J. Selkoe. 2002. 'Amyloid-beta oligomers: their production, toxicity and therapeutic inhibition', *Biochem Soc Trans*, 30: 552-7.

Walsh, D. M., and D. J. Selkoe. 2004. 'Deciphering the molecular basis of memory failure in Alzheimer's disease', *Neuron*, 44: 181-93.

Wang, Y. J., M. H. Pan, A. L. Cheng, L. I. Lin, Y. S. Ho, C. Y. Hsieh, and J. K. Lin. 1997. 'Stability of curcumin in buffer solutions and characterization of its degradation products', *J Pharm Biomed Anal*, 15: 1867-76.

Wilhelmsson, Ulrika, Eric A. Bushong, Diana L. Price, Benjamin L. Smarr, Van Phung, Masako Terada, Mark H. Ellisman, and Milos Pekny. 2006. 'Redefining the concept of reactive astrocytes as cells that remain within their unique domains upon reaction to injury', *Proceedings of the National Academy of Sciences*, 103: 17513-18.

Wilken, R., M. S. Veena, M. B. Wang, and E. S. Srivatsan. 2011. 'Curcumin: A review of anti-cancer properties and therapeutic activity in head and neck squamous cell carcinoma', *Mol Cancer*, 10: 12.

Wilms, H., J. Claasen, C. Rohl, J. Sievers, G. Deuschl, and R. Lucius. 2003. 'Involvement of benzodiazepine receptors in neuroinflammatory and neurodegenerative diseases: evidence from activated microglial cells in vitro', *Neurobiol Dis*, 14: 417-24.

Wright, A. L., R. Zinn, B. Hohensinn, L. M. Konen, S. B. Beynon, R. P. Tan, I. A. Clark, A. Abdipranoto, and B. Vissel. 2013. 'Neuroinflammation and neuronal loss precede Abeta plaque deposition in the hAPP-J20 mouse model of Alzheimer's disease', *PLoS One*, 8: e59586.

Wu, J. C., M. L. Tsai, C. S. Lai, Y. J. Wang, C. T. Ho, and M. H. Pan. 2014. 'Chemopreventative effects of tetrahydrocurcumin on human diseases', *Food Funct*, 5: 12-7.

Wyss-Coray, T. 2006. 'Inflammation in Alzheimer disease: driving force, bystander or beneficial response?', *Nat Med*, 12: 1005-15.

Xu, M. X., R. Yu, L. F. Shao, Y. X. Zhang, C. X. Ge, X. M. Liu, W. Y. Wu, J. M. Li, and L. D. Kong. 2016. 'Up-regulated fractalkine (FKN) and its receptor CX3CR1 are involved in fructose-induced neuroinflammation: Suppression by curcumin', *Brain Behav Immun*.

Yamada, J., and S. Jinno. 2013. 'Novel objective classification of reactive microglia following hypoglossal axotomy using hierarchical cluster analysis', *J Comp Neurol*, 521: 1184-201.

Yang, F., G. P. Lim, A. N. Begum, O. J. Ubeda, M. R. Simmons, S. S. Ambegaokar, P. P. Chen, R. Kayed, C. G. Glabe, S. A. Frautschy, and G. M. Cole. 2005. 'Curcumin inhibits formation of amyloid beta oligomers and fibrils, binds plaques, and reduces amyloid in vivo', *J Biol Chem*, 280: 5892-901.

Yoshida, T., S. K. Goldsmith, T. E. Morgan, D. J. Stone, and C. E. Finch. 1996. 'Transcription supports age-related increases of GFAP gene expression in the male rat brain', *Neurosci Lett*, 215: 107-10.

Youn, H. S., S. I. Saitoh, K. Miyake, and D. H. Hwang. 2006. 'Inhibition of homodimerization of Toll-like receptor 4 by curcumin', *Biochem Pharmacol*, 72: 62-9.

Yu, S., X. Wang, X. He, Y. Wang, S. Gao, L. Ren, and Y. Shi. 2016. 'Curcumin exerts anti-inflammatory and antioxidative properties in 1-methyl-4-phenylpyridinium ion (MPP(+))-stimulated mesencephalic astrocytes by interference with TLR4 and downstream signaling pathway', *Cell Stress Chaperones*, 21: 697-705.

Zhang, G., J. Li, S. Purkayastha, Y. Tang, H. Zhang, Y. Yin, B. Li, G. Liu, and D. Cai. 2013. 'Hypothalamic programming of systemic ageing involving IKK-beta, NF-kappaB and GnRH', *Nature*, 497: 211-6.

Zhang, J. M., and J. An. 2007. 'Cytokines, inflammation, and pain', *Int Anesthesiol Clin*, 45: 27-37.

Zhang, J., Q. Tang, X. Xu, and N. Li. 2013. 'Development and evaluation of a novel phytosome-loaded chitosan microsphere system for curcumin delivery', *Int J Pharm*, 448: 168-74.

Zhang, Q., and P. G. Haydon. 2005. 'Roles for gliotransmission in the nervous system', *J Neural Transm (Vienna)*, 112: 121-5.

Zhu, H. T., C. Bian, J. C. Yuan, W. H. Chu, X. Xiang, F. Chen, C. S. Wang, H. Feng, and J. K. Lin. 2014. 'Curcumin attenuates acute inflammatory injury by inhibiting the TLR4/MyD88/NF-kappaB signaling pathway in experimental traumatic brain injury', *J Neuroinflammation*, 11: 59.

Ziko, I., S. De Luca, T. Dinan, J. M. Barwood, L. Sominsky, G. Cai, R. Kenny, L. Stokes, T. A. Jenkins, and S. J. Spencer. 2014. 'Neonatal overfeeding alters hypothalamic microglial profiles and central responses to immune challenge long-term', *Brain Behav Immun*, 41: 32-43.